Chemical Engineering

Chemical Modification of PHEMA to Create an Improved Bioactive Biomaterial for Regenerative Applications

Elizabeth Monica Grenik

This thesis is presented for the Degree of

Doctor of Philosophy

of

Curtin University

May 2016

Declaration

To the best of my knowledge and belief this thesis contains no material previously published by any other person except where due acknowledgement has been made. This thesis contains no material which has been accepted for the award of any other degree or diploma in any university.

Signature:

Date:

Dedication: I would like to dedicate my work to a dear friend, Joe. His curiosity and enthusiasm in all things science and engineering was infectious and inspiring. His love of learning and teaching science and engineering has encouraged me to always strive to do my best.

Acknowledgements

Firstly I would like to thank my supervisors, Xia Lou and Deirdre Coombe for all of their support over the years. Without your knowledge and expertise I would have been lost. Thank you for taking the time to teach me so much and helping me to expand my skills. I would like to thank all of the people in my research groups. You were the ones who helped me out with all of the little things. I can't express how much I appreciated your constant support.

A very special thank you to Bev Kinnear who taught me everything I now know about cell culture and biological assay techniques. Your vast experience in the field has been priceless and inspiring. A big thank you to the Curtin University's Microscopy and Microanalysis Facility and the Curtin Health Innovation Research Institute for all of their support and for the use of their instrumentation which was essential for my project.

Another special thank you to all of the PhD students who were working through their projects at the same time as me. You were the day-to-day safety barrier between me and insanity. Without your support the whole process would have been significantly less enjoyable and worthwhile. A special mention to Guy Travers who ensured my thesis was perfectly formatted, thanks a million! Of course a big thank you to my friends and family for all of their emotional support. Your understanding and confidence in my abilities was sometimes the only thing that kept me going.

Abstract

RGD and heparan sulfate (HS) modified poly(2-hydroxyethyl methacrylate)-(PHEMA) was synthesised as a porous 3D sponge hydrogel. The synthetic pathway for the modification of PHEMA began with copolymerising HEMA with glycidyl methacrylate followed by the reaction of the glycol with hexamethylenediamine. This introduced a free amine onto the hydrogel which was used to covalently immobilise two different biomolecules using the same chemistry. The RGD peptide is well known as a biomolecule that can improve the adhesion of a variety of cells to a surface and HS provides the binding activity of all adherent cells to a wide variety of proteins. The binding activity of HS is known to mediate important cell behaviours such as cell adhesion, proliferation, differentiation and assist in wound repair. Therefore RGD and HS were used to improve cell adhesion and proliferation on PHEMA and to create a scaffold that had potential for tissue engineering applications.

The hydrogels were characterised with a variety of chemical and physical techniques. The immobilisation of RGD and HS was confirmed and quantified both individually on the hydrogels and also with the immobilisation of both biomolecules on the same hydrogel. The pores were interconnected and sufficiently large to enable cell migration into the material with diameters between 10-30 μm. The high swelling content of the hydrogels mimicked the in vivo environment of native tissue. Rheology measurements were performed to examine the elasticity and stability of the hydrogels under physiological conditions. The hydrogels were found to have elasticity similar to that measured for fibroblasts. These results indicated that the hydrogels had great potential as a scaffold for deep tissue regeneration.

The bioactivity of immobilised RGD and HS was accessed with cell culture work. Two mouse cells lines were used, 3T3 fibroblasts and C2C12 myoblasts. All modification steps were observed to improve the biocompatibility of the hydrogel in comparison to PHEMA. HS was shown to retain bioactivity after immobilisation resulting in improved cell adhesion, proliferation and differentiation. Incorporation of the RGD peptide showed a more moderate

improvement in cell behaviour when compared to the results from HS. The immobilisation of both RGD and HS on the same hydrogel resulted in the best cell behaviour. Most important was the finding that the presence of HS on the hydrogel was required for the successful differentiation of C2C12 cells into myotubes.

Additional characterisation of the bioactivity of the synthesised hydrogels involved immunofluorescence and an enzyme linked immunosorbant assay (ELISA). The immunofluorescence detected the fibronectin that had been produced by the cells while they were cultured on the hydrogels. The cells expressed more fibronectin on the modifed hydrogels, especially the end modifications. The differences in 3T3 cell adhesion and proliferation correlated well with the amounts of fibronectin produced by the cells, the differences with the C2C12 cells were more subtle. More importantly, the expressed fibronectin was more organised and mature on the HS hydrogels. The ELISA was designed to further confirm the activity of the immobilised HS. It used the known affinity between basic fibroblast growth factor (bFGF) and HS. The results clearly showed that the immobilised HS had retained its bioactivity and was readily able to bind bFGF. These results showed that the immobilised HS was able to bind and sequester molecules to control cell signalling, these signals enhanced cell behaviour and promoted cell differentiation. This mimicked the *in vivo* interaction between HS on the cell surface and soluble proteins in the extracellular matrix.

The project has shown that PHEMA can be effectively modified to create a bioactive hydrogel scaffold. The improved bioactivity of the hydrogel could be used for tissue regeneration applications. The hydrogel demonstrated important results such as: 1) the immobilised HS was able to bind a growth factor that is important for wound healing, 2) fibroblasts and myoblasts adhered and proliferated well on the modified hydrogels and 3) myoblast differentiation was only observed on the hydrogels with immobilised HS. These results showed that the synthesised hydrogels have potential for regenerative applications such as wound healing.

Contents

List of Figures

Chapter 1

Introduction

1.1 Introduction to Tissue Engineering

Tissue engineering is described by the National Institute of Health (NIH) as a topic of research that evolved from the field of biomaterial development and refers to the practice of combining scaffolds, cells and biologically active molecules into functional tissues. The NIH describes the goal of tissue engineering as: to assemble functional constructs that restore, maintain or improve damaged tissues or whole organs. Tissue engineering has also been described as 'the creation (or formation) of new tissue for the therapeutic reconstruction of the human body, by the deliberate and controlled stimulation of selected target cells through a systematic combination of molecular and mechanical signals'[1]. In a more simple form; tissue engineering involves the use of living cells, and seeding a biomaterial with cells before implantation, to aid in tissue formation or regeneration, thereby producing a therapeutic or diagnostic benefit[2–5].

A biomaterial is defined as any material, natural or synthetic, that is suitable to be placed in contact with living tissue. Biomaterials were traditionally designed to be relatively biologically inert to avoid unwanted inflammation responses. These biomaterials were designed as inert coatings for medical prostheses such as pacemakers and joint replacements, as well as with applications such as contact lenses. Such surfaces need to avoid the adhesion of cells and

biomolecules to maintain their functionality.

Now the focus has changed and biomaterials are designed to actively interact with the body to assist in the repair or replacement of tissue that has been damaged or lost. Biomaterials are required when the body is unable to completely or successfully repair its own tissues. The role of the biomaterial is to provide structural support to the affected area while initiating the body's own regenerative processes. Biomaterials can be designed as permanent implants, or as slowly degrading materials that are eventually completely replaced by native tissue. Biomaterials are applicable for any situation where the patient has suffered damage to tissue. The cause of the tissue damage could be due to disease, surgery, injury or birth defects or a combination of all four. The scarcity of replacement organs and tissues is one of the main drivers for the abundance of research in the biomaterial area[6]. The outcome of tissue engineering and biomaterial research is that a much greater number of patients could be treated for ailments caused by loss of tissue or organ function[6].

Engineering complex tissues is perhaps the most ambitious goal of all tissue engineers[5]. Engineering of functional vascular networks, interfaces, structural hierarchy and complex functional features is emerging as an unparalleled scientific and technical challenge for the next generation of tissue engineers[5]. As the field of tissue engineering expands and the complexity of biomaterials increases the definition of a biomaterial has broadened. Biomaterials can be made from synthetic or natural components, or the combination of both. These include tissue, and components of tissue, that are extracted from the body and are purified or modified. The functions of biomaterials have expanded to include applications that: completely replace native tissue, assist with the repair of native tissue, or provide therapeutic drugs. A current definition for a biomaterial is 'a substance that has been engineered to take a form which, alone or as part of a complex system, is used to direct, by control of interactions with components of living systems, the course of any therapeutic or diagnostic procedure, in human or veterinary medicine'[1].

1.2 The Extracellular Matrix

Native tissue is not made up solely of cells[7]. A substantial part of a tissue's volume is the extracellular area which is largely filled by an intricate network of macromolecules that constitute the extracellular matrix (ECM)[7]. The ECM is the body's natural tissue regeneration scaffold and consists of highly orchestrated supramolecular assemblies of hydrated and crosslinked fibrous proteins, proteoglycans, growth factors and other soluble molecules[8,9]. The ECM is an important component of every tissue and it often determines the physical properties of the tissue. However the ECM is not merely a physical support for native tissue, it is a dynamic and bioactive scaffold that regulates cell behaviour.

The ECM has the ability to communicate spatially and temporally with cells thereby directing cell behaviour via matrix interactions with cell-surface receptors[10]. It is dynamic due to cell-matrix communication occurring in both directions resulting in a matrix that is able to respond to cell signals and affect changes in its local microenvironment[10,11]. The ECM determines cell survival, development, migration, proliferation, shape and function as well as directing and organising tissue morphogenesis, homeostasis and regeneration in pathophysiological situations[7,8,10,11]. This influence is due to the highly specialised and complex molecular composition of the ECM and the adaptability of the ECM to the functional requirements of a particular tissue[7,9,10,12].

The main components of the ECM are fibrous proteins: collagens, elastin, laminins and fibronectin. Collagens are a family of fibrous proteins which collectively are the most abundant proteins in mammals[7]. Collagens are secreted by connective tissue cells (as well as other cell types) and are a major component of skin and bone[7]. Cells are known to interact with the collagen that they have secreted, aligning and compacting the collagen to create long-range order in the ECM[7]. For example fibroblasts (connective tissue cells) influence the alignment of collagen to create dense layers of connective tissue that bind cells within most organs in the body[7]. In contrast, elastin forms elastic fibers in the ECM which provide resilience and allows the matrix to stretch[7]. Elastin is the dominant ECM protein in arteries[7].

The laminins are a tri-glycoprotein complex that are important for the development and maintenance of cell organisation. For example, laminins have been demonstrated to stimulate cell growth and differentiation, promote neurite outgrowth and mediate cell communication[13]. Fibronectin is also a large glycoprotein that contributes to the organisation of the ECM and provides attachment sites for cells[7]. The tripeptide sequence RGD (arginine, glycine, aspartic acid) is a central feature of one cell binding domain of fibronectin[7]. This peptide sequence has often been used to increase cell binding to a surface.

Another important macromolecular component of the ECM are proteoglycans. Proteoglycans consist of a core protein that has covalently bound pendant chains of polysaccharides known as glycosaminoglycans (GAGs)[14,15]. Proteoglycans are diverse due to their different core proteins and different GAG chains. They are classified by the predominant GAG chain[15]. Proteoglycans are thought to play a major role in the chemical signaling between cells[7]. They bind various signaling molecules such as growth factors, proteases and protease inhibitors and have the ability to enhance or inhibit the activity of these proteins[7].

The binding of a protein to proteoglycans may lead to: restriction of the protein's action by steric hindrance of it's activity, sequestration of the protein and delayed release, protection of the protein from enzyme degradation or locally concentrate the protein to improve it's effective presentation to cell-surface receptors[7]. In particular the specific binding of growth factors to proteoglycans can effectively modulate cellular growth, cell development, angiogenesis and tissue regeneration[16,17]. Maintenance of the appropriate structure and concentration of proteoglycans is critical for a healthy tissue. Proteoglycans are strongly anionic polymers that absorb large amounts of water, this provides compressive strength to the ECM[18]. This is particularly important for tissues such as cartilage which are required to resist compressive loads[19,20].

Glycosaminoglycans are unbranched polysaccharide chains that are composed of repeating disaccharide units of D-glucuronic or L-iduronic acid and either *N*-acetylglucosamine or *N*-acetylgalactosamine[7,21]. They are highly negatively charged due to the abundance of sulfate and carboxyl groups on their chains[7].

The polysaccharide chains in GAGs are not able to fold into compact structures in the same way that polypeptide chains can. This allows them to form gels, even at low concentrations, which incorporate large amounts of water and creates a swelling pressure that can withstand compressive stress. These gels are also highly porous permitting the rapid diffusion of nutrients, metabolites and hormones[7].

There are 6 different types of GAGs; hyaluronan (also known as hyaluronic acid), dermatan sulfate, keratan sulfate, chondroitin sulfate, heparin and heparan sulfate (HS)[21,22]. It is the GAG chains which provide proteoglycans with an ability to function as: physiological barriers, reservoirs for signaling proteins and binding partners for structural macromolecules[21]. Indeed, GAG chains provide most of the bioactivity attributed to proteoglycans and play a pivotal role in biological processes like morphogenesis, angiogenesis and wound healing[23,24].

Another important component of the ECM are the soluble molecules that act as signaling molecules. These include chemokines, cytokines, hormones, vitamins and biological factors. There are three major classes of factors that act as extracellular signaling molecules; mitogens, growth factors and survival factors. These are usually soluble cell secreted proteins, proteins bound to the surface of cells or components of the ECM[7,25]. Mitogens are proteins that stimulate cell division, growth factors stimulate cell growth (increase in cell mass) and survival factors promote cell survival by suppressing apoptosis. Some extracellular signal proteins can act as both a growth factor and a mitogen to stimulate cell growth and cell division[7]. They can also direct cell migration, activate various cell types and initiate new gene expression[26]. These properties are recognised as playing important roles for wound healing processes and the direct application of growth factors to wounds has been shown to accelerate the normal healing process[26]. Platelet-derivated growth factor (PDGF), epidermal growth factor (EGF), transforming growth factor alpha (TGF-α), basic fibroblast growth factor (bFGF) and transforming growth factor-β1 (TGF-β1) are polypeptide growth factors that have significant activity in tissue repair processes[27].

Individual ECM components have many positive effects on cell behaviour. However, as native ECM is a matrix that is composed of multiple bioactive molecules, it is not surprising to find that these molecules also act synergistically *in vivo*. One example is the importance of the complex that is formed by heparan sulfate proteoglycans (HSPGs), growth factors and their receptors. This complex is required for optimal growth factor signaling, of members of the fibroblast growth factor (FGF) family[28,29].

In native ECM, some growth factors are stored in a latent form through their binding to the sulfated regions on the HS chains of HSPGs[16]. This can concentrate the growth factors close to cells. In addition, the binding of some growth factors to HS chains may protect the growth factor from normal proteolytic degradation. It may also enhance and stabilise interactions on the cell surface leading to the cross-linking of receptors and receptor activation[28,29]. The FGF family and their receptors (FGFR) interact with the HS chains of HSPGs and so coordinate cell-fate decisions such as cell growth, development, angiogenesis and tissue regeneration[16,28]. Hence, the ECM has enormous potential for regulating various signaling events that influence cell behaviour and effect tissue regeneration.

The influence of the ECM on cell behaviour extends to cell shape, attachment, proliferation, migration, differentiation and survival. The ECM affects cell shape through influencing the organisation of the cell's cytoskeleton[7]. For example a lack of fibronectin results in poorly adhered cells whilst abundant filbronectin commonly gives rise to well adhered cells, identified by their flattened shape and organised actin filaments[7]. Most cells require attachment to the ECM to proliferate and survive. Strong attachment of cells to the ECM and a spread morphology has been demonstrated to increase cell growth. This effect has been presumed to assist in the repair of tissues after injury[7]. The migration of cells through the ECM commonly occurs via the localised enzymatic degradation of the matrix. Cells secrete proteases that locally and specifically degrade the matrix allowing their migration while the structural integrity of the ECM is maintained[7]. The most common enzymes involved in this process are matrix metalloproteases which degrade matrix proteins such as collagen, laminin and

fibronectin[7].

Cell proliferation is affected by the strength of cell attachment to a substrate. This is due to the intracellular signals that are created when a cell attaches to a surface and forms focal adhesions. Focal adhesions are formed when ECM proteins such as laminin and fibronectin interact with cell-surface receptors known as integrins. This interaction leads to the activation of protein kinases which then activates intracellular signaling pathways that can promote cell division and survival[7]. Focal adhesions are composed of actin filaments that link the cytoskeleton to the ECM through integrins on the cell surface. Actin is a prevalent protein in the cell that polymerises to form filaments known as F-actin (or filamentous actin). These actin filaments form an assortment of networks and bundles that are interconnected to form the actin cytoskeleton[30]. Within a cell stress fibers are composed of actin and myosin bundles and are important for cell adhesion to ECM substrates and in cellular mechanotransduction (the cell converts mechanical signals from the arrangement/orientation of the actin fibers into a biochemical response)[7,31].

Cell fate decisions *in vivo* are largely controlled by exogenous signals presented on the ECM[32] and the ECM is essential for guiding cells through distinct development paths[33]. It contains extrinsic cell signals that creates a highly defined and specialised cell microenvironment, which is essential for correct tissue development and continued function[33]. The ECM has a variety of forms in different tissues and at different development stages in the same tissue[10,34]. The structural diversity observed in different ECMs is due to the combinations of specific molecular interactions involving different isoforms, ratios and geometrical arrangements of collagen, elastin, proteoglycans and adhesion proteins[33]. One example of how the ECM can be specialised is the stem cell niche. This is now assumed to exist in all adult tissues[9]. The stem cell niche is a specialised microenvironment where the ECM and growth-modulating factors stored within it help sustain a stem cell pool[9].

While there is much information about the ECM and it's effects on cells and tissues, there is still a lot of information that is lacking. The complex and dynamic nature of the ECM complicates results and makes it difficult to nail down which

component has exactly what effect. Moreover, the number of possible synergistic effects between individual components is overwhelming. It is most likely these collaborative molecular interactions within the ECM are what enables the ECM to provide such a successful template to communicate with cells and to guide tissue repair and maintenance.

1.3 Designing New Biomaterials

The need for better designed or more complex biomaterials is apparent from the limited applications of the currently available commercial products. The reliance on native tissue to create functional commercial biomaterials limits their widespread availability. Ultimately, it is hoped that these engineered tissues will alleviate the extreme shortage of tissues and organs for transplantation[35]. The underlying concept of tissue engineering is that cells have an inherent capability to organise into tissues and organs if given the proper environment of mechanical and chemical signals[6]. The basic assumption of this technology is that cells cultured in an environment that closely mimics the native, will develop into tissues that resemble natural tissues[6].

1.3.1 Physical Properties

Selecting the correct physical properties for a biomaterial is vital. The biomaterial needs to be able to provide the same physical support to surrounding tissue and cells as the native tissue. Without this physical support the biomaterial can fail in its application. This is especially true when the biomaterial is designed to be a permanent replacement for native tissue. Such instances normally involve joint or bone damage that can't be repaired by other means such as tissue grafts. In this application the biomaterial needs to be able to handle the same compressive and tensile stress as native bone. Additionally replacement joints need to have sufficient lubrication to allow for continual repetitive stress.

Physical support is equally important for biomaterials in soft tissue applications. In these applications the support is for the cells that will attach and grow on the biomaterial. The attachment site for a mammalian cell is typically another similar cell or the ECM and the elastic modulus of cells or ECM ranges from 10 to 10,000 Pa[36]. As the stiffness of the biomaterial has been shown to have an effect on how cells adhere to the material[37], it is important that materials for soft tissue applications are designed with the elastic modulus of the natural tissue in mind.

Cells possess their own contractile force that senses the substrate stiffness[12]. Hence, changing the substrate stiffness can affect cell secretion of ECM components and this may change the immediate microenvironment[12]. This in turn may induce or enhance cell differentiation, proliferation or apoptosis[38]. Therefore altering the stiffness of the biomaterial can have major effects on cell behaviour. The lack of stiffness in a biomaterial is referred to as the elasticity. The elasticity of the biomaterial should be matched to the native tissue ECM and a mismatch of elasticity can result in the failure of the biomaterial in vivo[12]. Cells placed on a biomaterial with an elastic modulus significantly less than that of the native tissue ECM are generally more rounded and less spread. This morphological difference is due to poor cell adhesion which often leads to low cell proliferation and enhanced apoptosis[39].

Other physical properties that are known to affect cell behaviour are: wettability, surface molecular mobility, surface free energy, porosity and topography. These physical properties of biomaterials tend to affect cell behaviour via affects on protein adhesion to the biomaterial surface. The wettability or hydrophilicity of a biomaterial is determined by the charge and polarity of the surface[40]. Wettability will affect the type and orientation of adsorbed proteins[40]. Hydrophobic surfaces irreversibly adsorb large quantities of albumin, a protein which does not support cell attachment whereas, hydrophilic surfaces tend to adsorb proteins that support cell adhesion such as fibronectin[40]. As a result cells on hydrophobic surfaces will generally retain a round morphology and weak attachment while those on hydrophilic surfaces will be more elongated and show better attachment.

Altering the molecular mobility and surface free energy of a biomaterial changes the morphology of adherent cells[37]. Generally an increase in either, or both, properties results in better cell attachment and spreading[37,41]. Highly dynamic polymer surfaces with high molecular mobility results in adherent cells with an elongated morphology while less mobile surfaces have adhered cells with a rounded morphology[37]. For example, the aspect ratio of fibroblasts was shown to increase (elongation of adhered cells) as the molecular mobility of the material was increased[37].

The surface free energy of a material determines the extent of protein adsorption to a surface and adsorption density of proteins affects the density of cell adhesion, the number of cells adhering, cell proliferation rate and projected cell area[37]. Interestingly a direct correlation was found between increasing the total surface free energy of a material and the density of adsorbed fibronectin[37]. Protein adsorption onto the biomaterial surface is the most important factor in determining cell behaviour. Most research with cells is done in media containing serum and the first proteins to interact with the biomaterial will be from the serum. Protein adsorption is a process that takes minutes compared to cell adhesion which can take hours[41–44]. Hence, modification of the physical properties of a biomaterial is primarily about optimising protein adsorption.

Manipulating the surface free energy of a biomaterial can also force the cell to follow a pattern designed on the surface[41], possibly because this determines the pattern of protein adsorption. As the surface free energy of a biomaterial is equal to the surface tension multiplied by the surface area[45], when the topography changes so too does the surface energy. This means surface topography can be considered as a component of surface free energy. It is well established that cells react to micrometer range topographic features such as grooves, ridges and wells[46]. Micro and nano-patterning of the surface can be used to manipulate cell shape, adhesion, migration, differentiation, protein synthesis and gene expression[47]. Recently the focus has been towards nanoscale changes in topography to cause changes in: cell adhesion, motility, cytoskeletal condensation, activation of tyrosine kinases, and modulation of intracellular signaling pathways that regulate transcriptional activity and gene

expression[46,48–51].

Multiple factors of the topography modulate cell behaviour, these include: the scale (micro down to nano), shape, type (grooves, steps, pillars), spacing and symmetry of the topographic features[46,48–51]. Generally the presence of features such as ridges, steps and grooves increases cell attachment and proliferation. Cells are also observed to align with ridges, steps and grooves. This alignment is due to the cells ability to sense the tension or stress in the surface which results in reorganisation of the cells cytoskeleton[47]. Ridges as thin as 70 nm are observed to guide cytoskeletal assembly and align the cells to the direction of the ridges[48,52]. Upon introduction of nano-topography to a biomaterial, an early cell response is to increase filopodia and microspikes[33]. Nano-features possibly modulate the interfacial forces that guide cytoskeletal formation and membrane receptor organisation[33]. Increasing the nanoscale roughness of the walls of pores in a biomaterial can increase cell attachment, proliferation and ECM component expression[42,53,54].

Several studies have established that similar nanoscale topography may elicit similar biological effects regardless of the chemistry of the biomaterial. One example is the similarity of smooth muscle cell behaviour on nanopatterned poly(methyl methacrylate) (PMMA) and poly(dimethylsiloxane) (PDMS). The differing surface chemistry of the two polymers is unlikely to result in the same adsorption of proteins[49] as PMMA is hydrophillic while PDMS is strongly hydrophobic. Yet the smooth muscle cells were very similar in their adhesion and morphology on the two surfaces.

In contrast different cell types prefer different surface morphologies. Work by Kubinova et al., showed that mesenchymal stem cells preferentially attached on the flat surface of the scaffold, outside of the pores[55]. The few that attached inside the pores were long and thin as they adapted their morphology to the pore surface. In contrast neural stem cells were observed to attach preferentially to the rhombus shaped pores of the scaffold. Thus, as the response to substrate topography is cell type specific it is important that the topography of the biomaterial is appropriate for the intended application.

1.3.2 2D versus 3D

The natural environment for cells is the three dimensional (3D) ECM. While many characteristics and behaviours of cells can be observed when cultured on the two dimensional (2D) surface of tissue culture plastic, to mimic native cell behaviours cells should be observed in a 3D environment. One of the first to demonstrate differences in cell behaviour from 2D to 3D culture was Peterson et al., with breast epithelial cells. Cell morphology and behaviour only mirrored that seen *in vivo* when the cells were grown within a 3D reconstituted basement membrane matrix[56].

Many researchers have demonstrated the substantial difference in the properties of cells in 2D culture compared to the native 3D environment[9,57–59]. 3D cell culture techniques aim to recapitulate the *in vivo* biology and has significantly impacted our understanding of ECM architecture and its role in tissue remodeling[9]. Therefore the new focus in biomaterials and tissue engineering research is on 3D biomaterials that are better at mimicking the native 3D environment. It has been established that cell attachment and morphology is distinctively different in a 3D biomaterial compared to a 2D surface[59]. Cells tend to be more spread on surfaces and have a more stellate spindle-shaped morphology within 3D scaffolds. This difference in morphology is due to the traction forces provided by contractile cell-matrix interactions at both the leading and trailing edge of the cells[59]. This difference in cell morphology also affects the cells motility and the process used by the cells to migrate through the biomaterial[59,60]. The benefit of 3D cell culture is that it allows for the investigation of cell signaling[61] and cell matrix interactions[62] in a more *in vivo* like environment[60].

Differences in cell proliferation can be observed when cells are grown in 3D as opposed to 2D culture. Rat bone marrow cells show significantly higher proliferation when cultured on a 3D alginate matrix compared to 2D alginate discs[63]. Mahoney et al., suggest that 3D matrices provide a more suitable environment for the expansion of neural precursor cells as their survival is significantly greater in 3D than 2D culture[64]. The importance of a 3D environment

for epithelial cells is recognised as it promotes normal epithelial polarity and differentiation[58]. Fibroblasts have an artificially induced polarity when cultured in 2D whereas fibroblasts are normally nonpolar cells. Fibroblasts adhere more effectively, have differing morphology and show enhanced proliferation and migration rates in 3D culture[57,59,65]. Fibroblasts in 3D culture show triple colocalisation of $\alpha_5$integrin, paxillin and fibronectin similar to the colocalisation that defines 3D-matrix adhesions *in vivo*[57]. 3D matrix adhesions enhanced cellular functional activities compared to 2D adhesions[57] therefore to investigate or replicate *in vivo* cell behaviour, it is vital to use a 3D culture system.

1.3.3 Chemical and Biological Properties

Chemical and biological modifications are often made to biomaterials in order to mimic the ECM. These modifications involve physical and chemical attachment of ECM components, their derivatives, synthetic versions of ECM components or other natural components. Researchers commonly incorporate full-length ECM proteins in biomaterials to take advantage of the innate bioactivity and functionality of these proteins. However there are limitations to using full-length proteins as they are susceptible to denaturation and degradation, require mild reaction conditions, have batch-to-batch variation and scale-up difficulties[35,66–68]. This results in the unavailability of binding domains, the development of antigenicity and loss of specificity[66]. As full-length proteins contain several binding regions their random folding makes it difficult to deduce which motif will be presented and therefore cell responses are unpredictable[68,69]. Additionally as these proteins are not human in origin, they may elicit undesirable immune responses and increase infection risks[68]. As a consequence much of the current research focuses on using shorter peptide sequences that mimic the binding domains of native ECM proteins.

There are many advantages associated with using short peptide sequences. These include: relatively easy synthesis, easier purification and characterisation, cost effectiveness, less antigenicity, greater specificity, higher stability against conformational change and more control is possible over the density

and orientation of the binding domains[67,68,70,71]. Due to their synthetic nature and smaller size, peptides are more easily incorporated into biomaterials, than the full-length protein from which they are derived[67,68]. The most commonly used peptide sequences are: RGD, KQAGDV, REDV, PHSRN, IKLLI, LRE, LRGDN, PDGSR, IKVAV, LGTIPG, YIGSR, DGEA, GFOGER and VAPG[69]. Short peptide sequences can be immobilised on biomaterials by a variety of methods. Immobilisation via covalent bonding can be achieved by plasma treatment, copolymerisation and by the direct reaction of biomolecules with the functionalised materials ith amine or thiol groups[69].

The RGD peptide is most commonly studied as it stimulates cell adhesion by cells that express the appropriate integrins[68,71]. RGD has been used to modify biomaterials for various applications including: fibroblast adhesion and spreading, neuronal regeneration, endothelial cell attachment and the culturing of human embryonic stem cells[69]. Massi et al., immobilised RGD onto poly(2-hydroxyethyl methacrylate) (PHEMA) and poly(ethyleneterephthalate) (PET) surfaces. The aim of the work was to produce bioadhesive biomaterials that were independent of adsorbed adhesion molecules from the culture medium. The addition of RGD to the PHEMA or PET surface resulted in a ~400-fold or ~4-fold increase, respectively, in the number of spread fibroblasts. Attachment and spreading of aortic endothelial cells on the RGD modified surfaces was serum independent and a complete monolayer formed by 24 hours[72]. Cook et al., used a copolymer of poly(lactic acid) (PLA) and lysine (PLAL) to introduce functional amino groups into degradable PLA. These amino groups were used to immobilise RGD containing peptides. This resulted in a 4-fold increase in the spreading of endothelial cells. This work, in the 1990's was the first demonstration of a synthetic, resorbable biomaterial that facilitated cell adhesion and spreading[6].

As research on peptide modified biomaterials continued, various techniques were explored to optimise the bioactivity of the immobilised RGD and other peptide sequences. Factors that affect the bioactivity of the peptide include: peptide concentration, peptide clustering or orientation, the method of immobilisation and the inclusion of synergistic molecules[71,73]. It is now common for a

spacer or linker to be used for the immobilisation of short peptides. The spacer prevents steric hindrance of adjacent peptides and helps to maximise receptor binding. This improves the biological activity of the peptide and enhances cell adhesion[69]. These RGD based peptides, can be completely synthetically produced or they can be obtained by recombinant gene technology. Synthesis of recombinant peptides can be controlled to increase batch consistency, this results in molecules that maintain native orientation with controllable structural and functional characteristics. As recombinant molecules are extracted from organisms they may trigger innate and acquired immune responses unlike peptides that are completely synthetic[69].

Kubinova et al., modified Poly(2-hydroxyethyl methacrylate-co-2-aminoethyl methacrylate) (P(HEMA-AEMA)) with a laminin derived peptide sequence[55]. The effect of the addition of the Ac-CGGASIKVAVS-OH peptide to the scaffold was examined by monitoring the behaviour of the mesenchymal stem cells. On unmodified scaffolds the cells were less spread and didn't show many branched structures. With the peptide present the cells formed numerous branched lamelipodia and membrane protrusions. Development of actin filaments were observed after 4 hours of culture with vinculin staining showing evidence of focal adhesions at the ends of the actin filaments after 3 days[55].

Recombinant peptides have been used with synergistic sequences to improve receptor specificity such as PHSRN with RGD. A spacing of 4nm between RGD and the synergy site PHSRN in the recombinant peptide mimicked the native spacing in fibronectin. Inclusion of the synergistic site lead to an increase in osteoblast adhesion, spreading, focal adhesion contact, actin organisation and cell function indicators but a decrease in ECM production[71]. These results mirror those by other researchers who found synergistic adhesion and spreading of hamster kidney cells and macrophages when using the two peptides together[74,75]. The synergistic effects are interesting and promising for improved cell adhesion and spreading on biomaterials however the down regulation of ECM production may be problematic for tissue engineering purposes.

ECM components other than proteins or their peptides have been used to modify biomaterials to improve their cell adhesion properties. Commonly used

molecules are proteoglycans and glycosaminoglycans (GAGs). These molecules play a critical role in regulating cellular adhesion, migration and proliferation and impart important physiochemical properties to tissues[76]. Whole proteoglycans have not been widely used to modify biomaterials. This is most likely due to their large size and limitations like those already described for whole proteins. Ingavle et al., incorporated a proteoglycan complexed with hyaluronan, aggrecan, into a scaffold[77]. Aggrecan was incorporated physically into the scaffold by creation of an interpenetrating polymer network (IPN). The effect of aggrecan on chondrocyte adhesion was shown to be comparable with that of RGD. The authors note that considering the comparable results from the two biomolecules immobilised the use of RGD is preferable as it is significantly more cost effective[77]. It is more common to use small sections of proteoglycans that replicate individual binding domains, or the relevant GAG chain to introduce bioactivity to a biomaterial.

In the early 2000's researchers began to chemically modify GAG molecules to create new biomaterials[14]. By modifying the GAGs, their physicochemical and mechanical properties could be tailored while maintaining their natural biocompatibility, biodegradability and lack of immunogenicity[14]. These biomaterials have been explored for the following tissue engineering applications: materials for localised drug delivery, barriers to prevent post-surgical adhesions and dressings and matrices for wound healing and bone repair[14,24].

Hyaluronic acid (HA), the only GAG that is not synthesised as a proteoglycan, has been chemically modified to form biocompatible, macroporous hydrogel biomaterials that provide new ways to store and release combinations of growth factors[24]. HA is the only non-sulfated GAG and is a strong inducer of angiogenesis, although this effect is dependent on its molecular weight as only low molecular weight HA stimulates endothelial cell proliferation and migration[24]. The use of HA as a drug delivery scaffold for growth factors combines an interactive biomaterial that can participate in tissue responses with the growth factor[24].

The possible synergistic effect of immobilising heparin (a sulfated GAG) within a HA biomaterial along with 2 growth factors was investigated by Riley et al.[78].

Vascular endothelial growth factor (VEGF) and angiopoietin 1 were the growth factors selected. They respectively, initiated an angiogenic response and promoted late-stage maturation of newly formed vessels[78]. The results showed that the delivery of multiple growth factors can significantly improve vascular growth.

Much of the biological activity of HSPGs has been ascribed to the HS chain[28]. It was shown that mutations in HS biosynthesis results in significant developmental defects that are not observed when mutations are introduced into the core protein[28]. Since this discovery HS has been increasingly implicated in cell-cell adhesion, cell-matrix adhesion, cell migration and proliferation, blood coagulation, inflammation and tissue regeneration[28]. HS is a variably sulfated, linear polysaccharide composed of repeating disaccharide units of gluronic acid and glucosamine[79]. HS sulfation tends to be irregular, therefore each tissue has a unique, characteristic HS profile that also varies according to the stage of tissue development[28,29,79]. The variation in sulfation results in different growth factor binding to HS from different cell types. As a consequence different tissues have different HS-growth factor complexes[28,79,80]. There is evidence that HS is expressed in tissue and developmental stage-specific forms that are required for embryonic organ formation[28]. HS has been shown to avidly bind to a variety of growth factors that are involved in controlling cell phenotype, these are the: FGFs, VEGFs, hepatocyte growth factor (HGF) and members of the TGF-β superfamily including the BMPs[79]. FGF signaling can be carefully and deliberately regulated by the application of appropriate HS chains. For example, Chipperfield et al., has shown that HS derived from adult neural tissue can be used to induce a neuronal phenotype in primary osteoblasts[28,81].

HS binds many species, not only growth factors but also chemokines, morphogens, most of the large glycoproteins in the ECM and a suite of proteases and synthetic enzymes[80]. A role of HS may be to allow extremely precise and specific interactions to occur at the correct time and place during the maturation and regeneration of tissue[80]. The fact that HS and HS-like molecules have been demonstrated to be important regulators of bone repair and regeneration

after injury through their growth factor modulation supports this view[29]. In addition HS in basement membranes assists the attachment of endothelial and epithelial cells and regulates vascular permeability[76]. *In vivo* administration of a synthetic polymer that mimics HS was shown to accelerate the regeneration and re-innervation of skeletal muscle[82]. All of these factors highlight the advantages of incorporating HS into biomaterials to increase their bioactivity and enhance their potential to assist in tissue regeneration.

1.4 Tissue Regeneration Scaffolds

Tissue regeneration scaffolds are biomaterials that are specifically designed to assist in the healing, growth and repair of damaged, lost or diseased tissues. Despite many early successes, there are few engineered tissue products available for clinical use, and significant challenges remain for long-term repair of biomechanically functional tissues[2]. The reasons for graft failure in animal studies and preclinical trials are not fully understood, but include a combination of biological and mechanical factors that can lead to the breakdown of repair tissues under physiologic loading conditions[2]. The challenge is not as simple as matching a single mechanical parameter, rather, most tissues possess complex viscoelastic, nonlinear and anisotropic mechanical and physicochemical properties that may vary between patients (eg. age, site)[2].

One area that has a range of commercially available products is the promotion of wound healing. These products consist of wound dressings or topical treatments that are often designed for the healing of ulcers. Xelma is an extracellular matrix protein treatment that has been shown to increase the healing of ulcers by approximately 22% when used weekly with appropriate bandaging[83]. Dermagraft is a human dermal fibroblast derived acellular matrix designed for the treatment of diabetic foot ulcers[84]. Both products require multiple applications over 2-3 months for complete healing of full thickness wounds. These products are limited in their application to skin wounds were no exposure of tendons, muscles, ligaments or bone occurs.

The other commercial products that are available are scaffolds designed to provide enhanced cell growth for experimental research. These include Extracel which is a 3D hydrogel matrix made of semi-synthetic components. Thiol modified hyaluronan (created by bacterial-fermentation), thiol modified gelatin and thiol reactive polyethylene glycol diacrylate, when mixed can form a hydrogel, sponge or film**.** This product is limited to experimental research applications and does not extend to *in vivo* tissue regeneration.

Another commercial product that is widely used for cell culture is Matrigel, a reconstituted basement membrane extract from Engelbreth-Holm-Swarm (EHS) mouse sarcoma. The main components are laminin, collagen IV, enactin and a variety of growth factors. Matrigel can be used as a 2D coating or a 3D matrix. Matrigel has demonstrated better performance as a substrate to support the adhesion and proliferation of many cell types. It has also been shown to promote better differentiation of muscle derived cells[85] and to maintain the differentiated state of zona glomerulosa cells[86].

The PuraMatrix Peptide hydrogel is composed of molecules with a repeating RADA peptide sequence (arginine-alanine-aspartic acid-alanine). It self-assembles into a 3D nanofiber scaffold and has been tested as a transplantation scaffold for Schwann cells in spinal cord regeneration applications[87]. The QGel matrix is a PEG based hydrogel that can be modified to contain different peptides. It has been used to develop a lab-on-a-chip system to isolate and culture cancer cells for potential applications as an early cancer diagnostic device[88].

There is an apparent lack of commercial products that are able to be used for wounds other than skin wounds. This is possibly due to the need for a 3D biomaterial that enables 3D healing. Such a material needs to be sufficiently porous to allow for cell migration into the material and diffusion of waste out of the material. The material is also required to produce structural support and provide the same elasticity and strength as the native tissue. The interaction between biomaterials and cells is not completely understood as the interactions are complex. This results in the current trial and error methodology that is used for most biomaterials research.

1.5 Introduction to Hydrogels

Hydrogels are polymers that are able to imbibe large amounts of water within their structure without dissolving. Hydrogels have a unique set of properties that resemble those of native tissue ECM: high water content, tissue-like elasticity, low interfacial tension as well as providing facile transport of nutrients and waste[89,90]. As hydrophilicity is one of the most important factors for biomaterials in medical use[91], their hydrophilicity along with other properties makes hydrogels ideal candidates for ECM mimetics[90]. Easy alteration of the physical form of hydrogels allows for precise control over molecular weight, degradation time and hydrophobicity, as well as other attributes, allowing hydrogels to be tailored for specific biomaterial applications[35,89]. Their unique set of properties makes them a highly attractive class of biomaterial and recently they have been used as *in vitro* cell culture platforms[90]. Biomaterials that are intended for clinical or commercial use need to be reproduced identically. Synthetic hydrogels are ideal candidates as their chemical and physical properties can be reproduced easily and they are inherently more homogeneous.

1.5.1 PHEMA

Poly(2-hydroxyethyl methacrylate) (PHEMA) is a hydrophillic polymer that has been extensively studied for biomedical applications[92]. PHEMA gels are highly biocompatible and are well tolerated as implanted prostheses due to their similarities in physical properties with that of native tissue[92,93]. The physical properties of PHEMA that resemble native tissue are its high water content, its elasticity and its low interfacial tension[91]. PHEMA gels are also optically clear and resilient and have been used in soft contact lenses[93].

PHEMA gels are easy to prepare, they can be fashioned into any shape and a wide variety of molecules that are difficult to immobilise can be stably incorporated into the gel[94]. PHEMA is chemically inert and stable in varying conditions of pH and temperature[95]. PHEMA is highly resistant to enzymatic digestion, as well as acid and alkaline hydrolysis, with the exception that alkaline hydrol-

ysis can occur at high pH and high temperature[89,91]. When alone PHEMA's inertness is reflected in the unwillingness of cells to attach to its surface[91,96], but PHEMA is easily copolymerised with other monomers to alter the chemical or mechanical properties of this hydrogel[89].

PHEMA has been used for a variety of applications that include: chemical gas sensors[95], *in vitro* toxin removal from plasma[97,98], red blood cell isolation[99], orthopaedic and dental implants[100], drug delivery[101–105], anti-coagulation treatment[106,107], immobilisation of enzymes and other biomolecules for improved bioactivity and bioreactor applications[92,108–110], contact lenses and artificial corneas[111,112], orbital implants[113], plastic surgery[114,115], advanced burn/wound dressings/artificial skin[116–119], nerve conduits[120–125], chromatography of proteins, as a substrate for a tumor model[126] and as an *in vitro* cell culture substrate[127]. PHEMA hydrogels are among the synthetic polymers that have been approved by federal agencies for biomedical and pharmaceutical applications[109]. This is an important factor that can assist in the approval of a PHEMA biomaterial, which is an essential step towards commercial use.

Most applications of PHEMA use the gel form of the hydrogel. Pore size in the gel form is limited to the nano- and low micrometer range[127]. When the water content of the hydrogel is kept low, generally less than 50 wt%, the gel formed is optically transparent, homogeneous and nanoporous. Alternatively when the initial water content is raised above 50 wt% a phase separation occurs during polymerisation. This is due to the limited solubility of PHEMA in water and the resultant polymer is an heterogeneous opaque white sponge with micro-sized pores[89]. Another form of PHEMA that has been widely studied is the brush morphology on the surface of a substrate. A review of PHEMA brushes on different surfaces revealed the ability of PHEMA brushes to be used to alter the cell adhesion properties of the surface. In general dense PHEMA brushes limit cell and protein adhesion while less dense brushes allow for the adhesion of both. This trend can be used to create tune-able surfaces by varying the density of the PHEMA brush[128].

1.5.1.1 PHEMA for Tissue Regeneration

The brush form of PHEMA has been demonstrated to be able to adsorb various ECM proteins. Brush PHEMA on a glass surface has been shown to improve the adsorption of fibronectin to the surface resulting in good adhesion of 3T3 fibroblasts[37]. PHEMA has also been modified with GRGD peptide to improve cell adhesion of 3T3 fibroblasts. The addition of GRGD increased the spreading behaviour of the cells by 3 orders of magnitude[72]. PHEMA has also been used to improve cell adhesion to the surface of other materials. Poly(dimethyl siloxane) (PDMS) films were modified with PHEMA via an interpenetrating polymer network (IPN) method and collagen I was covalently linked to the film. The films were tested with L929 fibroblasts. The cells maintained a spherical morphology with little spreading on plain PDMS films. Better cell adhesion and spreading was observed on the P(DMS-HEMA) IPN, but the most cells were observed on the collagen coated P(DMS-HEMA) surface[129].

PHEMA brushes on glass and silicone substrates have been modified with RGD and PHSRN peptides. The surface with only the PHSRN peptide did not perform well with fibroblasts. Surfaces with RGD alone or RGD mixed with PHSRN worked better, a ratio of 50:50 and 20:80 (RGD:PHSRN) worked best. These results demonstrate the specificity of peptides and the potential of synergistic effects[130].

Self-assembling rosette nanotubes have been formed within PHEMA. The rosette nanotubes were based on DNA base pairs, cytosine and guanine, modified with an aminobutyl group to point outwards while the DNA base pairs form the inner part of the nanotube structure. These macromolecules were incorporated into the monomer mixture and were observed to form the nanotubes during polymer synthesis. Human keratinocytes and skin fibroblasts showed high cell adhesion and better proliferation compared to the plain PHEMA[131].

Brush PHEMA on a glass slide has been modified with a peptide sequence using click-chemistry. The YIGSR peptide was added to the polymer with a controlled concentration gradient on the surface. Human vein endotheliocytes (EC) and human vein smooth muscle cells (SMC) were separately placed on

the brush gradient surface. ECs were observed to orientate themselves with the gradient and migrate preferentially in the direction of the concentration gradient. SMCs were less affected by the gradient showing less orientation and directed migration. The gradient was observed to assist in the preferential directional migration of the ECs over the SMCs, the ECs also had an increased migration rate over the SMCs[132]. This targeted cell specificity has potential in tissue regeneration applications as it could be used to ensure the migration of cell types that are most beneficial for the current step in the regeneration process and help to avoid the migration of cells that could hinder the process.

Another test was performed on the brush PHEMA using a confluent layer of cells on the peptide gradient. In this test the cells needed to over-come cell-cell interactions to migrate along the surface. Significant migration of the EC cells was observed in the direction of the gradient. Therefore the PHEMA brushes with peptide gradients were shown to be able to significantly affect cell migration and preferentially assist in the migration of one cell type over another[132].

A PHEMA brush has been used to direct cell migration. The molecular weight of the PHEMA was varied to adjust the brush height and create a gradient on the surface from 3 nm to 30 nm thick. Various brush gradients were created to adjust the slope between 0.8-3.2 nm/mm. Human vascular smooth muscle cells reacted to the gradients with their adhesion and spreading observed to decrease as the brush thickness increased. The cells were also observed to be preferentially orientated and migrate down the gradient. The steeper surfaces were observed to have higher cell migration down the slope with a maximum value of 87% for the 1.6 nm/mm slope compared with 58% on the 0.8 nm/mm slope. The orientation of the cells was affected by the PHEMA brush thickness and to a smaller extent by the gradient on the surface with the 15 nm thick brush showing the best cell orientation[133].

1.5.1.2 PHEMA for Stem Cell based Regeneration

PHEMA has been investigated as a culture material for embryonic stem cells. Initial work showed that embryonic stem cells grown for 48 hours on a PHEMA gel, that had been treated with gelatin, were comparable to those grown on gelatin coated tissue culture plastic[134]. This demonstrated the non-toxicity of PHEMA towards embryonic stem cells. The researchers extended this work by incorporating porogens and different crosslinkers into PHEMA. Embryonic stem cells were observed to proliferate best on PHEMA containing 40 wt% ethylene glycol dimethacrylate and an increase in pore size increased cell proliferation. Interestingly in this work no significant increase in cell proliferation was observed after the PHEMA was treated with gelatin[135]. PHEMA has been copolymerised with 2-dimethylaminoethyl methacrylate (DMAEMA) to increase the positive charge on the scaffold. The scaffold supported the proliferation of embryonic stem cells, but not the proliferation of fibroblasts[136]. This observation highlights the specificity of biomaterials in their support of only certain cell types.

PHEMA has been copolymerised with cholesterol to introduced hydrophobic areas into the scaffold, to increase protein adsorption to the material. The PHEMA-cholesterol polymer demonstrated mesenchymal stem cell (MSC) attachment, after the covalent attachment of laminin, via carbodiimide chemistry, the cells were significantly more spread and more uniform in shape[137]. The incorporation of cholesterol increased the protein adsorption to the surface which assisted in cell attachment. Interestingly the immobilisation of laminin improved cell adhesion to the non-porous polymer but no improvement was seen on the porous version. The lack of improvement after laminin attachment to the porous scaffold was thought to be due to the method of immobilisation, the laminin was immobilised via lysines which could have changed the structure of the protein[137]. To overcome this problem a peptide from laminin, Ac-CGGASIKVAVS-OH, was incorporated[55]. The peptide improved the number of adhered MSCs as well as increasing cell spreading. It also supported the attachment, proliferation and differentiation of neural stem cells. When

macro sized pores were introduced into the scaffold, the pores were preferentially colonised by the neural cells while the MSCs attached more to the flat surfaces (around the pores) of the scaffold[55]. These results highlight the sensitivity of cells to the topography of the scaffold, and indicates the physical characteristics of biomaterials can be optimised for certain cell types and therefore specific applications.

The effect of varying the surface chemistry on the performance of PHEMA has been studied. PHEMA was copolymerised with glycidyl methacrylate (GMA) as a film that could be easily modified with various functional groups by using the reactivity of the epoxy group. Glutaraldehyde was used to attach various single amino acids and amino acid analogues to the film. The surfaces modified with amino acids were observed to have the highest MSC number along with the hydrolysed P(HEMA:GMA)-OH surface. Specifically the films with 4-aminobenzoic acid and L-phenylalanine performed the best with cell numbers ~50% higher than the control[138]. This research demonstrates the importance of the surface chemistry of biomaterials as small changes in the chemistry can result in large changes in bioactivity and cell type specificity.

Gel PHEMA has also been soaked in collagen I in buffer solutions of different pH values to obtain optimum adsorption conditions. The PHEMA was then further soaked in laminin and fibronectin. PHEMA that had been soaked in collagen demonstrated better MSC and astrocyte attachment and proliferation than the plain PHEMA. Additional adsorption of laminin or fibronectin further improved cell attachment and proliferation of both cell types[139].

1.5.1.3 PHEMA for Nerve Regeneration

In the 1980's Carbonetto et al., prepared PHEMA gels for studying nerve fibre growth[93,94]. They permitted neuron attachment but did not support nerve fiber growth. The incorporation of various biomolecules into the PHEMA gel gave rise to degrees of improvement in nerve fiber growth. These biomolecules include: fibronectin, β nerve growth factor (βNGF) and several types of collagen. The biomolecules were added to the monomer mixture and upon polymeri-

sation the small pore size of the gel (~0.4 nm) caused them to remain permanently trapped within the gels. Best nerve fiber growth was observed with PHEMA gels that contained fibronectin, collagen or βNGF, while the incorporation of heparin, poly-L-lysine, cytochrome and wheat germ agglutinin showed no improvement on PHEMA alone[93].

A few examples of how PHEMA has been applied for nerve regeneration include; a PHEMA film with multi-walled carbon nanotubes (CNTs) to create a conductive film[140], a porous PHEMA sponge seeded with Schwann cells to improve integration with host tissue and enhance axon growth[141], a porous PHEMA cryogel with poly(lactic acid) to improve neuron cell adhesion and axon growth[142], and a copolymer of PHEMA with N-(2-hydroxypropyl methacrylate) (HPMA) and RGD to improve in vivo performance[124]. The P(HE-MA-co-HPMA) scaffold was successfully produced as a commercial product, NeuroGelTM, which is currently undergoing clinical trials by Aqua Gel Technologies[125].

A unique PHEMA scaffold has been created by spinning the monomer solution in a cylindrical mold during polymerisation. The resultant tubes were more porous on the inside graduating into a non-porous gel on the outside[143]. These tubes were later created as a copolymer of PHEMA with methyl methacrylate, in vivo testing showed the tubes to be biocompatible for 8 weeks[120] and able to facilitate the re-connection of the spinal cord in a rat model[122]. The tubes were additionally reinforced with a poly(caprolactine) (PCL) coil, these were able to out-perform autographs in a rat model over 16 weeks[121]. These results were astounding as they represent the ultimate goal for biomaterials which is to be a viable replacement for autographs. To achieve this they need to be able to perform equally to an autograph to produce new functional tissue that is identical to the native tissue.

1.5.1.4 Other Applications for PHEMA

The incorporation of biological molecules within the PHEMA network is still being explored. One example is the use of a methacrylated RGD sequence to

copolymerise the peptide into the PHEMA sponge. This improved the bioactivity of the PHEMA, as human corneal epithelial cells were shown to spread better on this surface than on a plain PHEMA sponge[144]. Sponge PHEMA has also been applied for drug delivery applications, it has been attached to the end of a catheter and shown to improve the delivery of insulin into surrounding tissue[102]. A PHEMA hybrid has been used to enhance hypoxic differentiation of MSCs into chondrocytes[145].

PHEMA has been grafted onto polyethylene to assist in the attachment of MC3T3-E1 osteoblasts[146]. A PHEMA cryogel was able to support the proliferation of MSCs, the cells expressed alkaline phosphatase (ALP) which is associated with the post-proliferative stage of ECM maturation[147]. A foaming agent has been used to create super porous PHEMA, the scaffold was modified with gelatin and shown to support the proliferation of MC3T3-E1 cells. Interestingly these scaffolds performed better than the hydroxyapatite (HA) material[148], this was a significant result as HA is a major component of bone and therefore one of the most commonly used materials for bone regeneration applications. These results suggest potential for PHEMA cryogels in bone regeneration applications**.**

1.6 Aim

The aim of this research is to investigate the synthetic methods to introduce biomolecules onto the 3D porous PHEMA hydrogels, to further evaluate the bioactivity of the modified PHEMA hydrogels by qualitatively and quantitatively examining the adhesion, proliferation and differentiation of cells on the hydrogels. Additionally to explore how different biomolecules can be used to optimise a scaffold for different tissue regeneration applications.

Various synthetic approaches will be studied to modify the porous PHEMA with limited interference of the 3D structure. The biomolecules, HS and RGD, have been selected for their ability to improve cell adhesion and cell development.

The immobilisation of both HS and RGD on the same hydrogel are explored for any synergistic effects. The potential of the modified hydrogels for use in deep tissue wound healing applications are investigated.

Chapter 2

Synthesis and Characterisation of Bioactive PHEMA

2.1 Introduction

The modification of PHEMA can be achieved in a variety of ways, it has been copolymerised[149], grafted[146], laser treated[150], soaked in biomolecule solutions[135], had macromolecules entrapped within it[140] and had biomolecules attached both physically[108] and chemically[144]. Most reported work on PHEMA has used the gel form. The sponge form of PHEMA was selected for this work as it is a 3D porous material with interconnected pores and the pore size is easily controlled by varying the water content during polymerisation[151]. This work built on knowledge gained from decades of research on PHEMA[100,152], yet it had the innovative twist of functionalising the sponge hydrogel with biomolecules to create a scaffold more appropriate for tissue engineering applications.

This chapter is focused on the synthesis and characterisation of PHEMA hydrogels with various biomolecules. The biomolecules chosen for this research were heparan sulfate (HS) and the RGD peptide. The RGD peptide was selected because it facilitates the adhesion of many cell types to substrates that carry this motif. The RGD peptide is a central feature of one of the cell binding domains of fibronectin[7], and its integrin ligands are present on a variety of different cell types. Importantly it can be produced synthetically which im-

proves reproducibility, reduces production costs and is amenable to scale-up if the scaffold is to be later manufactured on a commercial scale. While RGD has been attached to many surfaces, only one report exists of its incorporation into sponge PHEMA[144]. It was incorporated by methacrylating the peptide followed by copolymerisation with HEMA, cell quantification was not performed but microscopy showed differences in cell morphology with the presence of RGD. This work aims to produce an RGD immobilised PHEMA, with a different synthetic approach to extend the investigation by quantifying any cell proliferation improvement upon RGD immobilisation on PHEMA.

The other biomolecule, HS, was chosen because heparan sulfate proteoglycans (HSPGs) play pivotal roles in biological processes such as morphogenesis, angiogenesis and wound healing and much of this bioactivity can be attributed to their HS GAG chains[23,24]. Importantly HS chains interact with growth factors of the FGF family and their receptors (FGFR) and so coordinate cell-fate decisions such as cell growth and cell differentiation, which are key to tissue regeneration[16,28]. Interestingly HS immobilisation on PHEMA has not been previously reported. Although HS has been crosslinked through a collagen matrix[153], and incorporated in electrospun polycaprolactone[29] and poly(lactic-co-glycolic acid)[154]. The electrospun scaffolds were tested with stem cells, whereas the collagen scaffold was implanted into rats and it stimulated considerable tissue regeneration *in vivo*. It was therefore anticipated that the incorporation of HS into PHEMA would improve the bioactivity of PHEMA. The co-immobilisation of HS and RGD on a substrate has not been reported, however heparin and RGD have been immobilised on a PEG scaffold[155]. Therefore both HS and RGD were investigated for their potential to improve PHEMA bioactivity and create a hydrogel that could have tissue regeneration applications.

The hydrogels produced were then characterised chemically and physically using a series of techniques that included: chemical characterisation using Attenuated Total Reflectance-Fourier Transform Infra-Red spectrometry (ATR-FTIR), titration, UV-Vis absorbance and elemental analysis, physical characterisation using Thermogravimetric Analysis (TGA), rheometer, Brunauer, Em-

mett and Teller (BET) analysis, Scanning Electron Microscopy (SEM) and equilibrium water content (EWC%) determination. The rheology equipment also allowed for all measurements to be performed while the hydrogels were swollen and at 37ºC. This was ideal as the results were reflective of how the hydrogels would react *in vivo*. These techniques were used to investigate the properties of the hydrogels to determine the potential of the hydrogels for tissue engineering applications.

2.2 Materials

2-hydroxyethyl methacrylate (HEMA, Bimax), ethylene glycol dimethacrylate (EDMA, Bimax), ammonium persulfate (APS, BDH chemicals), heparan sulfate (HS, derived from procine intestinal mucosa with average Mw of 15,000 g/mol, Celsus Laboratories, Ohio, USA) and RGD tri-peptide (95%, GL Biochem, Shanghai, China) were used as received. Glycidyl methacrylate (GMA, 97%), N,N,N',N'-tetraethylmethylenediamine (TEMED, 99%), 1,9-dimethylmethylene blue (80%), glycine, hexamethylenediamine (98%), N-(3-dimethylaminopropyl)-N'-ethylcarb-odiimide hydrochloride (EDC, >98.0%), N-hydroxysuccinimide (NHS, 98%), sodium chloride (NaCl), hydrochloric acid (HCl), sodium hydroxide (NaOH), ethanol (70 vol%) and dimethylsulfoxide (DMSO) were all purchased from Sigma Aldrich. The purchased chemicals were used as supplied unless otherwise stated below.

Silicone tubing with inner diameter 20 mm and outer diameter 26 mm (GeckoOptical), 6x200x200 mm clear float glass plates (Perth City Glass). Basic ethanol was made by dissolving 20 g NaOH in 500 mL ethanol. Farndale reagent[156] consisted of 18 mg/L 1,9-dimethylmethylene blue, 3 g/L glycine and 2.4 g/L NaCl in deionised water with the pH adjusted to 3.0 with 2 M HCl.

2.3 Chemical Synthesis

2.3.1 Synthesis of PHEMA and P(HEMA:GMA)

Poly(2-hydroxyethyl methacrylate), (PHEMA) and poly(2-hydroxyehtyl methacrylate-co-glycidyl methacrylate), (P(HEMA:GMA)) hydrogels were synthesised as a sheet using the mould schematically illustrated in Figure 2.1. The chemical composition of the hydrogels is summarised in Table 2.1. The hydrogel codes for PHEMA and P(HEMA:GMA) are P and PG respectively.

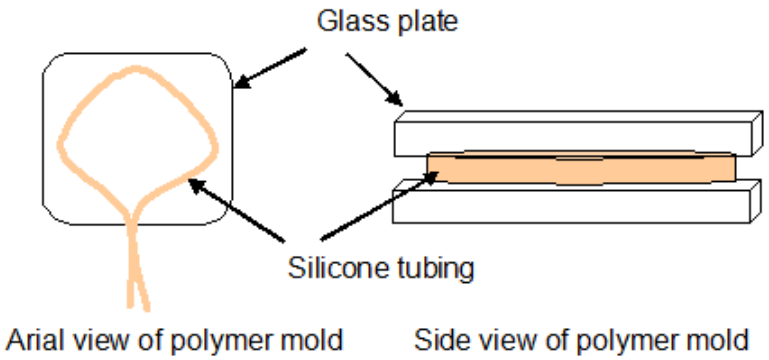

Figure 2.1: Diagram of the hydrogel mould.

The glass plates were soaked in basic ethanol for 16 h at room temperature before use. The polymer mould (Figure 2.1) was made by placing the silicon tubing (inner diameter 20 mm, outer diameter 26 mm) between 2 glass sheets. The appropriate amounts of reagents, summarised inTable 2.1, were mixed in the following order: HEMA dissolved in deionised water followed by addition of GMA, EDMA and APS. TEMED was added last and the solution was transferred into the pre-assembled mould within 5 min of the addition of TEMED. The mould was placed into an air-tight container with an open vessel of water to provide a humid environment. The container was left at room temperature for 3 h, followed by 50ºC for 12 h. The polymer was removed from the mould and transferred into 500 mL of deionised water. The polymer was rinsed and the water replaced daily for 2 weeks, to produce a hydrogel sheet that was 2-3 mm thick once swollen. The hydrogel sheet was cut into 9 mm diameter

discs using a metal punch and stored in deionised water at room temperature. PHEMA was synthesised with an identical procedure by omission of GMA.

Table 2.1: Chemical composition of hydrogel scaffolds.

Hydrogel	HEMA (g)	GMA (g)	Water (g)	EDMA (μL)	APS* (μL)	TEMED (μL)
PHEMA	8	0	32	34	136	68
P(HEMA:GMA)	7.4	0.6	32	34	136	68

*APS was used as a 10 wt% solution

2.3.2 Synthesis of P(HEMA:GMA)-NH_2

A modification of the procedure of Bayramoglu et al.[138], was used to aminate P(HEMA:GMA) discs to produce P(HEMA:GMA)-NH_2. Briefly; 100 discs (approximately 10 g) were added to a solution of hexamethylenediamine (2.3 g) in 40 mL deionised water. The solution was stirred at 170 rpm and 65ºC for 4 h then left at room temperature for 16 h with continued stirring at 170 rpm. The discs were rinsed 10 times with 100 mL deionised water and stored in deionised water at room temperature. Aminated discs were denoted by, P(HEMA:GMA)-NH_2 and the hydrogel code, PGN.

Back titration was used to determine the success of the amination and to quantify the free amine content. In brief, 6 discs of PG and PGN, were separately freeze dried and ground with a mortar and pestle, the final mass was 140 mg. The powdered hydrogels were suspended in 10 mL of 0.01 M HCl and agitated at 170 rpm for 4 h at room temperature. The solution was decanted from the hydrogels and the powder was rinsed 3 times with 1 mL deionised water. The rinses were added to the decanted solution and the solution was made up to 25 mL in a volumetric flask. The solution was back-titrated with 0.01 M NaOH using 0.5% phenolphthalein in ethanol as an indicator. The average titre from 3 titrations was used to determine the difference in titre between PG and PGN. The titre difference was used to calculate the n(NaOH) which had a ratio of 1:1

to the n(HCl) that reacted with the free amines on the hydrogel as described in equation 1 with units, μmol NH_2/g hydrogel.

$$\text{Equation 1: } \textit{Free amine content} = \frac{\dfrac{\textit{Volume (total solution)}}{\textit{Volume (solution titrated)}} \times \textit{n(NaOH from titre difference)}}{\textit{mass (hydrogel)}}$$

2.3.3 Synthesis of P(HEMA:GMA)-HS

A solution of 260 mg EDC, 80 mg NHS and 110mg HS in 30 mL deionised water was placed in an ice bath for 20 min. The mole ratio of EDC:NHS was 2:1, and EDC was used in a 5-fold excess with respect to the number of -COOH groups on HS (which was estimated to be 34/molecule). Approximately 5 g of PGN (50 discs) were added to the EDC solution and remained in the ice bath with shaking at 170 rpm for 3 h, then removed from the ice bath and agitated at room temperature for 16 h. The reaction solution was decanted from the discs and kept. The discs were rinsed 3 times with 10 mL deionised water for 10 min at 170 rpm. These rinses were combined with the decanted reaction solution and kept. The discs were further rinsed 10 times with 100 mL deionised water and stored in deionised water at room temperature until use. Discs that were functionalised with HS were denoted by, P(HEMA:GMA)-HS and the hydrogel code PGH.

To quantify the HS content, 2 mL Farndale reagent (details of Farndale reagent in section2.2) was mixed with 2 mL decanted reaction solution and the absorbance at 525 nm immediately measured in triplicate using a PerkinElmer UV-Vis Lambda25 spectrometer[156,157]. HS standards were made in deionised water at concentrations of 0.08, 0.16, 0.20, 0.25, 0.32, 0.39, 0.50, 0.63, 0.76, 1.01, 1.26, 1.57, 2.14, 2.57 and 3.14 mg/L. A standard curve was achieved by similarly measuring the HS standards by mixing equivalent volumes with Farndale reagent and reading absorbance at 525 nm as described.

2.3.4 Synthesis of P(HEMA:GMA)-RGD

PGN was also used to immobilise the RGD peptide. Briefly, 85 mg EDC, 25 mg NHS, 65 mg RGD were dissolved in 25 mL deionised water and placed in an ice bath. The molar ratio of EDC:NHS was 2:1, and EDC was used in a 1.2-fold excess with respect to the number of -COOH groups on RGD. Approximately 5 g P(HEMA:GMA)-NH_2 (50 discs) were added to the solution and agitated at 170 rpm at 4ºC for 3 h. The reaction and purification was carried out in the same fashion as described in 2.3.3. The rinses were added to the reaction solution and kept for further analysis. The discs were stored in deionised water at room temperature until use. Discs that were functionalised with RGD were denoted by, P(HEMA:GMA)-RGD and the hydrogel code PGR.

To quantify the immobilisation of RGD, the reaction solution was titrated against 0.01 M NaOH using 2-3 drops of 0.5% phenolphthalein indicator in ethanol. A calibration curve was created by titrating known amounts of RGD (0, 13, 26, 39, 52 and 65 mg) in a solution of 0.5 mM EDC and 0.2 mM NHS in deionised water.

2.3.5 Synthesis of P(HEMA:GMA)-HS&RGD

Following quantification of RGD immobilisation, P(HEMA:GMA)-RGD was further modified with HS as described in 2.3.3. A solution of 260 mg EDC, 80 mg NHS and 110mg HS in 30 mL deionised water was placed in an ice bath for 20 min. The molar ratio of EDC:NHS was 2:1, and EDC was used in a 5-fold excess with respect to the number of -COOH groups on HS (which was estimated to be 34). Approximately 5 g of P(HEMA:GMA)-RGD (50 discs) were added to the EDC solution and remained in the ice bath with shaking at 170 rpm for 3 h, then removed from the ice bath and agitated at room temperature for 16 h. The reaction solution was decanted from the discs and kept. The discs were rinsed 3 times with deionised water for 10 min at 170 rpm. These rinses were combined with the decanted reaction solution and kept. The discs were stored in deionised water at room temperature until use. Discs that were

functionalised with HS and RGD were denoted by, P(HEMA:GMA)-HS&RGD and the hydrogel code PGHR. Numbers have been used in the hydrogel codes to distinguish between hydrogel batches.

Table 2.2: Names and codes used for the synthesised hydrogels.

Hydrogel name	Hydrogel code
PHEMA	P
P(HEMA:GMA)	PG
P(HEMA:GMA)-NH_2	PGN
P(HEMA:GMA)-HS	PGH
P(HEMA:GMA)-RGD	PGR
P(HEMA:GMA)-HS&RGD	PGHR

2.4 Characterisation

2.4.1 Sample Preparation

For ATR-FTIR, elemental spectroscopy, thermogravimetric analysis, surface area determination and SEM imaging, the samples were frozen at -80ºC for 16 h followed by freeze drying at -54ºC for 2 h (ScanVac CoolSafe, LaboGene, Denmark). The freeze dried samples were ground to a fine powder for analysis unless otherwise specified. For other measurements the samples were dehydrated on Teflon sheets at 80ºC for 24 h.

2.4.2 Equipment and Operation Conditions

A Perkin Elmer Attenuated Total Reflectance Fourier Transform Infrared (ATR-FTIR) spectroscope was used to analyse samples. A scan range of 3600 - 600 cm^{-1} and resolution of 1.0 cm^{-1} was averaged over 250 scans.

A Perkin Elmer Series II CHNS/O Analyser 2400 was used in CHNS mode. The column was flushed by running 3 blanks and the calibration checked using cystine (29.99% C, 5.03% H, 11.67% N, 26.69% S) and acetanilide (71.09% C,

6.71% H, 10.36% N) as the analytical standards. 1-2 mg of the hydrogel was weighed and a minimum of 5 replicates run for each sample. For low sulfur detection the analyser was calibrated with acetanilide as a blank.

For TGA, about 11 mg of each hydrogel was weighed into 150 µL alumina crucibles. The samples were analysed with a flow rate of 20 mL/min of argon and 25 mL/min of oxygen. The samples were held at 25ºC for 10 min then heated at 5ºC/min up to 900ºC.

For SEM, a high resolution field emission electron gun Zeiss NEON 40EsB FIBSEM was used at an accelerating voltage of 3.00 keV, an aperture size of 30 µm and working distance between 2-3 mm. All samples were mounted on SEM stubs with carbon tape and coated with 3 nm of platinum prior to imaging.

A Micromeritics TriStar II BET was used to determine the surface area of the hydrogel discs via Brunauer-Emmett-Teller (BET) analysis. Three 9 mm diameter discs of each sample were analysed. Multipoint BET analysis was performed with the relative pressure range of 0.20 - 0.55, the de-gas time before BET analysis was set to 2 h. Outliers were removed to ensure a correlation coefficient of 0.93 or above. TriStar 3020 analysis program was used to calculate the surface area. All samples were de-gassed for 16 h prior to analysis.

2.4.3 Equilibrium Water Content

The equilibrium water content (EWC%) was determined by measuring the difference in hydrogel weight when hydrated and dry. The hydrogel was first weighed hydrated then placed in an 80ºC oven for 24 hours. The hydrogel was then weighed again and the EWC% calculated using equation 2 below. The average of 5 samples was calculated.

$$\text{Equation 2: } EWC\% = \frac{\text{mass(hydrated)} - \text{mass(dry)}}{\text{mass(hydrated)}} \times 100$$

2.4.4 Viscoelastic Properties

A Haake MARS II modular advanced rheometer system was used to perform shear testing of the hydrogel discs. 5mm thick discs were kept hydrated during analysis via oscillation stress sweep, oscillation frequency sweep and creep-recovery test measurements. A flat plate (PP35Ti) was used for all measurements, 240 grit sandpaper was attached to the top and base plate to reduce slipping of the hydrated scaffold discs. Measurements were taken at room temperature and at 37ºC.

The gap height for all measurements was determined by keeping the normal force between 0.2-0.4 N. The oscillation strain sweep was performed at a frequency of 1 Hz and the strain was swept from 0.05-3%. The oscillation frequency sweep was performed at a constant strain of 0.35% with a frequency range of 0.02-1 Hz. The creep/recovery test was performed with a stress of 10 Pa which was ramped up for 120 s. The stress was removed and the recovery monitored for a further 400 s. HAAKE RheoWin Data Manager software was used to extract the raw data. For repeated creep/recovery tests a stress of 10 Pa was applied over 30 s followed by a recovery of 240 s.

2.5 Results and Discussion

2.5.1 Synthesis of Hydrogels

The synthetic pathway used is summarised in the scheme in Figure 2.2. The first step involved copolymerising HEMA with glycidyl methacrylate (GMA), which has been widely used to react with primary amines to functionalise hydrogels[158]. The reasoning behind first synthesising the hydrogel and then modifying the GMA was to maximise the retention of control of the interconnected porous structure of sponge PHEMA. After the sponge was formed the glycidyl group of GMA was reacted with hexamethylenediamine. The incorporation of a free amine into the hydrogel enables a wide range of biologically

active molecules to be immobilised using the same, simple chemistry which does not require prior chemical modification of the biomolecule. In addition, because both HS and RGD could be immobilised via the same chemistry, synthesis of scaffolds containing either HS or RGD or both was possible.

The chemistry for the biomolecule immobilisation was a water soluble carbodiimide system. This involved the activation of carboxylic acid groups on the biomolecules with N-hydroxysuccinimide (NHS) with the simultaneous reaction of N-(3-dimethylaminopropyl)-N'-ethylcarbodiimide (EDC) to form a peptide bond with the free amine on the hydrogel. This chemistry is widely used and others have used this approach to covalently bind collagen to PHEMA[126] and to crosslink collagen and star-PEG with heparin[32,159]. The star-PEG-heparin scaffold was additionally post-modified with RGD using the EDC/NHS system[32].

2.5.2 Amination Determination

The success of the amination reaction was determined by measuring the amount of free amine present on the hydrogels by back titration. The results showed that 20-77 μmol of free amine was present per gram of hydrogel after the reaction of P(HEMA:GMA) with hexamethylenediamine. The assumption was made that all of the GMA added to the monomer mixture polymerised during synthesis of the hydrogels, the chemical conversion was in the range of 14-53%. Low conversion of GMA with free amines has been observed by others with 0.1% conversion realised when polyethylenimine was immobilised using identical chemistry[160]. Others have observed 36% conversion of GMA with hexamethylenediamine[138] but conversions as low as 0.01% have been reported[158]. The relatively low yields in the present study were likely due to the 3D nature of the hydrogels, where it was assumed that most of the conversion of the glycidyl groups happened on the surface of the discs. Additionally it was possible that some of the glycidyl groups were hydrolysed during polymerisation, this has been investigated during emulsion polymerisation of GMA

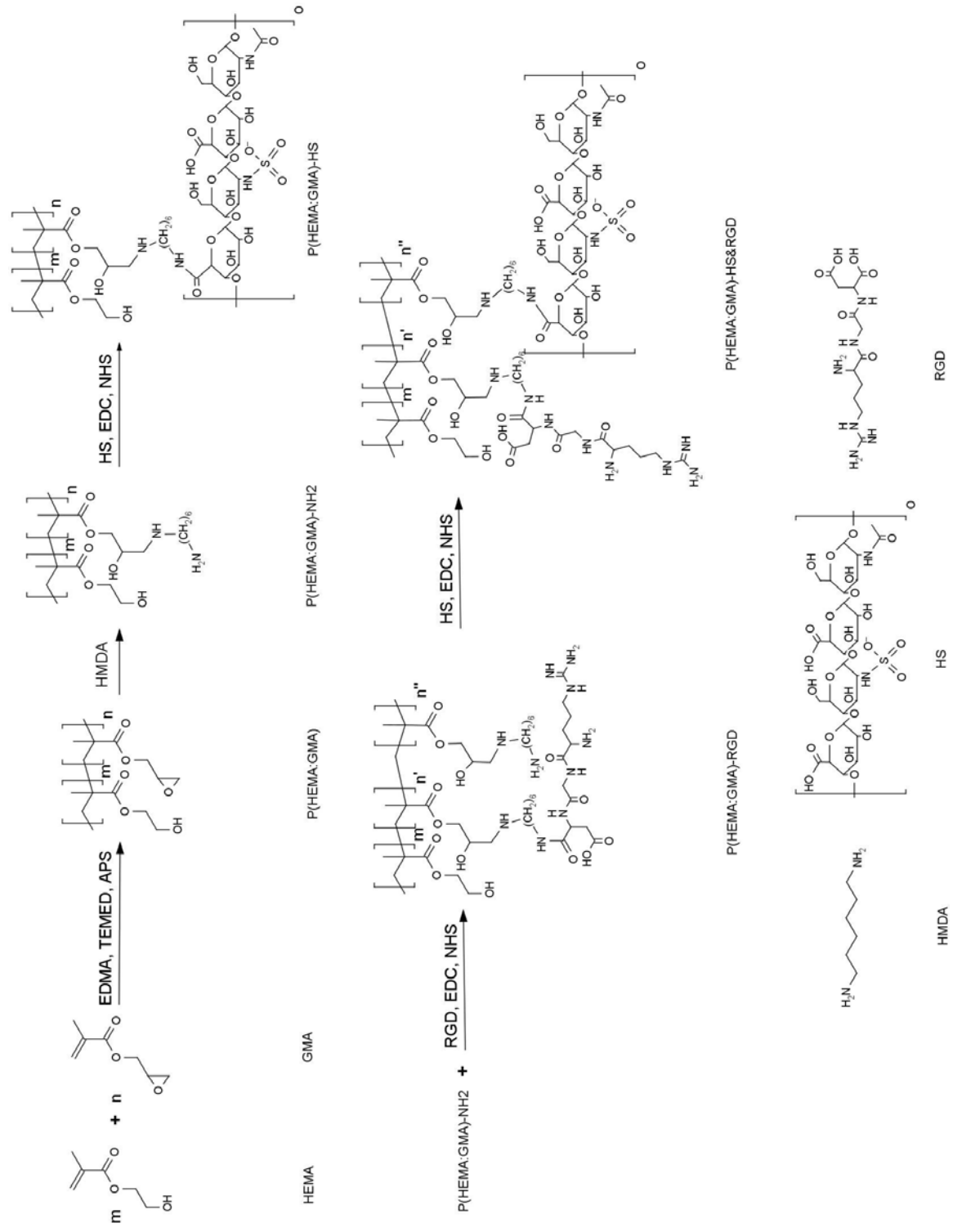

Figure 2.2: Scheme of hydrogel synthesis and modifications to immobilise biomolecules.

with up to 30% hydrolysis measured when polymerisation occurred at 60℃ [161]. The high standard deviation of the current results was likely due to the nature of the technique. The back titration relied on the protonation of all free amine groups on the hydrogel to consume the HCl, the reduction in HCl was then determined by titration with NaOH. The variability in the results could also have been due to the presence of unreacted glycidyl groups which may have been hydrolysed with HCl. The difference in titre from the titration of PGN and PG was used in an effort to reduce the effect of the unreacted GMA on the results.

Table 2.3: Quantified free amine present on the hydrogels.

Hydrogel code	GMA content (μmol/g hydrogel)	Free amine content[1] (μmol/g hydrogel)	GMA conversion[2] (%)
PGN8	150	66 ± 25	44
PGN12	142	40 ± 25	28
PGN21	147	48 ± 0*	33
PGN22	145	77 ± 14	53
PGN23	144	29 ± 15	20
PGN27	146	20 ± 13	14
PGN28	144	45 ± 12	31
PGN29	152	62 ± 14	41
PGN30	156	66 ± 18	42
PGN31	157	61 ± 16	39
PGN33	157	55 ± 38	35

[1]values determined by back titration, results were mean ± standard deviation, n = 3
[2]conversion was determined as the percentage of free amines that were reacted
*data for PGN21 had no standard deviation because the results were identical

2.5.3 HS Quantification

The amount of immobilised HS was quantified using a colourmetric dye and UV-Vis spectroscopy. The meta-chromatic dye, 1,9-dimethylmethylene blue in the Farndale reagent is electrostatically attracted to the highly negative charge

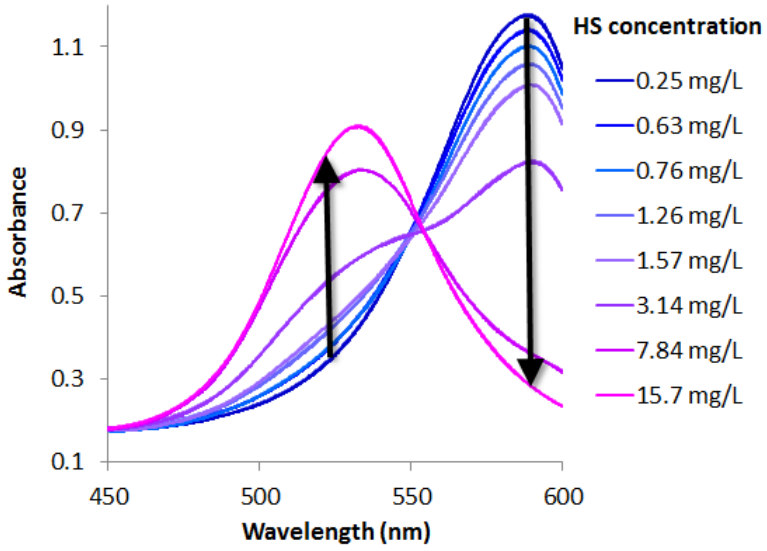

Figure 2.3: Change in absorbance of 1,9-dimethylmethylene blue (from Farndale reagent) with HS concentration. Not all concentrations of HS used in the calibration curve are shown for clarity of the figure.

of the sulfate groups on HS[156,157]. The coordination of 1,9-dimethylmethylene blue to HS results in a colour change from blue to purple (or pink) when the concentration of HS is sufficiently high. The colour change was monitored via UV-Vis spectroscopy as shown in Figure 2.3. As the concentration of HS increased the signal at 590 nm decreased and a new signal at 535 nm appeared. A calibration curve was created for HS by measuring the absorbance at 525 nm (Figure 2.4). The amount of HS left in solution after reaction with the scaffold was measured with UV-Vis and the value of unreacted HS calculated. This value was then subtracted from the initial amount of HS and the amount of HS immobilised on the scaffold was calculated.

Several batches of P(HEMA:GMA)-HS were synthesised. The summary table (Table 2.4) shows the reproducibility of the immobilisation technique. The amount of immobilised HS was consistently between 1.0 - 3.09 μg HS/g hydrogel. The 3 batches with lower amounts of immobilised HS were due to those batches having RGD immobilised on them first. Therefore the lower amount of HS was expected as there were fewer sites available for HS attachment. The

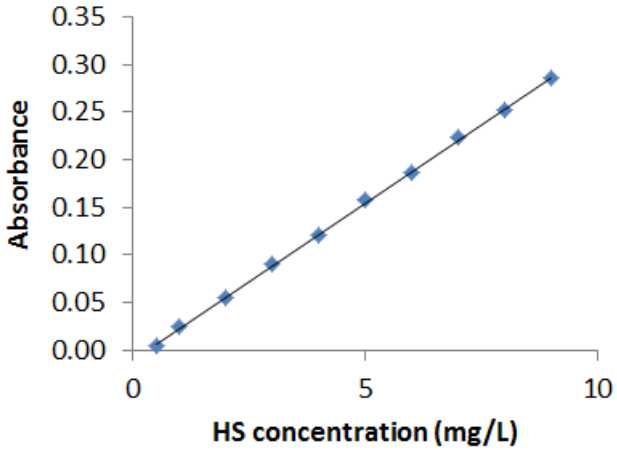

Figure 2.4: Calibration curve for 1,9-dimethylmethylene blue (from Farndale reagent). Linear relationship with increasing concentration of HS.

Table 2.4: Quantified amount of HS immobilised on hydrogels..

Hydrogel code	Free amine content (μmol/g hydrogel)	Amount of HS on hydrogel[1] (μmol/g hydrogel)
PGH8	66 ± 25	3.09 ± 0.05
PGH12	40 ± 25	1.0 ± 0.4
PGH23	29 ± 15	1.8 ± 0.3
PGH27	20 ± 13	2.4 ± 0.2
PGH33	55 ± 38	2.2 ± 0.1
PGHR21	48 ± 0	1.4 ± 0.3
PGHR30	66 ± 18	1.5 ± 0.2
PGHR31	61 ± 16	2.0 ± 0.5

[1]values determined by UV-Vis measurement with Farndale reagent as mean ± standard deviation, n = 3

amount of immobilised HS, 15-46 mg/g hydrogel, was similar to that achieved by others, for example, 60 ± 5 mg HS/g scaffold by crosslinking the HS through a collagen scaffold using EDC and NHS[23]. The HS used in the published report was of higher molecular weight, approximately 25 kDa, compared to the approximate 15 kDa form used in this work, which could have accounted for the higher mass immobilised on the collagen scaffold. Additionally it should be noted that the HS could have been tethered at multiple points on the hydrogel. The number of COOH groups per HS molecule was estimated at 34, therefore it was highly probable that the HS was anchored to the hydrogel by reaction with multiple amine groups.

2.5.4 RGD Quantification

Quantification of the amount of RGD peptide immobilised on the hydrogel discs was achieved via titration of the reaction solution against standardised NaOH. The deprotonation of RGD is shown in Figure 2.5 and the reaction resulted in a molar ratio of 2:1. As EDC and NHS interfered in the titration, a lower ratio of EDC:COOH was used for the RGD immobilisation, 1.2:1. To additionally reduce the interference of EDC and NHS, their amounts were held constant for all immobilisation reactions and calibration solutions. The calibration solutions were used to create a curve from which the amount of RGD left in solution after immobilisation could be determined.

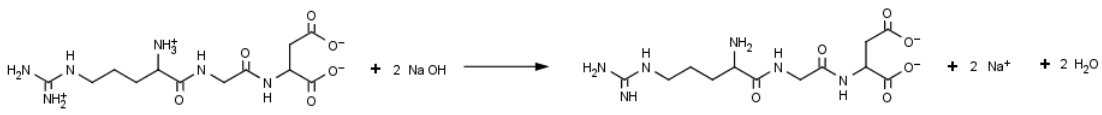

Figure 2.5: Chemical equation showing the reaction of RGD with NaOH.

The calculated amount of RGD immobilised on the hydrogel is summarised in Table 2.5. Some variability in the immobilisation amounts was measured, the immobilised RGD was between 22-87 μmol/g hydrogel. These results were for

the hydrogels with HS and RGD attached as well as RGD alone. The variability in the results was likely due to the reduced sensitivity of the titration as EDC and NHS were both present and also reacting with the NaOH. The conversion rates that were above 100% were likely due to a 2-fold effect, firstly the free amine content could have been under-estimated (as previously discussed in 2.5.2) and secondly the reduced sensitivity of the RGD titration may have contributed to an over-estimation of the immobilised RGD.

Table 2.5: Immobilised RGD on the hydrogels.

Hydrogel code	Free amine content (μmol/g hydrogel)	Amount of RGD[1] (μmol/g hydrogel)	Conversion[2] (%)
PGR22	77 ± 14	74	96
PGR28	45 ± 12	98	217
PGR29	62 ± 14	68	110
PGHR21	48 ± 0*	79	164
PGHR30	66 ± 18	85	129

Free amine content is mean ± standard deviation, n = 3
[1]values determined by titration with NaOH
[2]conversion determined as the percentage of free amine that reacted with RGD
*result for PGHR21 had no standard deviation because the results were identical

2.5.5 Elemental Analysis

Elemental analysis results are summarised in Table 2.6. The measured results fit the theoretical values well for carbon and hydrogen, being within 9%. From the difference between the measured and theoretical values, it can be concluded that the water content was approximately 5 wt% which was consistent with the TGA analysis results. The amination of P(HEMA:GMA) was confirmed by the increase in signal for nitrogen from 0% to 0.16% for P(HEMA:GMA)-NH_2. A further increase in the nitrogen signal to 0.19% for P(HEMA:GMA)-HS confirmed the immobilisation of HS.

Table 2.6: Elemental analysis results (wt%).

Hydrogel	Theoretical				Measured[1]			
	Carbon	Hydrogen	Nitrogen	Sulfur	Carbon	Hydrogen	Nitrogen	Sulfur[#]
P1	55.37	7.75	0	0	52.21	7.45	0	-
PG1	55.39	7.74	0	0	52.38	7.68	0	1.0*
PGN1	55.40	7.75	0.05	0	52.54	7.74	0.16[$]	1.2
PGH1	54.72	7.68	0.09	0.15	50.19	7.92	0.19[$]	1.6*

[1]values are the mean of 5 samples
[$]values determined to have increasing trend with respect to P1 & PG1 by Jonckheere-Terpstra test
[#]values determined after the equipment was calibrated for low sulfur samples on hydrogels: PG23, PGN23 and PGH23, average of 3 samples
*statistical significance determined by 2 tailed t-test with equal variances ($p<0.05$)

The theoretical calculations showed that the concentration for sulfur was just above the limit of detection of the analytical detector, which was 0.1 wt%. Despite this there was no significant difference observed in the sulfur signal. Therefore separate analysis was performed to determine the sulfur content of the hydrogels and this involved the column being specifically calibrated for low sulfur samples. The sulfur signal increased from P(HEMA:GMA) to P(HEMA:GMA)-HS, 1.0 - 1.6 wt% (Sulfur[#] in Table 2.6). The difference in signal for sulfur between P(HEMA:GMA)-HS and, P(HEMA:GMA) and P(HEMA:GMA)-NH_2, indicated that the amount of HS was between 3.6 and 5.9 μmol/g polymer. This result was higher than the UV-Vis results which measured 1.8 μmol HS/g polymer (Table 2.4). As these samples were bordering on the limit of detection for elemental analysis the UV-Vis results were used for further discussion.

Due to the over-estimation of the sulfur signal the remaining hydrogels were analysed with a CHN column. The measured results for carbon and hydrogen showed good agreement with the theoretical values with most results within ±10%. A better fit was realised with the addition of 5 wt% water in the samples, which was measured by TGA, and these results were consistent with the results on P(HEMA:GMA)-HS. The incorporation of amine, HS and RGD all resulted in increased nitrogen signals for PG31. The nitrogen signal also

Table 2.7: Elemental composition (wt%) of the hydrogels.

Hydrogel	Theoretical			Measured[1]		
	Carbon	Hydrogen	Nitrogen	Carbon	Hydrogen	Nitrogen
P2	55.37	7.75	0	52.72	7.26	0
P4	55.37	7.75	0	52.47	7.11	0
PG28	55.45	7.73	0	49.63	6.95	0.16*
PGN28	55.48	7.76	0.13	49.87	6.99	0.14*
PGR28	55.43	7.76	0.21	49.72	7.39	0.18*
PG31	55.45	7.73	0	52.45	7.23	0.16*
PGN31	55.50	7.77	0.17	52.27	8.46	0.21*
PGHR31	54.43	7.66	0.37	52.01	8.96	0.40*

[1]values were the average of 5 samples
*statistical significance was tested with a 2 tailed T-test with equal variances ($p<0.05$)

increased from P(HEMA:GMA)-NH_2 to P(HEMA:GMA)-RGD, 0.14-0.18 wt%, due to the immobilisation of RGD. These results were statistically significant and further confirmed the modifications that were quantified by titration.

2.5.6 ATR-FTIR

The ATR-FTIR spectrum for PHEMA is shown in Figure 2.6. The signals ascribed to PHEMA were; a strong and broad signal observed at 3400 cm^{-1} due to the O-H stretch[162]. Medium absorption bands at 2950 cm^{-1} and 2885 cm^{-1} were ascribed to the antisymmetric stretching vibration of C-H in the methyl and -CH_2 groups[163]. Another strong signal was observed at 1720 cm^{-1} due to the carbonyl C=O stretch[162]. Medium to strong signals in the range 1250-1070 cm^{-1} (maybe also 1030 peak) were ascribed to the C-O and the antisymmetric stretching of C-O-C[163]. The signal at 1450 cm^{-1} corresponded to $CH_3$and CH_2 bending deformations and the signals 970-900 cm^{-1} were due to C-O-C deformation[92]. The signal at 750 cm^{-1} was associated with the bending vibration mode of CH_2 and CH_2 rocking that is characteristic of methacrylic polymers.

A change in the relative intensity of the signals at 1020 cm^{-1} and 1075 cm^{-1} was observed as the hydrogels were modified. The copolymerisation of HEMA

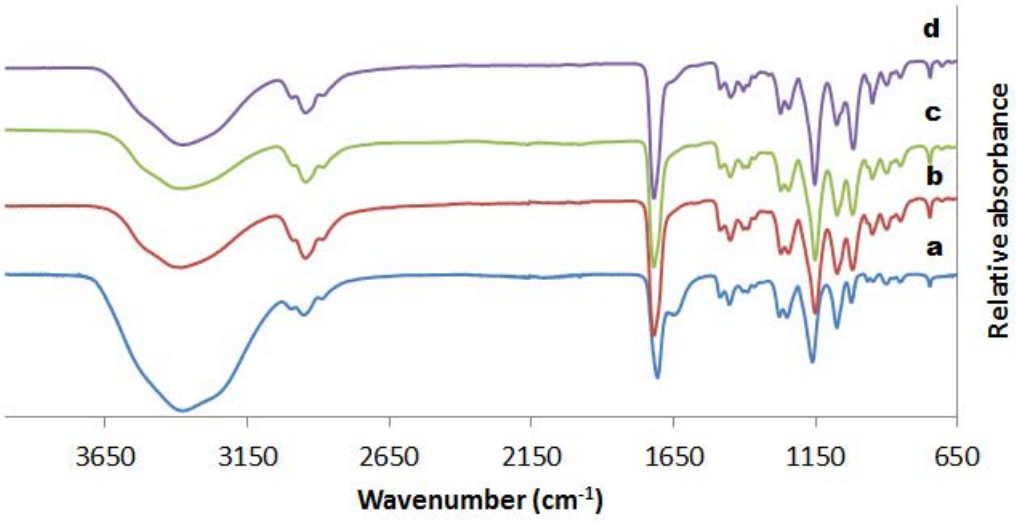

Figure 2.6: ATR-FTIR spectra of PHEMA (a), P(HEMA:GMA) (b), P(HEMA:GMA)-NH_2 (c) and P(HEMA:GMA)-HS (d).

with GMA increased the 1020 cm^{-1} signal due to the introduction of more C-O-C groups. The signal further increased after the immobilisation of HS due to the multiple C-O-C groups contained in the biomolecule. No further characteristic signals were observed from the modifications performed on PHEMA due to the overlap with the strong signals from PHEMA. For example, the characteristic amine signals from hexamethylenediamine were obscured by the broad O-H stretch and strong carbonyl stretch of PHEMA. The strongest characteristic signals for HS were due to the carboxylic acid groups which also produce signals within the range of the PHEMA O-H and carbonyl stretches.

An indirect approach was used to confirm the reaction of HS to the free amine groups on the hydrogels. Briefly, 94 mg HS was reacted with 24 mg hexamethylenediamine, 206 mg EDC and 64 mg NHS in deionised water at room temperature for 24 h. The product was dried with a rotor evaporator and the IR spectra taken. The spectra of the product had 2 signals at 2940 cm^{-1} and 2860 cm^{-1} which corresponded to the hexamethylenediamine signals (Figure 2.7). Additionally the reaction was confirmed by the retention of the primary amine signal at 1630 cm^{-1} and a new signal at 1550 cm^{-1} which indicated the presence of a secondary amine. This showed that the HS was attached to one end

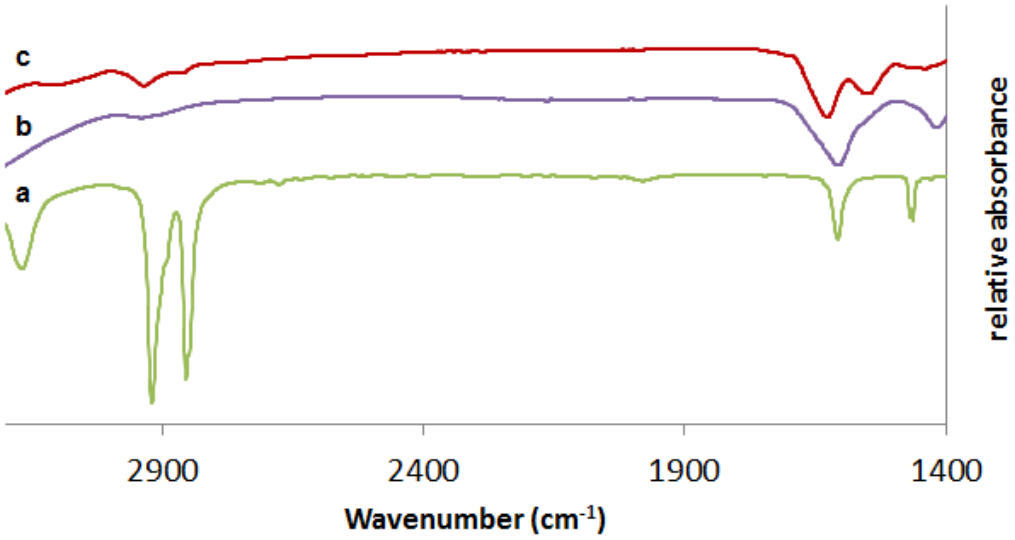

Figure 2.7: ATR-FTIR spectra demonstrated the reaction of HS with hexamethylenediamine. Hexamethylenediamine (a), HS (b) and aminated HS (c).

of the hexamethylenediamine. These results were further strengthened by the UV-Vis results which were able to quantify the amount of HS that had been immobilised on the hydrogels.

2.5.7 TGA

The TGA results showed a gradual weight loss between 25-210ºC followed by the primary weight loss which occured between 210-440ºC (Figure 2.8). The initial weight loss between 25-100ºC was due to the evaporation of water from the hydrogels, and this was between 4.6 - 5.7%. The water was probably absorbed from the atmosphere before analysis. This result was used in the elemental analysis which showed a great fit with theoretical results with 5 wt% water in the hydrogels. The primary weight loss was due to the decomposition of the hydrogels, this began at 210ºC for PHEMA, while decomposition of P(HEMA:GMA) was delayed until 276ºC. The copolymer displayed increased thermal stability due to the incorporation of GMA. Examination of multiple batches of the hydrogel showed low variability between the batches, as seen in Figure 2.9. The thermal stability of PHEMA was consistent with

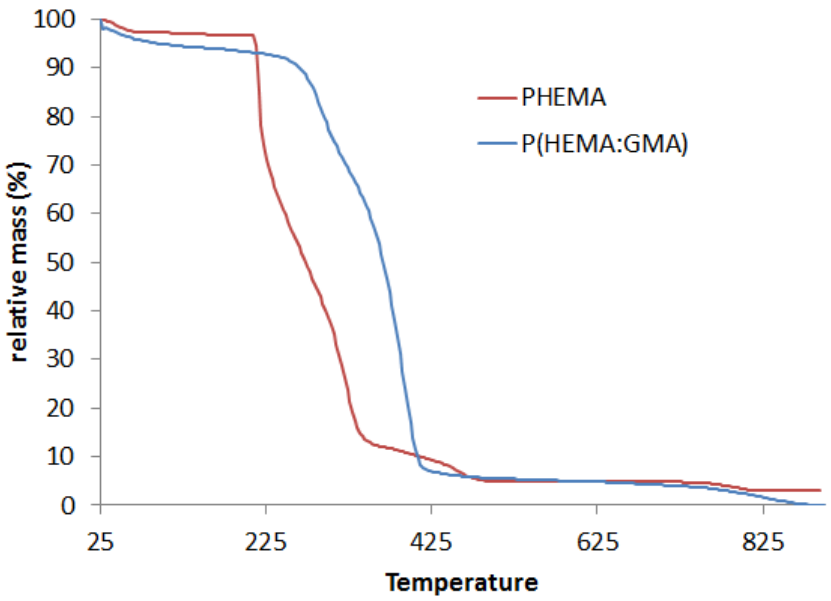

Figure 2.8: TGA curves for PHEMA and P(HEMA:GMA).

TGA results obtained by others[105,164] and the copolymerisation of PHEMA with methylmethacrylate similarly delayed thermal decomposition[165]. The decomposition of the hydrogels after the further modification with hexamethylenediamine and HS was unchanged from that of P(HEMA:GMA). These results demonstrated that the modified hydrogels had improved thermal stability over PHEMA and were stable at physiological temperature.

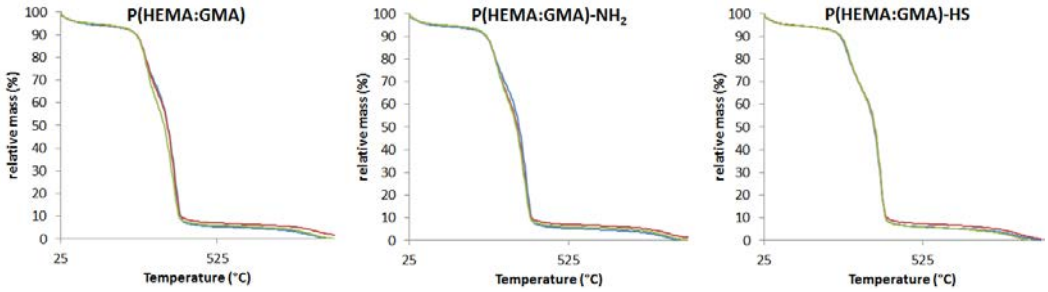

Figure 2.9: TGA curves for 3 batches of hydrogel showing low batch-to-batch variability. PG10 (red), PG12 (blue) and PG23 (green).

2.5.8 Pore Structure, Surface Area and EWC%

The SEM images showed the porous structure of the hydrogel scaffolds and the spherical structure of the polymer. The pore structure of the hydrogels was maintained after the chemical modifications as seen in Figure 2.10. The PHEMA hydrogel had some areas with thin string-like structures, these were likely an artefact and have been observed by others in PHEMA sponges[166]. Interestingly the pores for PG10 were the most distinct and large with the spherical structure of the polymer appearing smaller than all other hydrogels. Smaller spherical structure of the hydrogel has been attributed to the early onset of phase separation which reduces the droplet size[166]. The solubility of GMA in water is 2.3 wt%, therefore it was possible that the early onset of the polymerisation was enhanced by the higher solubility of GMA in PHEMA than in water. Another possible cause was the increased temperature used for the synthesis of PG10, 60ºC for 20 h followed by 70ºC for 3 h. All other hydrogels were synthesised at 50ºC for 12 h, the difference in synthesis temperature may have caused an earlier onset of the phase separation resulting in the formation of smaller polymer spheres and pronounced pore size.

The pores in the copolymer appeared to have contracted after modification with hexamethylenediamine. There were no observable differences in pore size or polymer morphology between P(HEMA:GMA)-NH_2, P(HEMA:GMA)-HS and P(HEMA:GMA)-RGD. All hydrogels were seen to contain pores with the same spherical structure. P(HEMA:GMA)-HS&RGD appeared more dense than the other hydrogels, this could have been due to variations during sample preparation (freezing and freeze drying) or due to the angle at which the hydrogel was imaged (imaging pores at an angle can make them appear narrower). All hydrogels showed the effect of freezing as striations that were created across the samples, these were most obvious on PG10, PGN10 (diagonally) and PG30 (vertically).

All of the average EWC% results were similar which indicated that all hydrogels

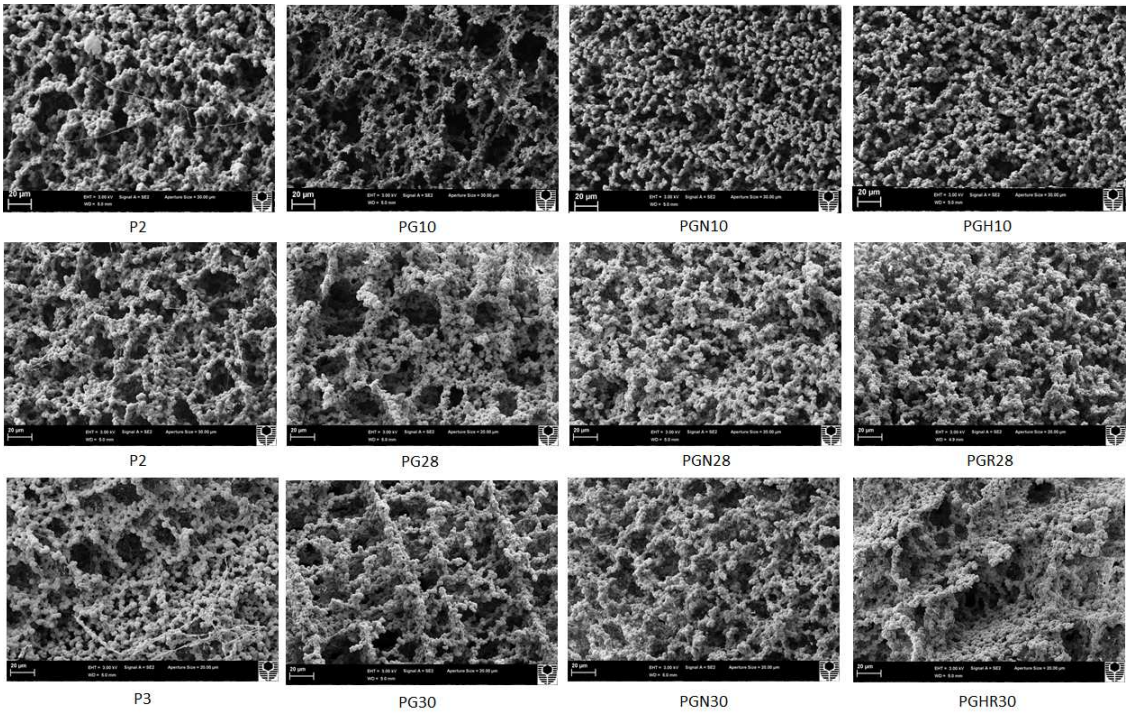

Figure 2.10: SEM images of the cross-sectional area of hydrogels. All images were taken at 3keV with a working distance of 5.0 mm giving 500x magnification, the scale bar was 20 μm.

Table 2.8: EWC% values for the hydrogels.

Hydrogel number	EWC%[1]			
	PG	PGN	End modification	
6	80.3 ± 0.4	79.9 ± 0.5	PGR	79.4 ± 0.2
8	82.3 ± 0.4	-	PGH	-
9	79.0 ± 0.5	80.4 ± 0.5	PGR	79.5 ± 0.5
10	81.4 ± 0.7	-	PGH	-
15	81.5 ± 0.2	80.0 ± 0.1	PGHR	79.7 ± 0.6
16	81.8 ± 0.5	80.1 ± 0.4	PGHR	79.5 ± 0.3

[1]values were the average of 5 samples ± standard deviation

maintained their hydrated nature after modification (Table 2.8). The EWC% for PHEMA was: 76 ± 4, 76 ± 1 and 76.5 ± 0.6 for P2, P3 and P4 respectively. The modified hydrogels had higher EWC% values between 79-82% indicating an increase in swellability over PHEMA. The amount of GMA in the hydrogels was kept low to avoid the large reduction in equilibrium water content which was observed by Santander-Borrego when they used greater than 6 mol% incorporation of GMA in HEMA[167]. These results contrasted with the SEM images which showed an apparent decrease in pore size, therefore the contraction in the pores did not affect the EWC%. These results demonstrated that the hydrogels maintained a constant degree of swelling in water after all modifications.

The surface area of the hydrogels was measured using BET analysis. PHEMA had a surface area of 24 ± 5 m^2/g and the modified hydrogels: 21 ± 3 m^2/g, 39 ± 2 m^2/g, 36 ± 5 m^2/g for PG10, PGN10 and PGH10, 36 ± 2 m^2/g, 17 ± 3 m^2/g, 28 ± 7 m^2/g for PG28, PGN28 and PGR28, 36 ± 10 m^2/g, 22 ± 11 m^2/g, 39 ± 4 m^2/g for PG30, PGN30 and PGHR30 respectively. None of the differences between the various hydrogels were statistically significant. These results indicated that the apparent pore contraction observed in the SEM images did not result in a significant decrease in the surface area. The EWC% and surface area values were similar to those obtained by others when PHEMA was crosslinked with EDMA, others have observed an EWC% of 65% and surface area of 25.61 m^2/g[127]. When PHEMA was crosslinked with N,O-dimethacryloylhydroxylamine, EWC% values of 68 and 67% and surface areas of 43.83 m^2/g and 54.31 m^2/g were obtained[135]. Therefore taking the SEM, EWC% and surface area results together, all of these results demonstrated that the modifications on PHEMA maintained the hydrated nature, surface area and porosity of PHEMA.

2.5.9 Viscoelastic Properties

The viscoelastic properties of the hydrogels were measured with a rheometer as this equipment measured the hydrogels response to shear stress. The rheology equipment also allowed for all measurements to be performed while the

hydrogels were swollen and at 37ºC. The water content of PHEMA has been demonstrated to affect the viscoelastic properties as it has a plasticising effect (increases the elasticity/stretch-ability)[168]. This was ideal as the results were reflective of how the hydrogels would react *in vivo*. The values determined for the hydrogels were the: elastic modulus, viscous modulus and elastic recovery. The elastic modulus is also known as the storage modulus and it described the solid behaviour of the hydrogels, the greater the elastic modulus the more the material reacts as an ideal elastic solid (resists deformation and returns to its original shape). The viscous modulus, also known as the loss modulus, described the flow or liquid characteristic of the hydrogels. The larger the viscous modulus the more the material is able to dissipate energy, usually as heat. Most materials exhibit both characteristics to varying degrees and are therefore known as viscoelastic.

Table 2.9: Elastic and viscous moduli of the hydrogels at room temperature and 37ºC.

Hydrogel code	G' (kPa)[1]	G" (kPa)[1]	G' (kPa)[2]	G" (kPa)[2]
P3	2.9 ± 0.4	0.48 ± 0.06	2.48 ± 0.04	0.34 ± 0.03
PG17	2.7 ± 0.2	0.37 ± 0.02	-	-
PGN17	2.6 ± 0.1	0.40 ± 0.02	-	-
PGH17	3.4 ± 0.3	0.40 ± 0.03	2.52 ± 0.09	0.31 ± 0.06
PG24	2.7 ± 0.4	0.32 ± 0.08	-	-
PGN24	2.5 ± 0.1	0.32 ± 0.06	-	-
PGR24	3.0 ± 0.4	0.36 ± 0.03	3.0 ± 0.1	0.19 ± 0.02
PG25	2.7 ± 0.1	0.37 ± 0.02	-	-
PGN25	2.4 ± 0.2	0.33 ± 0.06	-	-
PGHR25	2.7 ± 0.2	0.46 ± 0.05	3.0 ± 0.2	0.36 ± 0.02

G' = Elastic modulus, G" = Viscous modulus

[1]values were the average of 20 measurements from 5 samples ± standard deviation at room temperature

[2]values were the average of 20 measurements from 3 samples ± standard deviation at 37ºC

The oscillation stress sweep was used to determine the linear viscoelastic re-

gion of the hydrogels, which is the region where the elastic and viscous moduli are independent of the strain in the material. An oscillation strain sweep within the linear viscoelastic region was then used to measure the moduli, these are summarised in Table 2.9. The elastic modulus of PHEMA was 2.9 ± 0.4 kPa. In order to determine whether any of the modifications on PHEMA had a significant effect on the viscoelasticity of the hydrogels, all intermediates (P(HEMA:GMA) and P(HEMA:GMA)-NH_2) corresponding to the 3 end modifications were tested. The 3 batches of P(HEMA:GMA) had similar elastic moduli to each other and PHEMA. P(HEMA:GMA)-HS had the highest elastic modulus of 3.4 ± 0.3 kPa, followed by P(HEMA:GMA)-RGD which had 3.0 ± 0.4 kPa. The slight increase in the elastic modulus was due to the immobilisation of HS and RGD on the hydrogel. Interestingly P(HEMA:GMA)-HS&RGD had elastic modulus of 2.7 ± 0.2 kPa which was not markedly different to PHEMA. The viscous modulus was highest for PHEMA and P(HEMA:GMA)-HS&RGD at 0.48 ± 0.06 kPa and 0.46 ± 0.05 kPa respectively. The viscous modulus was constant for 2 of the P(HEMA:GMA) batches, P(HEMA:GMA)-NH_2 and P(HEMA:GMA)-RGD. All of the hydrogels displayed solid-like behaviour as the elastic moduli were greater than the viscous moduli.

Table 2.10: Elastic recovery of the hydrogels at room temperature.

Hydrogel code	**Recovery (%)[1]**
P3	73.0 ± 0.9
PG17	80.6 ± 0.4
PGN17	72.5 ± 0.9
PGH17	79.5 ± 0.4
PGR24	74.0 ± 1.1
PGHR25	68.5 ± 0.5

[1]stress of 10 Pa was applied gradually over 120 s followed by a recovery of 400 s. Results were the average of 5 samples ± standard deviation

PHEMA and the end modification hydrogels were tested at 37ºC to mimic physiological conditions. All of the hydrogels demonstrated similar mechanical properties when tested at physiological temperature. These results showed

that the hydrogels would retain their mechanical properties for *in vivo* applications which is essential for successful tissue engineering applications. The moduli values obtained for the hydrogels was within the range measured by AFM for fibroblasts, 3-12 kPa[169], as individual cells and a reconstituted tissue model, 1-2.5 kPa[170,171]. The AFM results were a measure of Young's modulus which is typically a little larger than the shear modulus, which was measured in this work. These data suggested that the hydrogels have an appropriate elasticity to support fibroblast adhesion.

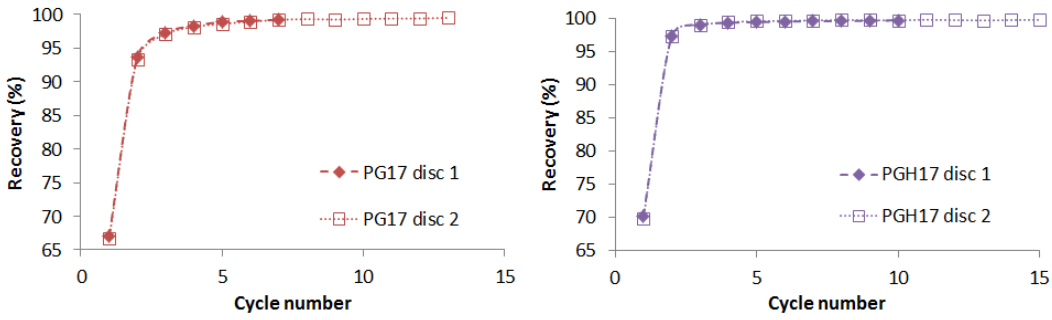

Figure 2.11: Elastic recovery of hydrogels after application of repeated stress at 20℃. Stress of 10 Pa was applied over 60 s (30 s for P(HEMA:G MA)) followed by a recovery of 240 s.

The creep/recovery analysis was used to determine the ability of the hydrogels to recover after the application of stress. The elastic recovery of the hydrogels was determined by the difference in the maximum and minimum strain measured with the physiologically relevant shear stress of 10 Pa. This stress is indicative of the shear stress in skin associated with movement such as running[172]. The hydrogels were observed to recover well with values from 68.5-80.6% (Table 2.10). The recovery was similar for PHEMA, P(HEMA:GMA)-NH_2 and P(HEMA:GMA)-RGD, and higher for P(HEMA:GMA) and P(HEMA:GMA)-HS. These results may have indicated some improvement in the elastic recovery of the scaffolds due to the copolymer and modification steps. However the results from P(HEMA:GMA)-NH_2 and P(HEMA:GMA)-HS&RGD did not comply with that hypothesis. Interestingly P(HEMA:GMA)-HS&RGD demonstrated the lowest recovery which correlated with it also having the lowest elastic modulus

of all the end modifications. As this hydrogel had the highest viscous modulus it was possible that the immobilisation of both biomolecules enhanced the fluid characteristics of the hydrogel while simultaneously impairing the elastic properties.

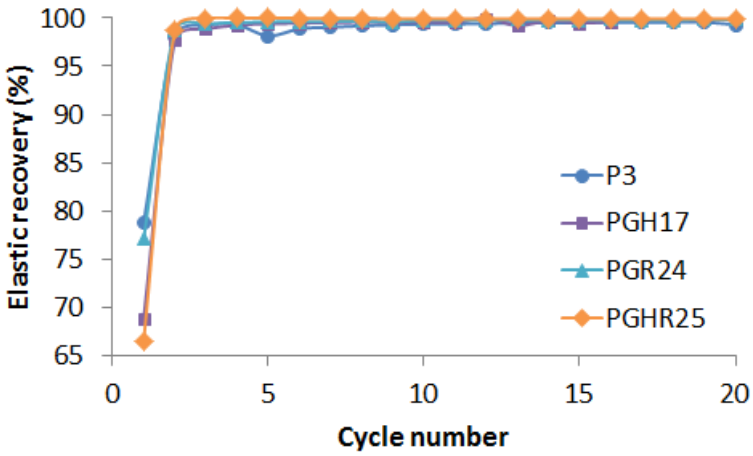

Figure 2.12: Elastic recovery of hydrogels after repeated application of stress at 37ºC. Stress of 10 Pa was applied over 30 s followed by a recovery of 240 s.

Additionally the amount of HS immobilised on PGH17 and PGHR25 varied, 0.84 ± 0.05 and 2.9 ± 0.1 μmol HS/g hydrogel respectively. As more HS was attached to PGHR25, it was possible that greater crosslinking occurred on this hydrogel. More immobilised HS, covalently bound to the hydrogel at multiple points would restrict the movement of the hydrogel. This restriction in movement would impair the hydrogels ability to recover elastically from an applied stress, resulting in the reduction of the recovery by 11%.

The overall high recovery values for the hydrogels indicated good elastic properties which are essential for a permanent implant. A permanent implant would undergo repetitive compression and tension moments as well as shear stress. These results showed that the hydrogels have great potential to cope with applied stress without permanent deformation as they have the ability to spring back into shape once the stress is removed. To extend these results P(HEMA:GMA) and P(HEMA:GMA)-HS hydrogels were tested for repeated creep/recovery to determine their performance after multiple stress events, this

was in effect, an attempt at a shear fatigue test. Fatigue testing is most often performed on hard materials (moduli >100kPa) with tensile or compressive systems, however the long term success of soft implants is also reliant on maintained mechanical properties that match the surrounding tissue. Repetition of the test showed that the recovery of P(HEMA:GMA)-HS approached 100% after 5 cycles and P(HEMA:GMA) demonstrated the same trend. These results meant that the hydrogel underwent some rearrangement or small deformation during the first 2 cycles and remained stable thereafter. These results indicated that the hydrogels should be able to withstand the repeated stress that would be encountered by a permanent implant.

The elastic recovery from repeated creep/recovery tests of the hydrogels was also determined at 37ºC. The recovery of PHEMA approached 100% by cycle 14, P(HEMA:GMA)-HS by cycle 7 while P(HEMA:GMA)-RGD and P(HEMA:GMA)-HS&RGD were seen to approach 100% recovery by cycle 4. These results showed that the modified hydrogels were able to recover their shape more rapidly after multiple applications of stress than PHEMA. These results confirmed that the hydrogels would be stable and provide consistent physical support under repeated stress conditions at physiological temperature under physiological shear stress. This suggested that the hydrogels have potential to provide long term support to soft tissue when implanted.

2.6 Conclusions

Several modifications of PHEMA were achieved. PHEMA was copolymerised and modified to enable immobilisation of HS and RGD. The amination of the P(HEMA:GMA) was confirmed by titration and elemental analysis. Immobilisation of HS was confirmed indirectly with ATR-FTIR, directly by elemental analysis and quantification of HS and RGD immobilisation was by UV-Vis and titration respectively. The results showed consistent immobilisation of 1-3.09 μmol HS/g polymer and 22-87 μmol RGD/g polymer. Immobilisation of both

HS and RGD resulted in 1.4-2.0 μmol HS/g polymer and 22-87 μmol RGD/g polymer.

The synthesised hydrogels were all porous with high EWC%, which indicated high water content similar to that of native tissue. The results from TGA demonstrated that P(HEMA:GMA) had increased thermal stability over PHEMA. The surface area of the modified hydrogels as well as the other physical properties measured did not vary significantly from that obtained with PHEMA, which indicated that the modifications did not adversely affect the biocompatible characteristics of PHEMA.

Measurement of the viscoelastic properties of the hydrogels showed that the hydrogels had elasticity similar to soft tissue and relaxed muscle. The highest elastic modulus measured was for P(HEMA:GMA)-HS, 3.4 ± 0.3 kPa at room temperature. Interestingly the highest elastic modulus measured at 37ºC was for P(HEMA:GMA)-RGD and P(HEMA:GMA)-HS&RGD at 3.0 ± 0.1 kPa and 3.0 ± 0.2 kPa. The elastic recovery of the hydrogels was tested and found to be high, 68.5 - 80.6% at room temperature with similar results at 37ºC. Repeated creep/recovery tests showed the hydrogels ability to retain their shape after multiple applications of stress. These results showed that the elastic recovery of the hydrogels approached 100% after 4-7 cycles. This indicated that the hydrogels had some small re-arrangement in their structure during the first few applications of stress but were stable thereafter. Therefore the hydrogels demonstrated stable physical properties that are compatible with an application as a permanent implant.

In conclusion the synthesised hydrogels were characterised chemically and physically. Chemically the hydrogels were successfully modified to incorporate HS and RGD. The elasticity of the hydrogels was shown to be close to that of soft tissue and relaxed muscle. Lastly the hydrogels showed the ability to withstand repeated stress at physiological temperature and shear stress. These hydrogels have potential for use in soft tissue regeneration applications.

Chapter 3

Biological Characterisation of HS Modified PHEMA and Intermediates

3.1 Introduction

Heparan sulfate (HS) is a co-receptor acting in the formation of some cell-cell adhesions and cell-matrix adhesions. In addition its interactions with cell surface receptors contribute to cell proliferation, cell motility and differentiation[173]. HS is known to bind fibronectin, laminin and collagens in the ECM, all of these have been found to be important for cell adhesion. Additionally, cell interactions with some matrix proteins can facilitate differentiation, for example fibronectin has been found to enhance the differentiation of murine myoblast cells, C2C12[174]. The contribution of HS to the normal physiological function of a wide range of different cell types was recognised when HS was discovered to bind members of the FGF family of growth factors. This binding was required for sustained signaling through the various cell surface FGF receptors[80,173]. More recently, HS has been recognised as a required biomolecule for the binding of FGF family members to direct the change from cell proliferation to differentiation[80].

Surprisingly, HS immobilisation on sponge PHEMA has not been previously re-

ported. Heparin, a GAG similar to HS but more sulfated, has been immobilised on PHEMA for therapeutic drug delivery and antithrombogenic activity[107,175], but its effect on cell differentiation was not investigated. Interestingly, heparin incorporated into a fibrin scaffold to allow for the binding of bFGF, resulting in significant improvements in neurite behaviour, specifically the enhancement of neurite extension formation[176]. Heparin, of a similar molecular weight to the HS used in this study, was shown to improve fibroblast adhesion and proliferation in a way that was superior to the results obtained with another GAG, chondroitin sulfate[177]. In connective tissue, fibroblasts are the main cells that are involved in the deposition, maintenance and remodeling of the ECM[177] and as a result are important for tissue regeneration. Of particular interest to the present study was the finding that the expression of HS proteoglycans (HSPGs) were up-regulated during muscle regeneration[178]. They are essential for the transmission of mechanotransduction signals which are important for cell spreading, assembly of the actin cytoskeleton and cell contractility[179]. Collectively all of these data demonstrate the likely importance of HS in tissue regeneration applications.

When developing a scaffold for tissue regeneration that contains HS it is not enough to quantify the amount of HS immobilised on the hydrogel, it also needs to be shown that the immobilised HS is active. Quantitative analysis in Chapter 2 showed that 1-3.09 μmol HS/g polymer was immobilised. To examine the bioactivity of the immobilised HS, two approaches were taken in this chapter, one was a binding assay to assess whether the HS that was immobilised could bind a growth factor likely to be involved in tissue regeneration. The second approach was to assess the effect of the immobilised HS on cell behaviour in tissue culture.

A review of the literature suggested that basic fibroblast growth factor (bFGF) could be a growth factor that both binds to HS and is involved in tissue regeneration. For example, bFGF is a major growth factor involved in skin wound repair[173], and the introduction of bFGF and HS into a scaffold has been demonstrated to improve cellular invasion *in vivo*[153]. Also a PHEMA copolymer soaked in HS solution then bFGF solution has been shown to improve neu-

ral stem cell growth[180]. As there is a known strong affinity between HS and bFGF, it was possible for an assay to be designed to assess the bioactivity of the immobilised HS by how much bFGF was bound. Accordingly, an Enzyme Linked ImmunoSorbant Assay (ELISA) was designed using bFGF as the HS binding growth factor. The analysis of the hydrogels with a bFGF ELISA had the dual approach of testing the bioactivity of the immobilised HS, and of indicating whether the hydrogels are likely to sequester bFGF *in vivo* thereby enhancing their tissue regeneration potential.

The second way the bioactivity of the synthesised hydrogels was examined was through cell culture. It was argued that an increase in cell adhesion or cell development would indicate that the HS is active. Having considered the measured elasticity of the hydrogels, 2 cell types were chosen that are derived from tissues of soft and intermediate stiffness. These were 3T3 mouse fibroblasts and C2C12 mouse myoblasts. It has been reported that HS facilitates the bioactive processes of bFGF which are critical for fibroblasts and myoblasts[181]. Fibroblasts are one of the most abundant cells in connective tissue and myoblasts are cells that have the potential to differentiate into myotubes which is the first step towards developing muscle fibre. Accordingly these cell types will provide evidence of whether the hydrogels may be suitable for use in deep tissue wound healing applications. Cell behaviour was observed by fluorescent microscopy and cell proliferation was measured by assay.

3.2 Experimental Procedure

3.2.1 Reagents and Buffers

Chloroform 99% pure (Merck, Melbourne, Australia), ultrapure water (Baxter Healthcare, Sydney, Australia), Hank's Buffered Saline Solution (HBSS, HyClone, Thermo Fischer Scientific, Waltham, USA), tissue culture phosphate buffered saline (TC PBS, Hyclone, Thermo Fischer Scientific), 0.05% Trypsin-EDTA (0.05% (w/v) trypsin in 5 mM ethylenediamine tetraacetic acid (EDTA), Gibco, Thermo Fischer Scientific), CellTiter AQueous One (Promega, Sydney,

Australia), alamarBlue (Invitrogen) and CellTiter Glo 3D Cell Viability Assay (Promega), rhodamine phalloidin (200 units/mL, Molecular Probes, Invitrogen, Thermo Fischer Scientific) were all used as supplied.

Carboxylic acid diacetate succinimidyl ester (CFSE, CellTrace Oregon Green® 488, Molecular Probes) was dissolved in dimethylsulfoxide (DMSO, Sigma Aldrich) to give 2 mM solution and stored at -20°C.

Phosphate buffered saline (PBS) was made as a 10x concentrate and consisted of 150 mM NaCl (VWR, Prolab, Brisbane, Australia), 8.4 mM Na_2HPO_4 (Chem Supply, Adelaide, Australia) and 1.6 mM $NaH_2PO_4.H_2O$ (AnalaR BDH, VWR) dissolved in MilliQ water, pH was adjusted to 7.4 using 1M HCl (Sigma Aldrich) and filtered with 0.2 μm filter and stored at room temperature. PBS was made by diluting 100 mL of concentrate in 900 mL MilliQ water.

HEPES buffered saline (HBS) consisted of 150 mM NaCl (VWR, Prolab), 10 mM 4-(2-Hydroxyethyl)piperazine-1-ethanesulfonic acid) (HEPES, Life Technologies, Thermo Fischer Scientific), 1 mM $MgCl_2$ and 1 mM $CaCl_2$, stored at 4°C.

4', 6-diamino-2-phenylindole (DAPI**,** Sigma Aldrich) was diluted in HBSS to give 2 μg / mL solution.

Tris buffer consisted of 5 mM tris(hydroxymethyl) aminomethane (VWR Prolab) dissolved in ultrapure water, pH adjusted to 7.6 using 1M HCl, sterile filtered with 0.2 μm filter, stored at room temperature.

0.05 M carbonate/bicarbonate buffer consisted of 0.016 M Na_2CO_3 (Sigma Aldrich) and 0.034 M $NaHCO_3$, (Selby Biolab, Thermo Fischer Scientific) dissolved in MilliQ water, the pH was adjusted to 9.6, filtered with 0.2 μm filter and stored at 4°C.

Tween 20 was prepared as a 0.05% (v/v) solution of polyoxyethylene sorbitan monolaurate (Tween 20, Sigma Aldrich) dissolved in 1xPBS.

Bovine serum albumin in PBS (BSA, fraction V, culture grade, HyClone, Thermo Fischer Scientific), was prepared as a 1% (v/v) solution in TC PBS .

Paraformaldehyde (Sigma Aldrich) was prepared as a 4% (w/v) solution dissolved in TC PBS, the pH was adjusted to 7.4, the solution was filtered with

0.45 μm and 0.2 μm filters and stored at 4°C in the dark.

Triton X-100 (TX-100, Amresco, Cleveland, USA) was prepared as a 0.1% (v/v) solution dissolved in TC PBS and stored at 4°C.

3.2.2 Cell Culture

3T3 murine fibroblasts (European Collection of Cell Cultures, Porton Down, UK) were cultured in proliferation media: RPMI (Gibco, Thermo Fischer Scientific) supplemented with 10% (v/v) fetal bovine serum (FBS, CSL Limited, Melbourne, Australia), 2 mM of L-glutamine, 10 mM HEPES and 1 mM sodium pyruvate were purchased from Gibco BRL. C2C12 murine myoblasts (American Type Culture Collection, Manassas, VA, USA) were cultured in proliferation media: Dulbecco's modified Eagle's medium (DMEM, Gibco BRL) with 10% (v/v) FBS and 2 mM L-glutamine, 10 mM HEPES and 1 mM sodium pyruvate. For differentiation the C2C12s were cultured in differentiation media that consisted of DMEM with 2% (v/v) horse serum (Gibco BRL) and 2 mM L-glutamine, 10 mM HEPES and 1 mM sodium pyruvate.

Cells were cultured under sterile conditions at 5% CO_2 and 37°C to approximately 70% confluency in 25 cm^2 tissue culture flasks (Nunc, ThermoFisher Scientific). Cells were harvested by rinsing with PBS and EDTA and incubating with 0.05% (w/v) trypsin in 0.5 mM EDTA (Gibco), for 3 min at 37°C. The 3T3 cells were subcultured at $20x10^4$ cells / flask and C2C12 cells at $5x10^4$ cells / flask. Cell numbers were determined using a Coulter Multisizer (Coulter Electronic, Sydney, Australia). Cells cultured on hydrogel scaffolds for experiments that involved cell imaging used phenol red free RPMI (Sigma) or DMEM (HyClone).

3.2.3 Cell Culture on Hydrogels

The hydrogel scaffolds were sterilised before being used in ELISA or cell culture. The discs were sterilised using chloroform[182]. Forty hydrogel discs were placed inside dialysis tubing (SnakSkin, 3.5 K MWCO, Thermo Scientific) with

20 mL PBS. Up to 4 dialysis tubes filled with hydrogel discs were placed in 2 L of 0.5% (v/v) chloroform in PBS and left stirring at 4°C for 16 h. Dialysis tubes were removed from the chloroform solution and placed into 2 L PBS with stirring at 4°C for an hour, this was repeated twice. The discs were removed from the dialysis tubing under sterile conditions and stored in sterilised containers in TC PBS at room temperature.

Hydrogel discs (9 mm in diameter) were pre-incubated in 0.5 mL phenol red free proliferation medium in 24 well plates for 2 h at 37°C before cell seeding. The media was removed and the 3T3 and C2C12 cells were seeded onto the discs at 1.0-1.2x10^4 cells/disc and 1.4-2.2x10^4 cells/disc respectively in 25 μL of the appropriate cell culture medium. The cells were incubated at 37°C for 30 min, then 1 mL phenol red free proliferation medium was added, the culture media was changed every 48 h.

3.2.4 Cell Staining

Cells were stained with CFSE as follows: the hydrogels were rinsed 3 times with 1 mL warm HBSS then 50 μL of 20 μM CFSE in HBSS was added and incubated for 10 min at 37°C followed by 3 rinses with 1 mL warm HBSS. The cells on the hydrogels were covered with a glass cover-slip and visualised using fluorescent microscopy (Zeiss Axioskop) with $\lambda_{excitation}$ = 494 nm and $\lambda_{emission}$ = 522nm and imaged using Spot Advanced software (SPOT™ Imaging solutions).

For rhodamine phalloidin staining, the cells were fixed on the hydrogels by incubation in 0.5 mL of warm 4% (w/v) paraformaldehyde at room temperature for 30 min in the dark. The hydrogels were rinsed twice with 1 mL PBS and the cells were permeabilised with 0.5 mL cold 0.1% (v/v) TX-100 and incubated at 4°C for 4 min. The discs were rinsed twice with 1 mL PBS and then incubated in 5% (v/v) rhodamine phalloidin in HBS for 2 h in the dark at room temperature. The discs were rinsed 3 times with 1 mL HBS and counter-stained with DAPI by incubation in 0.5 mL of 2 μg/mL DAPI at 37°C for 5 min followed by 3 rinses with 1 mL warm HBS. The cells on the hydrogels were covered with a glass cover-

slip and visualised using fluorescent microscopy (Zeiss Axioskop, Gottingen, Germany) with $\lambda excitation$ = 554 nm and $\lambda emission$ = 573 nm for rhodamine phalloidin, $\lambda excitation$ = 340 nm and $\lambda emission$ = 488 nm for DAPI and imaged using Spot Advanced software (SPOT™ Imaging solutions, Sterling Heights, Michigan, USA).

3.2.5 Immunofluorescence of Cell Expressed Fibronectin

Hydrogels were seeded with 3T3 or C2C12 cells and the cells were cultured for 2-3 days. The hydrogels were rinsed 3x1 mL HBS at 37°C for 2 min then incubated in 1 mL 4% paraformaldehyde at room temperature for 10 min. The hydrogels were rinsed 3x1 mL HBS with 300 rpm shaking for 5 min, then incubated in block solution (10% FCS and 1% BSA in HBS) at 4°C for 16 h before incubation with 100 μL of 50 μg/mL rabbit polyclonal fibronectin antibody (Abcam, ab2413) in block solution or 100 μL buffer solution at room temperature for 3 h. The hydrogels were rinsed 3x with 1 mL HBS with shaking at 300 rpm for 2 min, then incubated with 100 μL of 10 μg/mL secondary antibody (Alexa Fluor® 488 F(ab')2 goat anti-rabbit IgG, Molecular Probes, Invitrogen) in block solution at room temperature for 2 h. The hydrogels were rinsed 3x with 1 mL HBS with 300 rpm shaking for 2 min followed by incubation in 0.5 mL of 2 μg/mL DAPI in HBS at room temperature for 10 min. The hydrogels were rinsed 3 times with HBS and imaged with a glass coverslip on a Nikon A1+ confocal microscope (Nikon, Tokyo, Japan) using NIS-Elements AR analysis version 4.1 software.

3.2.6 Enzyme Linked ImmunoSorbant Assay (ELISA)

An ELISA to detect basic fibroblast growth factor (bFGF, Peprotech, Rocky Hills, USA) was as follows: 96 well plates (Maxisorp Immuno Plate, NUNC) were coated with 50 μL of 2 μg/mL anti-bFGF mouse monoclonal antibody (mAb, R&D systems, Minneapolis, USA, IgG_{2B} clone: 10060) in 0.05 M carbonate/bicarbonate buffer (pH 9.6). The plate was incubated at 4°C for 16 h

and then rinsed 3 times with 200 μL 0.05% (v/v) Tween 20 in PBS.

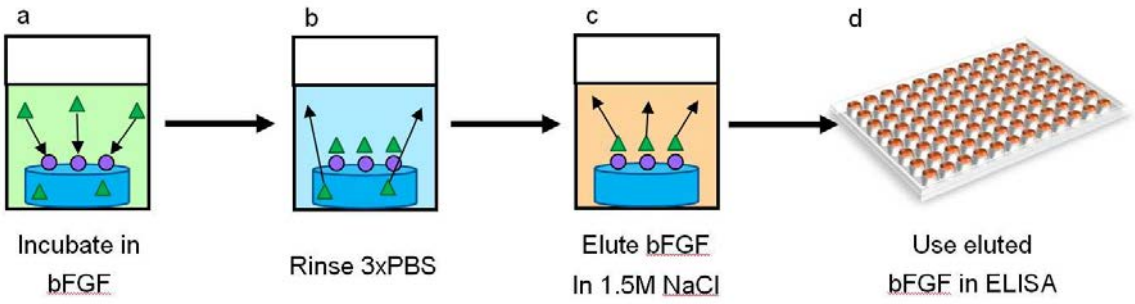

Figure 3.1: Procedure for testing the bioactivity of the immobilised HS on the hydrogels. (a) Hydrogel discs (blue) with immobilised HS (purple circles) were incubated in bFGF (light green), the green triangles are bFGF molecules. The arrows indicate the binding of bFGF to HS. (b) Hydrogels were rinsed with PBS (light blue) to remove any non-specifically incorporated bFGF. (c) Bound bFGF is eluted off the hydrogels in a solution of sodium chloride (orange) and (d) this eluent was used in the ELISA.

The hydrogel scaffolds were incubated in 100 μL bFGF (25 μg/mL, Peprotech) diluted in 5 mM Tris buffer (pH 7.6) at room temperature for 2 h with shaking at 500 rpm. The discs were rinsed 3 times for 10 min in 0.5 mL of 5 mM Tris buffer with shaking at 500 rpm. The bFGF bound to the HS in the discs was eluted in 1 mL of 1.5 M NaCl in PBS for 30 min with shaking at 500 rpm at room temperature. The eluted bFGF was diluted 1/10 in PBS and then added to the immobilised anti-bFGF mAb in the wells of the ELISA plate and incubated for 2 h at room temperature (see Figure 3.1).

A calibration curve was created using 100 ng/mL bFGF in 1.5 M NaCl in PBS and serially diluting across the plate, the solutions were then transferred to the ELISA plate and incubated for 2 h at room temperature. 100 μL of 1 μg/mL biotinylated anti-bFGF mouse mAb (R&D systems, IgG_{2A} clone: 10043) in 1% (v/v) BSA was incubated at room temperature for 1 h. The plate was rinsed 3 times with 200 μL 0.05% Tween 20 and then 100 μL of 1/1000 dilution streptavidin-biotinylated horseradish peroxidase complex (GE Healthcare, Hatfield, UK) in 1% BSA in PBS was incubated at room temperature for 30 min. The plate was rinsed 3 times with 200 μL 0.05% Tween 20 and once with 200

μL PBS before addition of 100 μL of 3,3',5,5'-tetramethylbenzidine (TMB, Microwell Peroxidase Substrate System, KPL, Maryland, USA) and incubation at room temperature for 10 min. 100 μL of 1 M orthophosphoric acid (APS Chemicals) was added and the absorbance was measured at 450 nm using a Perkin Elmer (Waltham, Massachusetts, USA) multimode plate reader, EnSpire 2300**.**

3.2.7 Cell Quantification with ImageJ

ImageJ (version 1.46r, National Institutes of Health, Bethesda, MD, USA) was used to process images of CFSE stained cells on the hydrogel discs. A minimum of 9 images taken at 120x magnification were used, the objective field area was randomly selected across the disc to obtain a representative sample. The images were converted to binary images and processed to subtract background and reduce noise. Objects above 113 μm^2 were counted, this area was calculated from the minimum cell diameter used for cell number determination, 12 μm for C2C12 cells (therefore π x 6 μm^2).

3.2.8 Cell Quantification with AQueous One

The assay used the CellTiter AQueous One Solution from the Cell Proliferation Assay kit (Promega). The cells were cultured on the hydrogels for 5 days, harvested with trypsin diluted 1/10 in EDTA and plated at $0.2x10^4$ cells/well in a 96 well plate for 3 days. On day 0, 1, 2 and 3 after subculture, 20 μL AQueous One was added and incubated at 37°C for 2 h, absorbance was measured at 490 nm using an Enspire 2300 plate reader.

3.2.9 Cell Quantification with alamarBlue

For cell adhesion the cells were seeded onto 4 mm diameter hydrogel discs at a concentration of $3.6x10^4$ cells/disc and incubated at 37°C for 30 min. Proliferation media (200 μL) was added to the wells and the plate incubated at 37°C for an hour, 10 μL alamarBlue was added and incubated at 37°C for 4

h. Fluorescence was measured using an excitation wavelength of 560 nm and an emission wavelength of 590 nm using an Enspire 2300 plate reader. The cell number was determined by comparison with a calibration curve of cells grown on tissue culture plastic. Cell concentrations were within the range that showed a linear relationship between cell number and the fluorescent signal.

For cell proliferation the cells were seeded onto 4 mm diameter hydrogel discs at a concentration of $0.4x10^4$ cells/disc and incubated at 37°C for 30 min. Proliferation media (200 μL) was added to the wells and the plate incubated at 37°C for an hour, 10 μL alamarBlue was added and incubated at 37°C for 4 h. Fluorescence was measured as described in 3.2.9. This procedure was repeated on day 1, 2 and 3 with the medium changed every day before and after the addition of alamarBlue. The cell number was quantified by referring to a calibration curve of cells grown on tissue culture plastic at concentrations within the linear range of the assay (i.e. there was a linear relationship between cell number and fluorescent signal).

3.2.10 Cell Proliferation with CellTiter-Glo

The assay used the CellTiter-Glo Luminescent Cell Viability Assay (Promega). 3T3 and C2C12 cells were seeded onto 8 hydrogel discs, 5 mm diameter, at a concentration of $2x10^5$ and $2.6x10^5$ cells/mL respectively and incubated at 37°C for 45 min. Proliferation media was added and the discs were further incubated at 37°C for 2 h. For the day 0 timepoint, 4 of the discs were used, these were transferred to a white plate and 50 μL CellTiter-Glo reagent was added. The plate was agitated at 500 rpm for 5 min and left at room temperature for another 25 min before luminescence was measured with a Perkin Elmer EnSpire 2300 multimode plate reader. The other 4 discs were incubated for 2 days and the assay procedure was repeated, this procedure was repeated with different time points.

3.3 Results and Discussion

3.3.1 Method Development

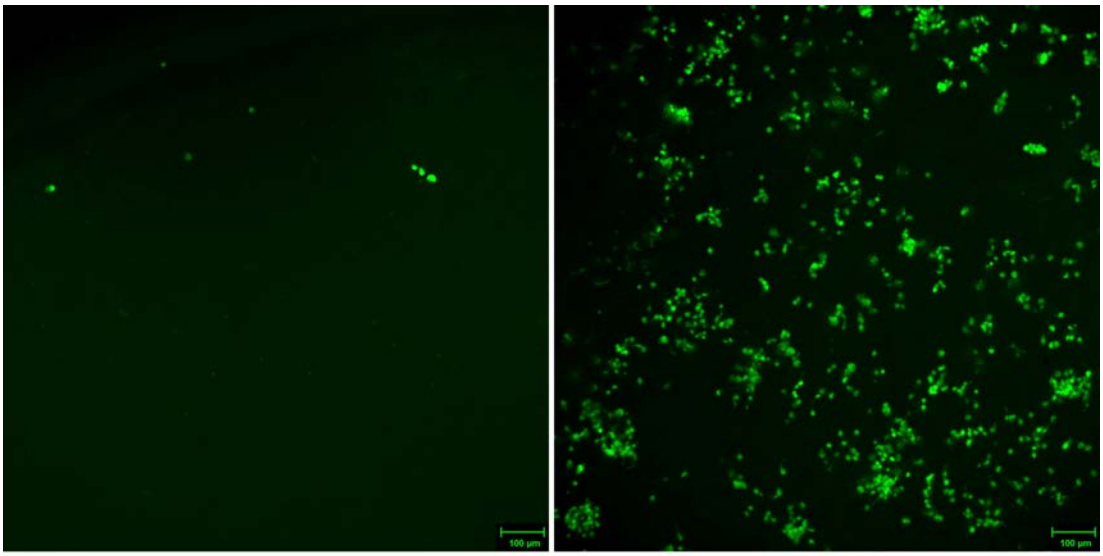

Figure 3.2: Adhesion of 3T3 cells on the hydrogels. On day 3 the cells were treated with trypsin as per standard cell harvesting protocol and the hydrogels stained with CFSE, scale bars show 100 μm.

To assess if the immobilisation of HS improved the bioactivity of the hydrogels, experiments were designed to examine if there were differences in cell behaviour. The cell behaviours examined were cell adhesion, cell proliferation and cell differentiation. Quantification of cell numbers on the hydrogels was difficult because of the nature of the hydrogels; as they were 3D, opaque and white. This meant that direct observation and imaging of the cells on the hydrogels was not possible. The following subsections provide the details of the trialled but unsuccessful methods for cell number quantification. These 3 techniques have been used with hydrogels and other scaffold materials but were ultimately unsuccessful due to the various difficulties created by the nature of the 3D porous hydrogel created in this work. The details of the successful method that was proven reliable and reproducible can be found in section 3.3.3.1.

A commonly used alternative approach for cell quantification involves harvesting the cells; this was attempted but it was not possible to remove all of the cells from the P(HEMA:GMA)-HS hydrogels using trypsin as the harvesting reagent (Figure 3.2). Another approach is to degrade or dissolve the scaffold to release the cells, but this was also not possible as PHEMA is not degradable. This suggested cell quantification would require a colorimetric or fluorescent stain followed by microscopic imaging. Images could then be analysed with software, such as ImageJ, to quantify the cell number present on each hydrogel. Cell proliferation determination can also be done with image analysis, however accurate quantification may be difficult at later time points due to cells migrating into the hydrogel, aggregating or fusing together as was the case with the C2C12 cells.

3.3.1.1 ImageJ

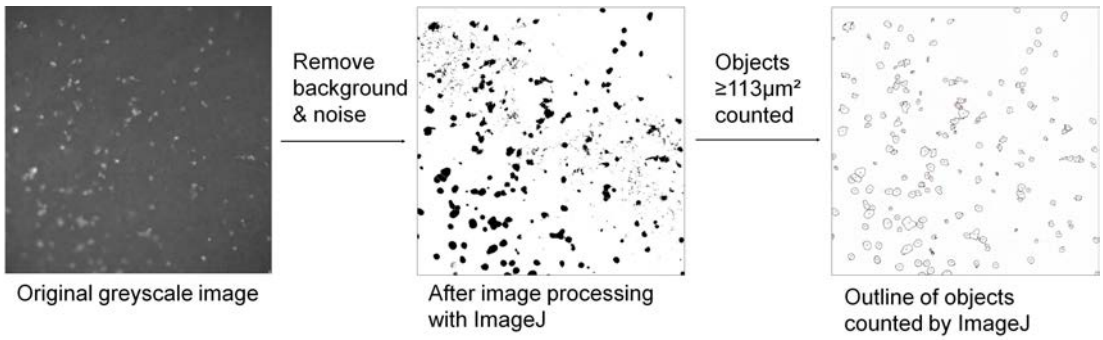

Figure 3.3: Scheme showing the image processing steps for cell counting using ImageJ.

The processing of images, of the CFSE stained cells grown on the hydrogels, using ImageJ was straight-forward. Analysis of 3 cell culture experiments with C2C12 cells was performed, the results showed the total cell number from 3 randomly selected fields on the hydrogels. The highest cell number was found on P(HEMA:GMA)-HS, which indicated that more cells had adhered to P(HEMA:GMA)-HS (Figure 3.4). Lower cell numbers were observed on P(HEMA:GMA) and the lowest cell numbers were on PHEMA. These results

demonstrated that the modifications on PHEMA improved the bioactivity of the hydrogel resulting in higher adhesion of C2C12 cells.

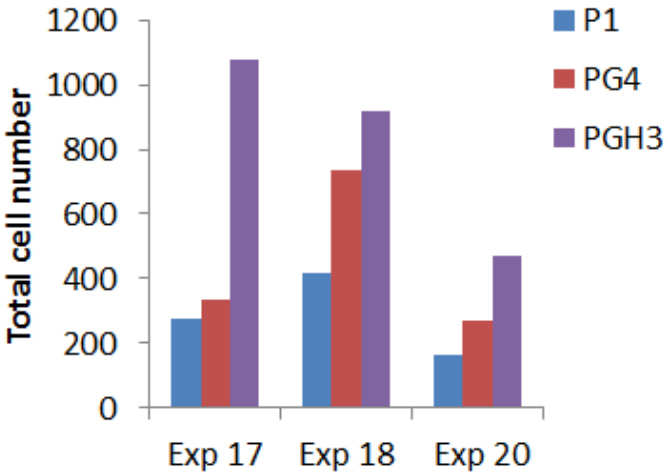

Figure 3.4: Total number of C2C12 cells on the hydrogels on day 1, n = 3. $1.7x10^4$ cells were seeded/disc for experiment 17 and $1.9x10^4$ for experiments 18 and 20.

However, due to situations where the cells were not evenly distributed across the hydrogel and where the cells aggregated or made contact with one another, it was difficult to determine how many cells were contained in the group. This affected the accuracy of the cell count and although it was observed to be an issue on day 1, giving rise to assay to assay variability, this variability was even more apparent from day 3 onwards. As the hydrogels were 3D, it was probable that the cells were at different levels in the hydrogels, with some being directly beneath or on-top of others. In this situation the signal from two cells was assessed as being from one very bright cell by the software. Due to these limitations, this method was not used further.

3.3.1.2 AQueous One Assay

The more recently developed AQueous One assay uses a tetrazolium salt that is reduced by cells to form a soluble formazan product. However, in my experiments not all of the formazan product remained in solution and variable

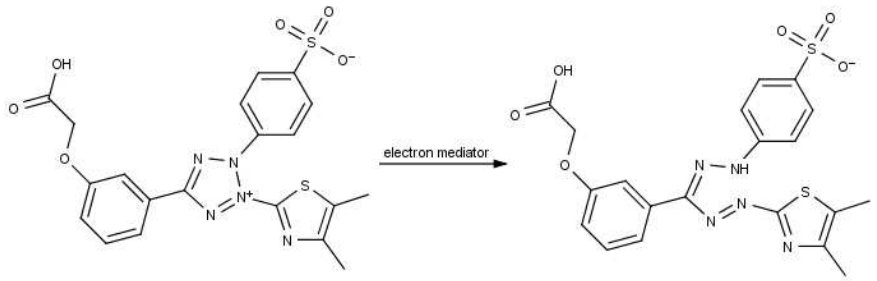

Figure 3.5: Bioreduction of AQueous One. The tetrazolium compound in AQueous One is bioreduced by cells to form the formazan product which can be detected in solution by absorbance measurements.

amounts of this product were deposited on the hydrogel and could not be solubilised for measuring in the plate reader, therefore direct quantification of cell number on the hydrogels was not possible. This assay was used to determine whether cell viability and cell proliferation were affected by cell exposure to the hydrogels. Accordingly cells grown on the hydrogels were harvested and re-plated onto tissue culture plastic and cell numbers were determined using the AQueous One assay at various times after plating. As seen in Figure 3.6 the proliferation of 3T3 cells that were harvested from the hydrogels very closely resembled the proliferation of the control cells (cells grown on tissue culture plastic for the entire time). Therefore, the 3T3 cells were not adversely affected after being cultured on any of the hydrogels.

The proliferation rate of C2C12 cells was also not affected by these cells having been cultured on the hydrogels for 5 days. Cell numbers increased after the cells were harvested from the hydrogels and plated on tissue culture plastic (Figure 3.7). Cell proliferation was similar for the cells harvested from each hydrogel and followed that of the control cells that were cultured on tissue culture plastic for the entire experiment. It is therefore reasonable to conclude that the hydrogels did not adversely affect the metabolic activity of either cell type and normal cell proliferation was maintained.

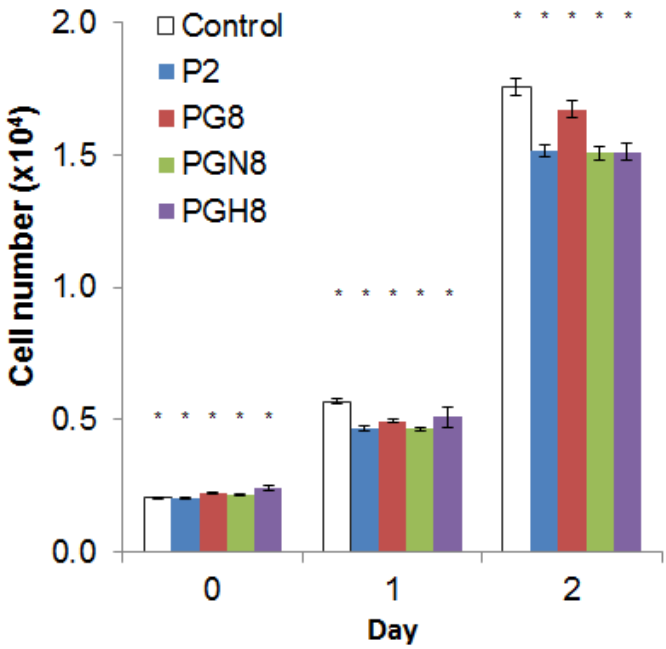

Figure 3.6: Cell proliferation of 3T3 cells after culture on the hydrogels. The cells were grown on the hydrogels for 3 days, harvested with trypsin and re-seeded onto tissue culture plastic for 2 days. The re-seeded cells were assayed everyday, control = cells on tissue culture plastic for entire experiment, n = 4, error bars show standard deviation, *non-parametric comparison of medians across timepoints.

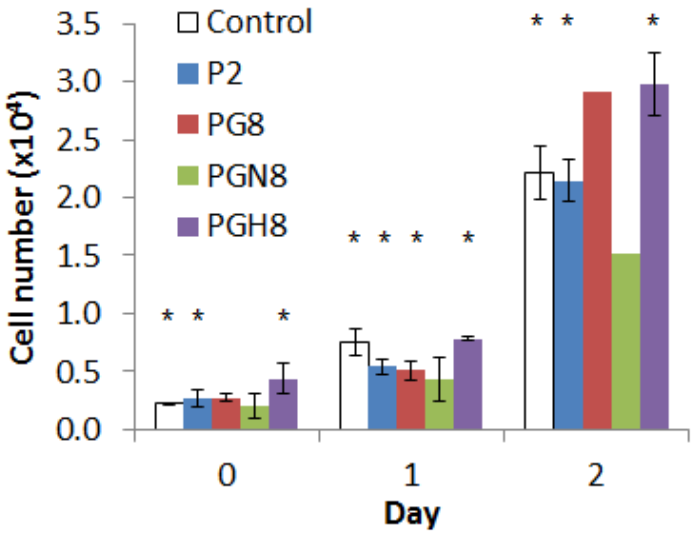

Figure 3.7: Cell proliferation of C2C12 cells after culture on the hydrogels. The cells were grown on the hydrogels for 5 days, harvested with trypsin and re-seeded onto tissue culture plastic for 2 days. The cells were assayed everyday, control = cells grown on tissue culture plastic for the entire experiment, n = 4, error bars show standard deviation. No standard deviation was calculated for PG8 and PGN8 on day 2 as only 2 results were obtained. *non-parametric comparison of medians across timepoints.

3.3.1.3 alamarBlue

The alamarBlue assay was tested to determine if direct quantification of the cell numbers on the hydrogels was possible. The active component in alamarBlue is resazurin which is a weakly fluorescent compound that is reduced by cells to the highly fluorescent resorufin (Figure 3.8). Unfortunately, as seen in Figure 3.10 the P(HEMA:GMA)-HS discs which had been incubated for 2 h with increasing numbers of C2C12 cells had higher fluorescent signal than the same number of cells seeded on tissue culture plastic. This indicated that there was a large background signal from the hydrogels and that a cell number of 5,000, or below, would not be detected. Nevertheless, an assay was conducted to assess whether it was possible to use alamarBlue to examine C2C12 proliferation. The number of cells on all hydrogels increased from day 0 to day 1 and 2 as measured by this assay (Figure 3.9). These results correlated well with the AQueous One results (Figure 3.7) except for PHEMA (P2 discs), where the cell number was markedly higher on day 2 than that deter-

mined previously with AQueous One. The results on day 3 were similar to day 2, but increased cell numbers were obtained when the discs were assessed on day 6. The plateau in cell proliferation observed from day 2 to 3 was unexpected, (a typical growth curve for C2C12 cells can be found here[183]), however the overall trend involved increased cell numbers over time.

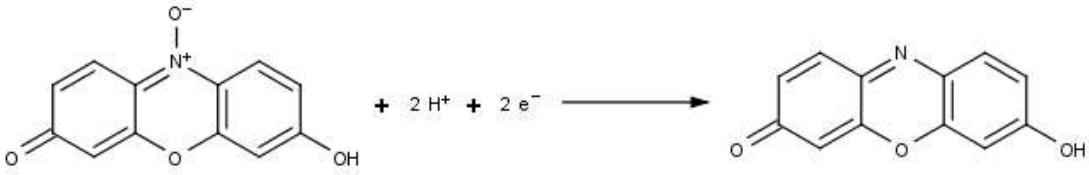

Figure 3.8: Reduction of resazurin to resorufin. Resazurin is the active component in alamarBlue which is reduced to fluorescent resorufin.

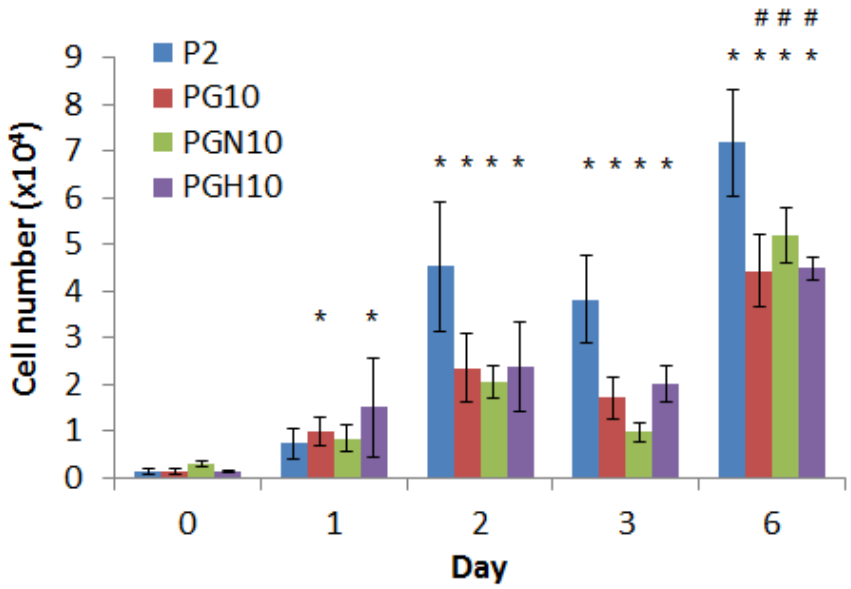

Figure 3.9: Proliferation of C2C12 cells on the hydrogels as determined by alamarBlue assay. Cells were seeded at a density of 400 cells/disc in proliferation medium, n = 4, error bars show standard deviation, *non-parametric comparison of medians across timepoints compared to day 0, #compared to day 1, except PGH10 which is compared to day 3.

An adhesion assay was performed on the hydrogels with alamarBlue. The cells appeared to have adhered better on PHEMA and P(HEMA:GMA)-HS than the

other hydrogels, the percentage of cells that adhered to the surfaces compared to the total number that was seeded was calculated (Table 3.1). The results showed that almost all of the cells seeded onto P(HEMA:GMA)-HS, 98%, adhered successfully to the surface. A large percentage of cells, 82%, adhered to PHEMA, while the other surfaces had about 60% adherence.

Table 3.1: Adhesion of C2C12 cells on the hydrogels as determined by alamarBlue.

Surface	Cells adhered (%)[1]
Control	64 ± 3
P2	82 ± 22
PG10	60 ± 22
PGN10	59 ± 23
PGH10	98 ± 44

[1]assay was performed 2 h after C2C12 cells were seeded onto the hydrogels in proliferation medium, control cells were on tissue culture plastic, n = 3, number of cells seeded was 36,500.

There were very large variations in the alamarBlue data, the standard deviation was much higher than that observed with the AQueous One assay (Figure 3.6 & Figure 3.9). The highest variability was seen with the cell number on PHEMA (Figure 3.9). The variability was likely due to the high background measured with alamarBlue and the hydrogels (with no cells present). This was also observed to be highly variable as 5 randomly selected discs had very different signals (Figure 3.10), 29-65% deviation. This was likely to have caused the apparent plateau in the proliferation assay from day 2 to 3 (Figure 3.9). It could also have affected the variability more at later time points as the background signal was observed to increase over the length of the experiment. This should not have occurred since alamarBlue has been reported to be stable in media (without cells present) for up to 3 days with 2-3% deviation in the fluorescent signal[184]. These results indicated that either the alamarBlue was not as stable as reported, or that there were interactions between the alamarBlue and the hydrogels that resulted in the reduction of alamarBlue without the presence of cells.

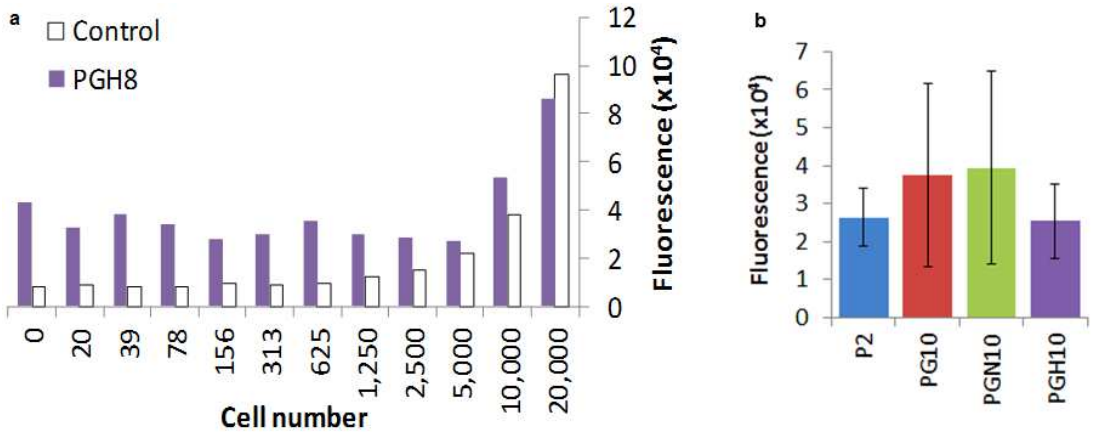

Figure 3.10: Assessment of the background fluorescent signal of alamarBlue with the hydrogels, a) C2C12 cells were assayed 2 h after seeding on PGH8 discs in proliferation medium and incubated for 4 h in alamarBlue, control = cells on tissue culture plastic, n = 1, b) hydrogels in the absence of cells, n = 5, error bars show the standard deviation.

Results from alamarBlue are known to be affected by the presence of proteins in the culture media during the incubation time of the assay. Studies have demonstrated that fetal bovine serum (FBS) and bovine serum albumin (BSA) can interfere with the reduction kinetics of the alamarBlue. The reduction in the rate of reduction of the alamarBlue has been shown to decrease the fluorescent signal by up to 35%[185]. Due to the potential interference and inhibition of the redox reaction of alamarBlue, it has been demonstrated to over-estimate cell numbers by 21-64%[186]. For these reasons some literature advises care in the conduct and verification of assay results while others recommend that the assay not be used for cell quantification[186,187]. Others have noted changes in cell morphology which suggested alamarBlue interference with normal cell function and possible cytotoxic effects[188]. Taking these facts into account it was likely that the high variability in the assays was due to an interaction between the hydrogels and cells, and alamarBlue. As a consequence of the variability no further experiments with alamarBlue were performed.

3.3.2 Cell Attachment

The cell adhesion to the hydrogels is shown in Figure 3.11 and Figure 3.12. The adhesion of both the 3T3 and C2C12 cells was very sparse on PHEMA.

Poor adhesion was indicated by the spherical, not spread cell morphology. In addition, the majority of cells were observed to clump together to form large cell clusters, suggesting the cells preferred to attach to one another rather than attaching to the PHEMA. This result was expected as PHEMA is well established as a biologically inert material[189] which is not attractive for cell adhesion[96].

Poor cell adhesion to PHEMA has been observed by others. The adhesion of human lung fibroblasts (IMR-90) to PHEMA gels showed spherical cell morphology with a significantly smaller projected cell area than the control, up to 5 times smaller. The poor cell adhesion diminished the total protein expression by the cells, specifically the expression of collagen and correlated with the inhibition of RNA expression and DNA synthesis[190]. The DNA synthesis was used as an indication of cell proliferation which was minimal on PHEMA. Poor or inhibited 3T3 cell adhesion was highlighted in work by Lewandowska[66], where the addition of a soluble RGD peptide to the culture medium resulted in spherical cell morphology and the 3T3 cells attaching to one another. Poor cell adhesion of 3T3 and MC3T3E1 (preosteoblasts) cells has also been shown on printed PHEMA scaffolds, the addition of poly-L-lysine was required for successful cell spreading and proliferation of both cell types[191].Cell morphology is closely linked to cell adhesion as the strength and success of cell adhesion is often determined by the morphology. In general a more spread morphology is indicative of better cell adhesion, the relationship between spread morphology and greater strength of 3T3 cell adhesion has been verified[192]. The morphology of 3T3 cells that are well adhered to a surface changes from dendritic to stellate or bipolar indicating that the cell-matrix interactions have matured[193].

The adhesion of the 3T3 cells to P(HEMA:GMA) and P(HEMA:GMA)-NH_2 was similar, with more cells seen on P(HEMA:GMA) (Figure 3.11). The cells remained spherical but did not form clusters, suggesting they had adhered to the hydrogel. The GMA content of the hydrogels was in the range of 142-157 μmol/g hydrogel. Work by Bayramoglu et al., incorporated 50 wt% GMA, resulting in 3.82 mmol GMA/g polymer[138], mesenchymal stem cells grown on the

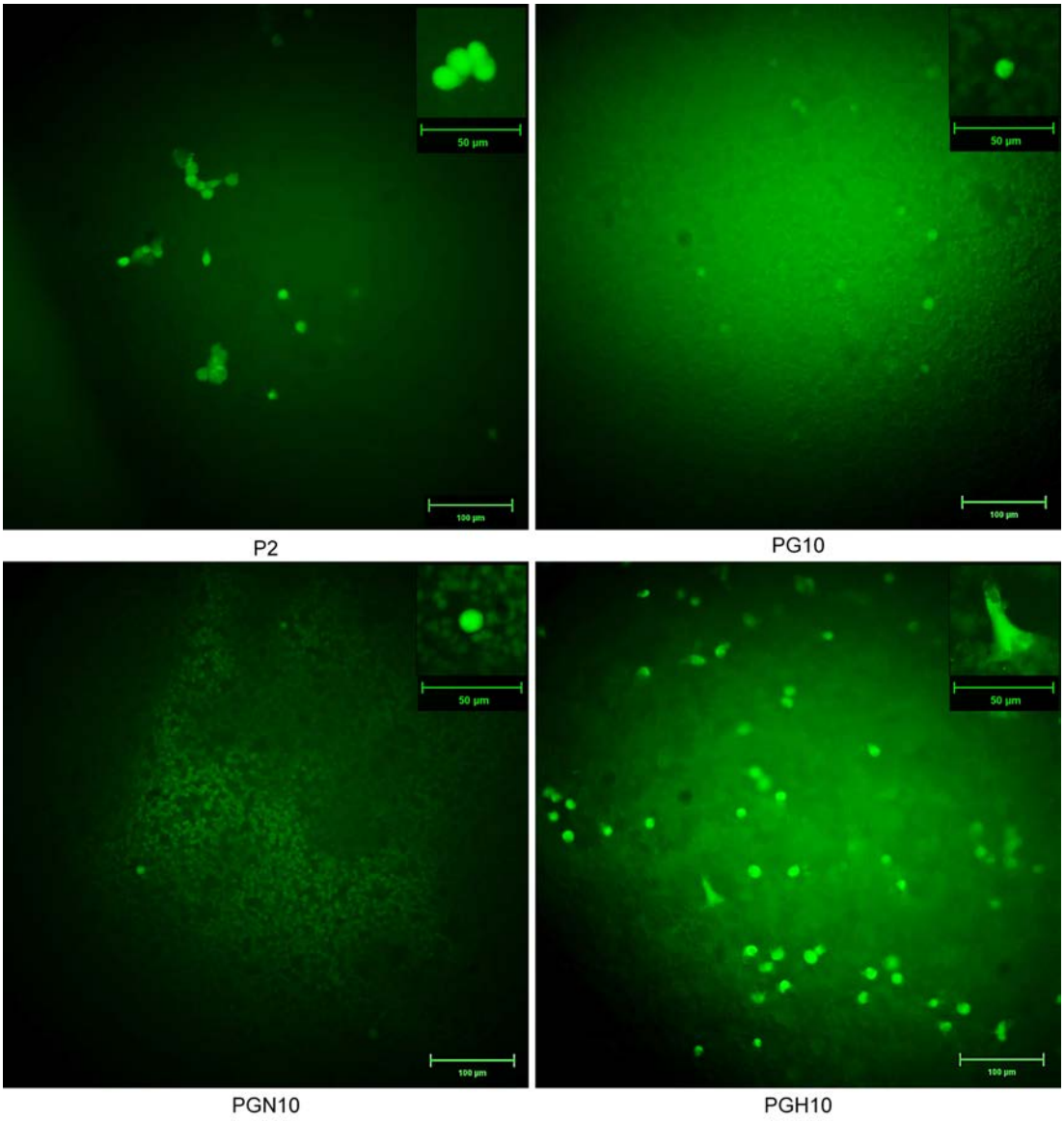

Figure 3.11: 3T3 cell adhesion to the hydrogels. The cells were stained with CFSE, 2 h after seeding on the hydrogels and imaged with fluorescent microscopy (Zeiss Axioskop), scale bars show 100 µm. Inserts show cell morphology, scale bars show 50 µm.

copolymer showed similar cell viability as the control cells (on tissue culture plastic). The incorporation of GMA and other hydrophobic polymers in PHEMA has shown improvements in cell adhesion and proliferation, as the addition of polycaprolactone improved cell adhesion and proliferation of fibroblasts[190].

The best substrate for 3T3 cell adhesion were the P(HEMA:GMA)-HS hydrogels. On this substrate many cells had spread morphology indicating that they

had attached firmly to the surface. Improved cell adhesion was also implied by the cell protrusions. The increased cell size and formation of small protrusions from the cells indicated a rearrangement of the cell cytoskeleton as the cells formed attachments to the surface[194]. These results indicated that the modifications to the PHEMA enhanced 3T3 cell adhesion; copolymerisation and incorporation of amine assisted the cells to adhere whereas immobilisation of HS produced the best cell adhesion.

More C2C12 cells adhered to the P(HEMA:GMA) and P(HEMA:GMA)-NH_2 hydrogels compared to PHEMA (Figure 3.12). On these hydrogels the cells adhered to the surface as single cells rather than the cell clusters seen on PHEMA. On P(HEMA:GMA)-NH_2 some cells were larger than those on PHEMA and had small protrusions indicating a more spread morphology. Therefore by visual comparison, the increase in cell spreading suggested the cells adhered better to P(HEMA:GMA) and P(HEMA:GMA)-NH_2. These results were supported by the literature as others have also found the introduction of amine groups, on PHEMA and other surfaces, assisted with cell adhesion and cell spreading[195,196]. It has been reported that the presence of amine groups increased the density of positive charge, which increased protein adsorption and adsorbed proteins, such as fibronectin, were orientated in a way that supported cell adhesion[197,198]. This improved cell spreading and resulted in cells that were more strongly attached due to the formation of more mature focal adhesion complexes and better organised actin stress fibres[196].

P(HEMA:GMA)-HS hydrogels were the most favoured for C2C12 cell adhesion. C2C12 cells on this hydrogel had a spread morphology indicative of stronger adhesion than on the other hydrogels and the cells had multiple protrusions.

These protrusions were visible after 2 hours (Figure 3.12), and became more obvious following rhodamine phalloidin staining, which stains polymerised actin (Figure 3.13). Single protrusions were seen on the C2C12 cells on P(HEMA:GMA)-NH_2, while those on P(HEMA:GMA)-HS had multiple (white arrows). The filamentous actin, stained by rhodamine phalloidin, is linked via a multi-protein complex to integrin cell adhesion molecules[194]. Rhodamine phalloidin is there-

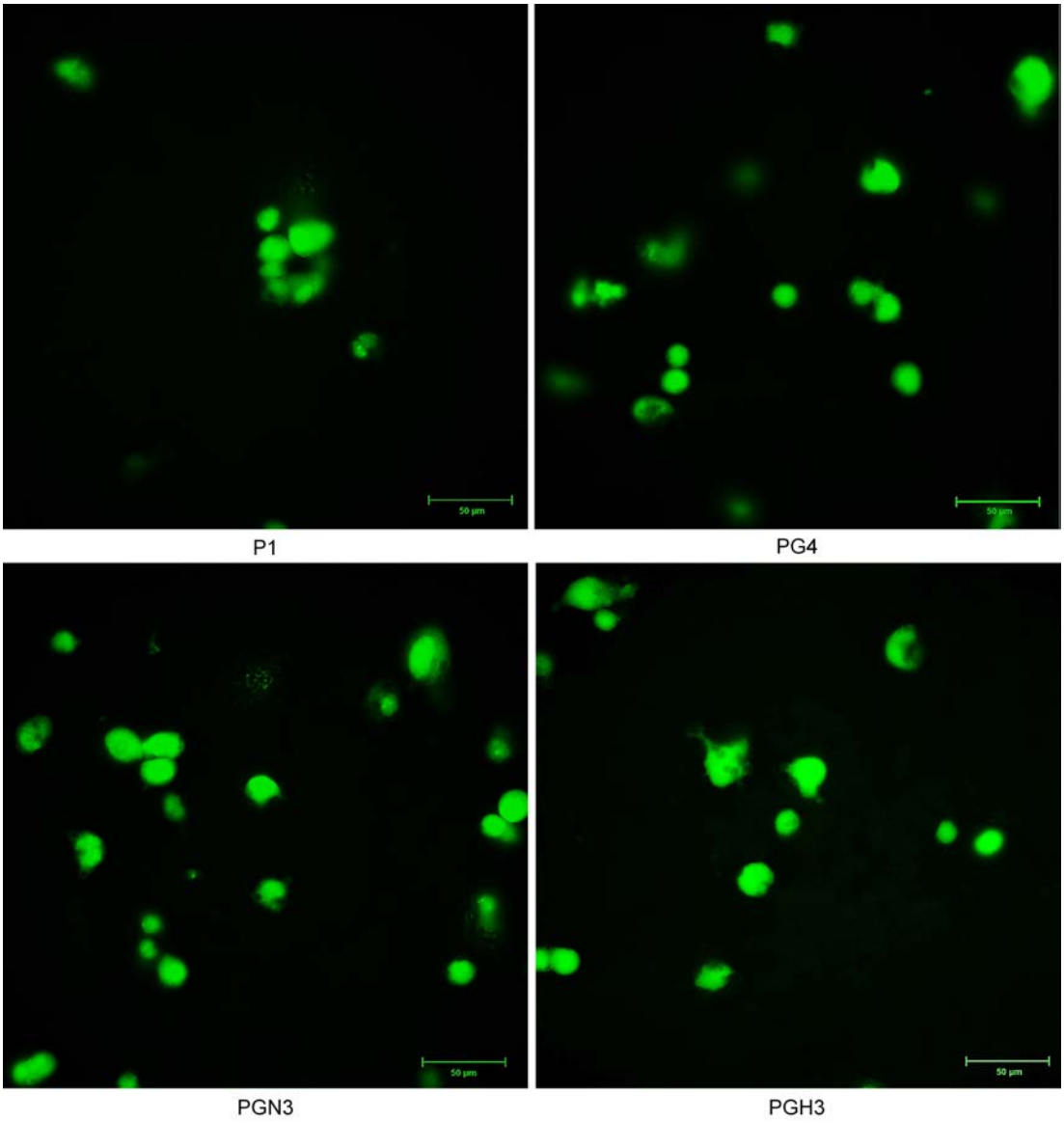

Figure 3.12: C2C12 cell adhesion to the hydrogels. The cells were stained with CFSE 2 h after seeding on the hydrogels and imaged with fluorescent microscopy (Zeiss Axioskop), scale bars show 50 μm.

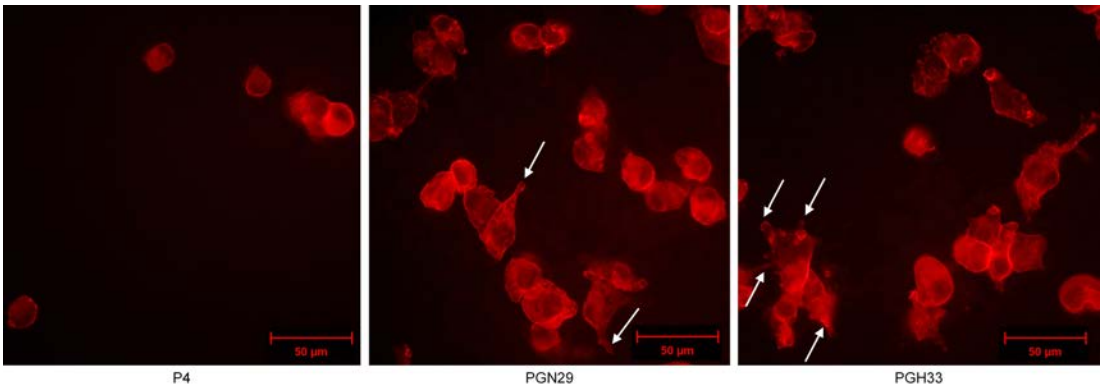

Figure 3.13: C2C12 cell adhesion to the hydrogels 2. The cells were stained with rhodamine phalloidin 2 h after seeding on the hydrogels and imaged with fluorescent microscopy (Zeiss Axioskop). Arrows indicate cell protrusions, scale bars show 50 µm.

fore often used to investigate cell spreading and the formation of cell adhesions[71,72].

Similarly to the 3T3 cells, the C2C12 cells adhered better following modification to the PHEMA hydrogel. The copolymer had some improvement in cell adhesion, the introduction of amine further improved adhesion and the best cell adhesion was observed on P(HEMA:GMA)-HS, where multiple cell protrusions were seen. These results revealed incremental increases with each modification in the ability of the hydrogels to support cell adhesion, but the final modification with the immobilisation of HS markedly improved the adhesion of both cell types to the hydrogel. The presence of soluble HS has been shown to increase the number of adhered cells and vinculin staining of astrocytes, these results indicated that the HS enhanced cell adhesion and increased the number of focal adhesions formed[199]. Therefore the presence of immobilised HS has been demonstrated in this work to act similarly to soluble HS by activating the integrin-based focal adhesions, increasing cell adhesion and cell spreading.

Considerable research has been done on the importance of HS proteoglycans and their roles in cell behaviour, cell adhesion, proliferation and differentiation. However HS has rarely been immobilised onto tissue engineering scaffolds, with most research focussed on the similar bioactivity of heparin. Some work

has used HS to load scaffolds with growth factors but few have tested the effects of immobilised HS alone. Of the few that have, they have been focussed on *in vivo* results. Therefore there is limited literature that investigates the potential benefits of immobilised HS with regards to increased cell adhesion. In the current work the immobilised HS was shown to drastically improve cell adhesion of both cell types.

3.3.3 Cell Proliferation

The proliferation of 3T3 and C2C12 cells was low to non-existent on the PHEMA hydrogels (Figure 3.15 and Figure 3.14). Little increase in 3T3 cell number was observed and compared to the other hydrogels, the lowest cell number was seen on day 4. The large cell clusters were clearly visible from day 2 on PHEMA, but absent on other hydrogels. Similar cell clusters were formed by C2C12 cells on PHEMA (Figure 3.15), with little cell proliferation observed over 6 days. This was probably because adherent cells require stable adhesion to a surface to be able to proliferate and grow[200].

By visual observation the proliferation of both cell types on P(HEMA:GMA) was similar to that on PHEMA. Some small 3T3 cell clusters were observed on P(HEMA:GMA) however the number and the size of these clusters was less than those observed on PHEMA. C2C12 cells were observed to migrate towards one another and form cell clusters on days 4 and 6. These clusters were also smaller than those observed on PHEMA, but may have attributed to the low proliferation observed as by day 6, the cell number on P(HEMA:GMA) had not increased. The cell morphology on P(HEMA:GMA) was more typical of C2C12 cells grown on tissue culture plastic, being elongated and fusiform shaped. These results indicated that both cell types had better morphology on P(HEMA:GMA) than on PHEMA but no observable difference in cell proliferation.

Few 3T3 cells were observed on P(HEMA:GMA)-NH_2 on days 1 and 2, however more cells were present on days 3 and 4 (Figure 3.14). This indicated that the cell proliferation was delayed but resulted in higher cell number on day

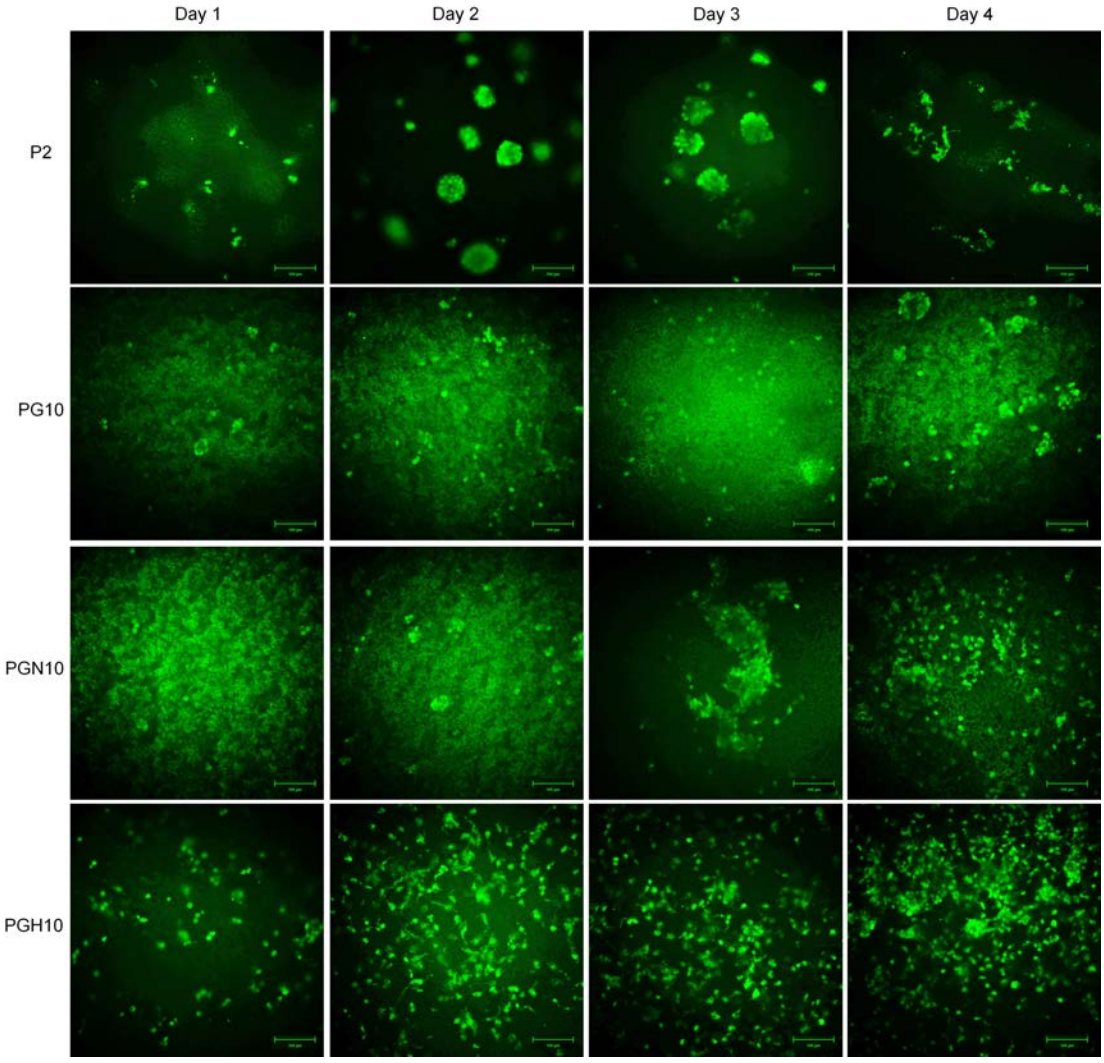

Figure 3.14: 3T3 cell proliferation over 4 days on the hydrogels. The cells were stained with CFSE and imaged with fluorescent microscopy (Zeiss Axioskop), scale bars are 100 μm.

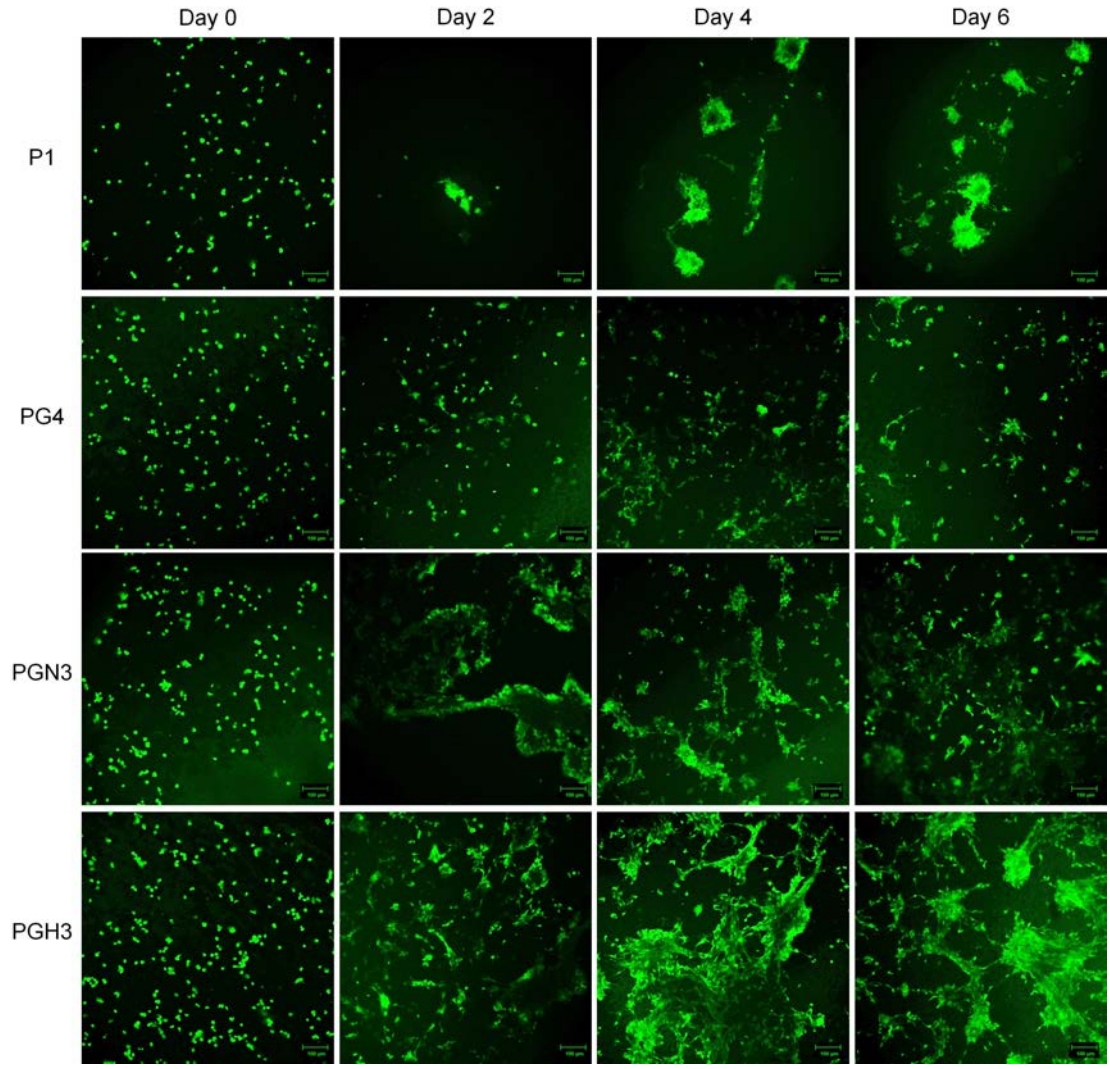

Figure 3.15: C2C12 cell proliferation over 6 days on the hydrogels. The cells were stained with CFSE and imaged with fluorescent microscopy (Zeiss Axioskop), scale bars are 100 μm.

4 than on PHEMA or P(HEMA:GMA). This was in contrast to the C2C12 cells on P(HEMA:GMA)-NH_2 which were more highly populated than PHEMA and P(HEMA:GMA) on days 2-6 (Figure 3.15). After several days, it was clear the C2C12 cells had proliferated more on P(HEMA:GMA)-NH_2 than on PHEMA or P(HEMA:GMA). As they proliferated they formed larger colonies of cells, however they maintained their elongated and fusiform morphology. These colonies were probably formed by proliferation and re-population of the hydrogel surface, than by the migration of cells towards one another, as overall there appeared to be more cells on these surfaces at the later time points. Others have observed that the introduction of free amines to PHEMA was compatible with increased fibroblast proliferation[195]. Similarly, nerve cells on chitin and chitosan scaffolds had improved growth following the introduction and increase of amines[201,202]. Here the introduction of free amines has affected and improved the proliferation of myoblasts more markedly than the fibroblasts.

The highest cell proliferation of both cell types was observed on P(HEMA:GMA)-HS. The proliferation of 3T3 cells was observed visually after 2 days (Figure 3.14) and continued to day 4 so that on P(HEMA:GMA)-HS there were more cells than on any of the other hydrogels. Similarly, by day 6, C2C12 cells on P(HEMA:GMA)-HS were observed to have increased markedly in number (Figure 3.15). In some areas the cells were approaching confluency and in these areas they organised and became aligned. Interestingly HS modified scaffolds are rarely investigated for their direct effect on cell proliferation, more commonly they are treated as a delivery device for growth factors. Soluble HS has been shown to increase cell proliferation of human mesenchymal stem cells (hMSC) in a dose dependent manner with enhanced results compared to soluble heparin[29]. In contrast soluble HS has been shown to enhance the cell proliferation of neural progenitor cells only when in the presence of a fibroblast growth factor (FGF)[81]. Since the hMSC were cultured with fetal calf serum (which contains basic FGF, bFGF) it is possible that the increased cell proliferation was also due to the combined presence of HS and bFGF. In this work fetal calf serum was also used therefore it is possible that the enhanced cell proliferation on P(HEMA:GMA)-HS was due to the presence of bFGF that

had been bound to the hydrogel by the immobilised HS. This possibility is supported by literature that reported the presence of HS and bFGF was required for fibroblast proliferation[181]. Therefore these results demonstrated that the immobilised HS retained its ability to promote fibroblast proliferation and extended its influence to also improve myoblast proliferation.

3.3.3.1 Cell Quantification with CellTiter-Glo

The data from the CellTiter-Glo assays is represented with box plots. The box plots show the interquartile range (IQR) with a coloured box, the box limits are the 1st and 3rd quartiles. The median is indicated with a horizontal black line within the coloured boxes and the whiskers extend to the highest and lowest data points that are within 1.5 times the IQR from the 1st and 3rd quartiles (tukey definition of whisker extent).

The results with the 3T3 cells showed that there was a statistically significant increase in cell number on the hydrogels from day 0 to day 2, except on PHEMA. On day 2 the number of 3T3 cells was significantly greater on P(HEMA:GMA)-HS compared to the number on PHEMA and P(HEMA:GMA)-NH_2 (a inFigure 3.16). These results confirmed the visual observations of the cells on the hydrogels (discussed in 3.3.3).

The results for the cell number on PHEMA on day 2 were quite varied. This was most likely due to the formation of large cell clusters as seen in Figure 3.14. These clusters were loosely attached to the PHEMA surface and could therefore be easily rinsed off during medium exchange. This would account for some of the results being quite low and close to the values from day 0 (as the cell clusters were rinsed off), while the other values were much higher and likely due to the presence of the cell clusters in the assay. A repeat of the assay showed the same general trend in the results, with a significant increase in cell number on P(HEMA:GMA)-HS (b inFigure 3.16). These results indicated that the 3T3 cells proliferated better and more quickly on P(HEMA:GMA)-NH_2 and P(HEMA:GMA)-HS compared to PHEMA. This demonstrated that the modification of PHEMA was successful in improving the bioactivity and enabling 3T3

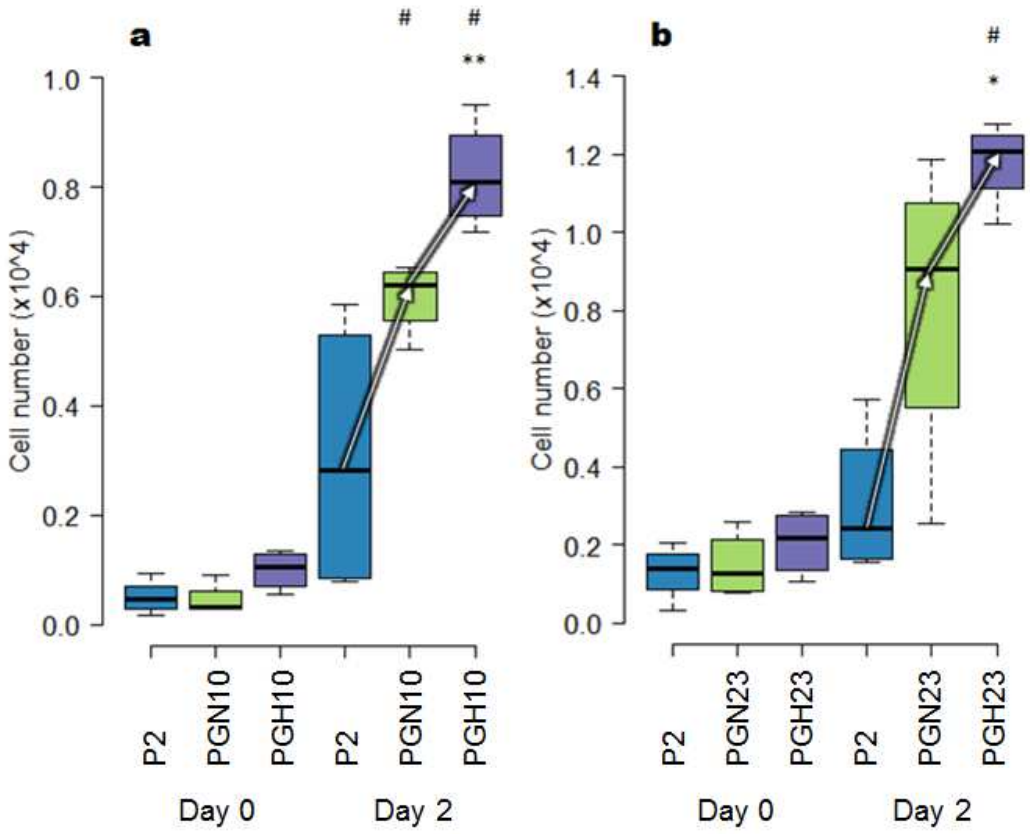

Figure 3.16: Proliferation of 3T3 cells on the hydrogels as determined by CellTiter-Glo, n = 4. Statistics were analysed using a non parametric comparison of median values and for an increasing trend with the Jonckheere-Terpstra test ($p<0.05$). a) **PGH10 > P2 and PGN10, # day 2 results > day 0, b) * PGH23 > P2, # day 2 results > day 0.

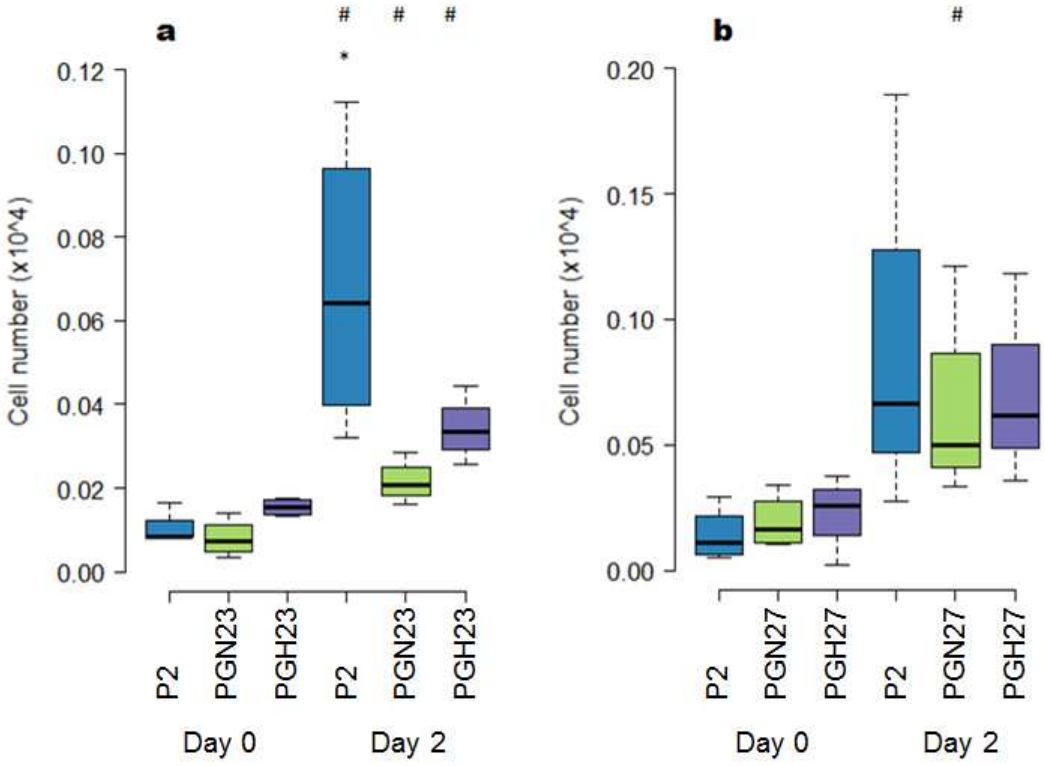

Figure 3.17: Proliferation of C2C12 cells on the hydrogels as determined by CellTiter-Glo, n = 4. Statistics were analysed using a non parametric comparison of median values ($p<0.05$). a) *P2 > PGN23, # all day 2 results > day 0, b) # day 2 PGN27 > day 0 PGN27.

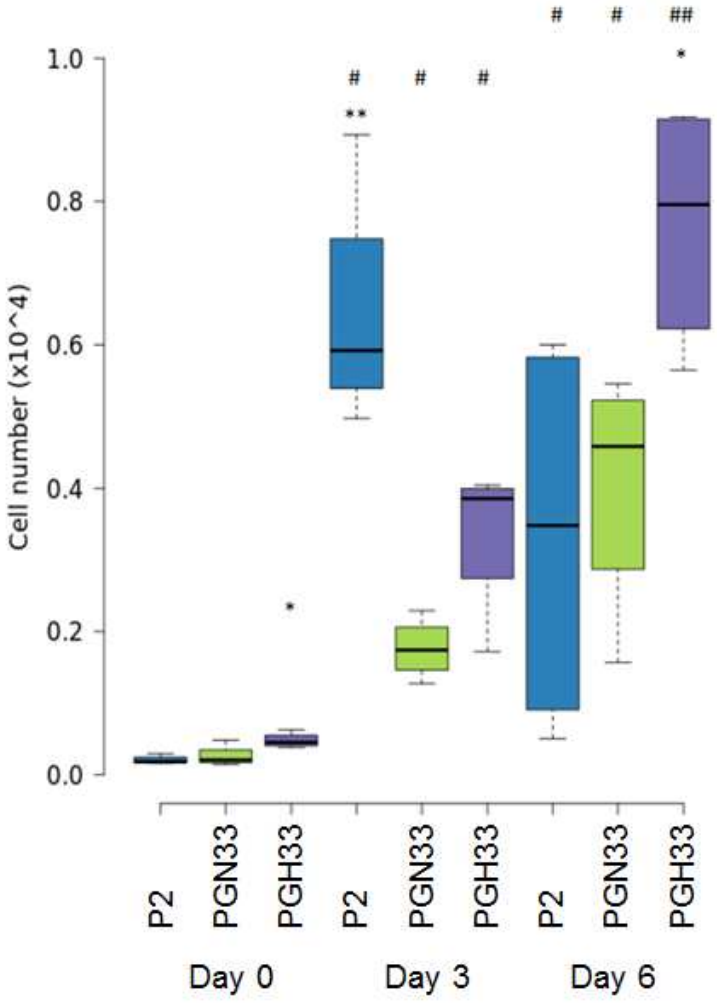

Figure 3.18: Proliferation of C2C12 cells on the hydrogels as determined by CellTiter-Glo 2, n = 3. Statistics were analysed using a non parametric comparison of median values ($p<0.05$). *day 0 PGH33 > P2, *day 6 PGH33 > PGN33, **day 3 P2 > PGN33 and PGH33, # all day 3 & 6 results > day 0, ## day 6 PGH33 > day 3 PGH33.

cells to proliferate better on the hydrogel.

C2C12 cells were observed to increase in cell number from day 0 to 2 on all of the hydrogels. The increase in C2C12 cell number on day 2 was statistically significant for each hydrogel (a in Figure 3.17). The increase in cell number was not as large as that seen for the 3T3 cells, this was likely due to the slower proliferation rate of C2C12 cells. There was a large variability observed for the cell number determined on PHEMA (Figure 3.17). This variability was likely due to the formation of cell clusters on PHEMA, these were observed in Figure 3.15. When the assay was repeated similar results were obtained. The results showed a small increase in cell number on P(HEMA:GMA)-NH_2 on day 2 compared to day 0 (b in Figure 3.17). The variability in the cell number was higher for all hydrogels than in the previous assay. The small difference observed in cell number was most likely due to the selection of day 2 as a time point, C2C12 cells are slow proliferators therefore a later time point would be more appropriate.

The assay time points were adjusted from day 2 to day 3 and an additional time point at day 6 was added. The results from the assay showed more significant differences in cell number between time points (Figure 3.18). The number of C2C12s on PHEMA increased significantly from day 0 to day 3 and on day 6 appeared to be similar to that on day 3 or slightly decreased. In contrast the cell number on P(HEMA:GMA)-NH_2 and P(HEMA:GMA)-HS increased significantly from day 0 to day 3 and 6. The results showed that the later time points were more appropriate to validate the proliferation of the C2C12 cells and that the C2C12 cells proliferated better and more quickly on P(HEMA:GMA)-NH_2 and P(HEMA:GMA)-HS compared to PHEMA. These results supported the visual observations of the C2C12s as seen in Figure 3.15. These results further confirmed that the modification of PHEMA was successful in increasing the bioactivity of the hydrogel resulting in improved proliferation of C2C12 cells.

The literature shows that minimal cell proliferation is observed on neat PHEMA scaffolds. Generally molecules are added to PHEMA to improve cell proliferation, such as gelatin[203], poly-L-lysine[191], fibronectin[66] and RGD[204]. The variability in cell number measured in the current work could be due to a few

factors. The first possibility was due to the method of polymerisation, in a glass mould, which resulted in the formation of a skin layer along the surfaces that were in contact with the glass. The formation of a skin layer has been observed by others[102,205]. The variability in the cell number measured could therefore have been due to the presence of a thin skin which was easily broken, such areas could have provided a better surface for cell adhesion resulting in the patchy distribution of cells on PHEMA from day 1 onwards. Another possibility was the formation of the cell clusters. The large size of the cell clusters meant that the large cell counts on PHEMA could have been solely due to the cells within the clusters. This would have indicated that the cells counted by the assays were present on PHEMA but in a quiescent form.

These results showed the improved bioactivity of PHEMA after modification, especially after HS immobilisation. HS is a coreceptor for many growth factors that are involved in cell proliferation[173], therefore its immobilisation on the hydrogel might be expected to assist cell proliferation. Interestingly, the incorporation of heparin (a GAG similar to HS, but more sulfated) onto a collagen scaffold was shown to similarly improve fibroblast proliferation[177]. HS has been shown to increase the proliferation of preosteoblast cells in a concentration dependent manner when introduced as a soluble protein in the medium**?** . Here it has been shown that HS not only assists in fibroblast proliferation but has a similar effect on the proliferation of myoblasts.

The CellTiter-Glo assay had the ability to be used directly on the hydrogels to determine the number of cells. This was a large advantage over the other assays that were tested and this assay was found to be the most reliable for cell proliferation data with these hydrogels. The signal produced was luminescent which resulted in markedly lower background than those measured with the other assays (see method development section). This improved sensitivity enabled comparison between cells grown on the different hydrogels. As the hydrogels were 3D there were some diffusion issues which produced some variability in the data, however this assay was best able to demonstrate differences in cell numbers on the hydrogels. The CellTiter-Glo system created quantitative results that correlated well with the visual observations of the cells

on the hydrogels.

3.3.4 Cell Differentiation

The beginning stages of C2C12 cell differentiation was observed when the cells were cultured in proliferation media. After 6 days of culture on P(HEMA:GMA), P(HEMA:GMA)-NH_2 and P(HEMA:GMA)-HS the C2C12 cells appeared to be in the early stages of differentiation as evidenced by their fusiform morphology (Figure 3.20). This was not observed on PHEMA. The next step in differentiation involves the re-organisation of the cells to align themselves parallel to one another. Little to no cell organisation was observed on P(HEMA:GMA) and P(HEMA:GMA)-NH_2, but alignment occurred on P(HEMA:GMA)-HS (white arrows) and some cell fusion was evident. As C2C12 cells approach confluency their morphology changes to bipolar as the cells change into myocytes. The myocytes align and fuse to form multinucleated myocytes which mature into myotubes[206], as depicted in Figure 3.19.

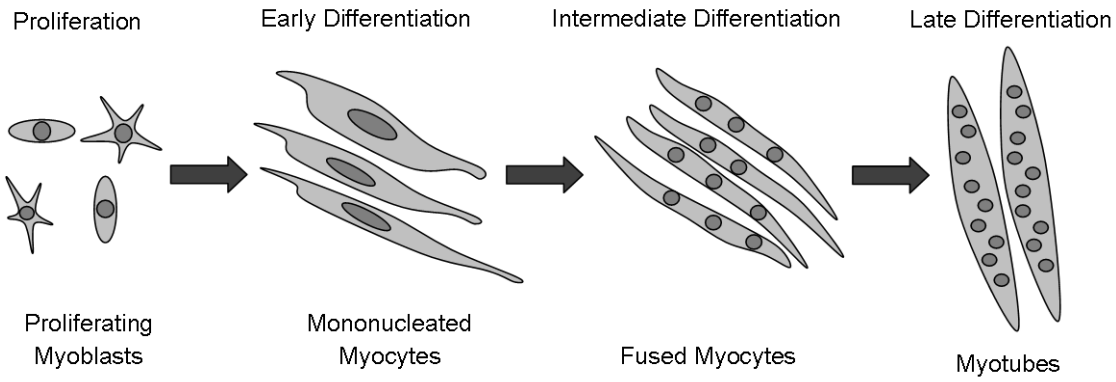

Figure 3.19: Schematic diagram of the stages of C2C12 differentiation.

The differences in C2C12 cell morphology and behaviour were more pronounced following rhodamine phalloidin staining. The cells on PHEMA were spherical with diffuse staining suggesting relatively unorganised filaments (Figure 3.21). In contrast, the cells on P(HEMA:GMA)-NH_2 had fusiform morphology showing

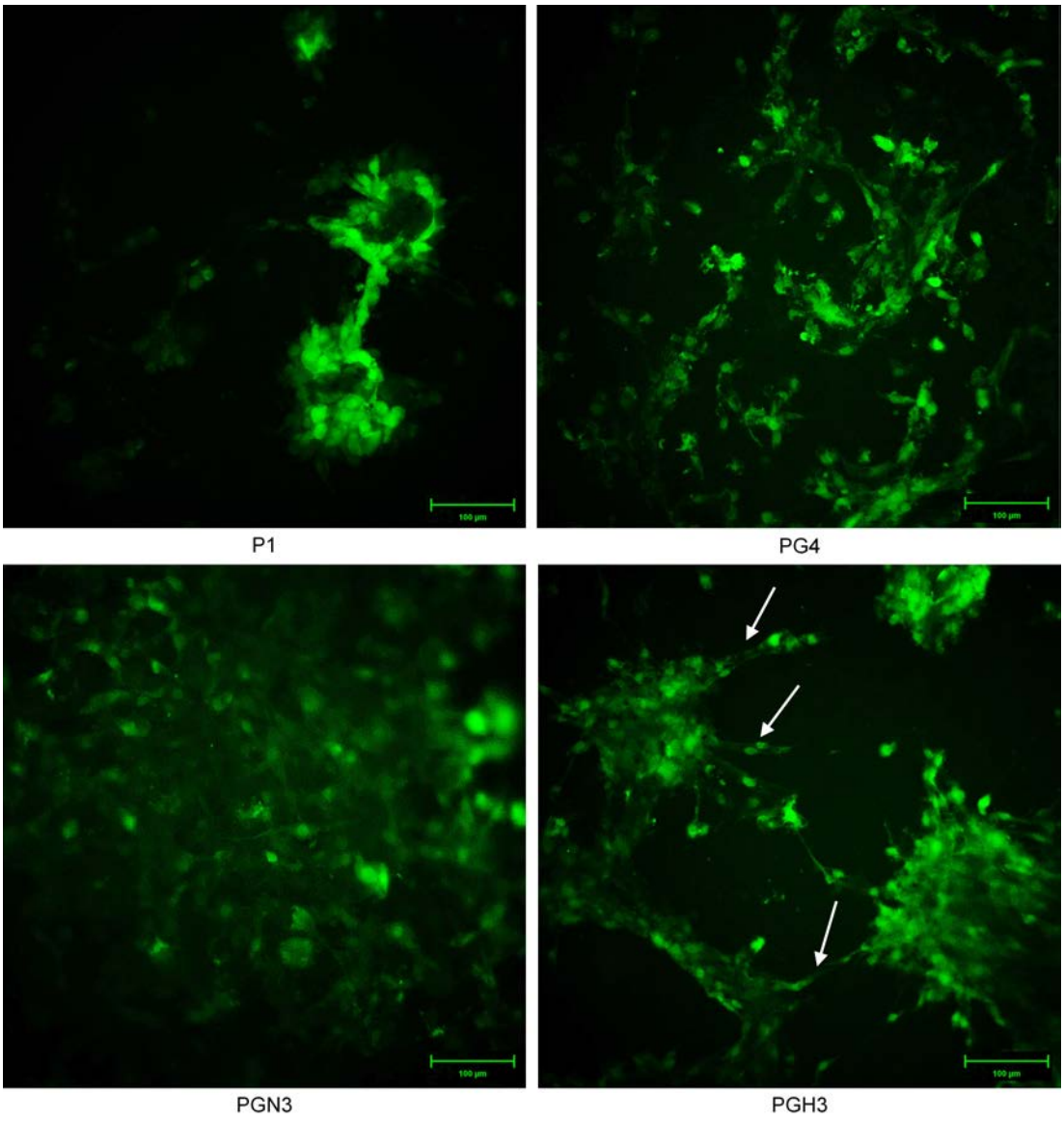

Figure 3.20: Beginning stages of C2C12 cell differentiation on hydrogels. The C2C12 cells were cultured in proliferation media and stained with CFSE on day 6. Imaged with fluorescent microscopy (Zeiss Axioskop), scale bars show 100 μm.

that the filaments were organised, the cells were elongated and by day 6 were beginning to become aligned. On P(HEMA:GMA)-HS the cells were fusiform in low cell density areas and in confluent areas had aligned and begun to fuse (Figure 3.21). Hence, all the modifications of PHEMA assisted in C2C12 cell differentiation but the inclusion of HS had the greatest effect on differentiation when the cells were cultured in proliferation media. These results indicated the requirement of HS immobilisation on the hydrogels to facilitate cell differentiation of the C2C12 cells. HS is involved in strengthening cell-cell adhesions and as a coreceptor involved in differentiation[173], it is required for the binding of growth factors to coordinate the change from proliferation to differentiation[80]. It has been demonstrated that the inhibition of syndecan-3 (a HSPG) expression in C2C12 cells impeded cell differentiation[178]. Additionally the requirement of both HS and bFGF for the differentiation of myoblasts has been reported[181]. Therefore its immobilisation on the hydrogel in an active form resulted in successful myotube formation.

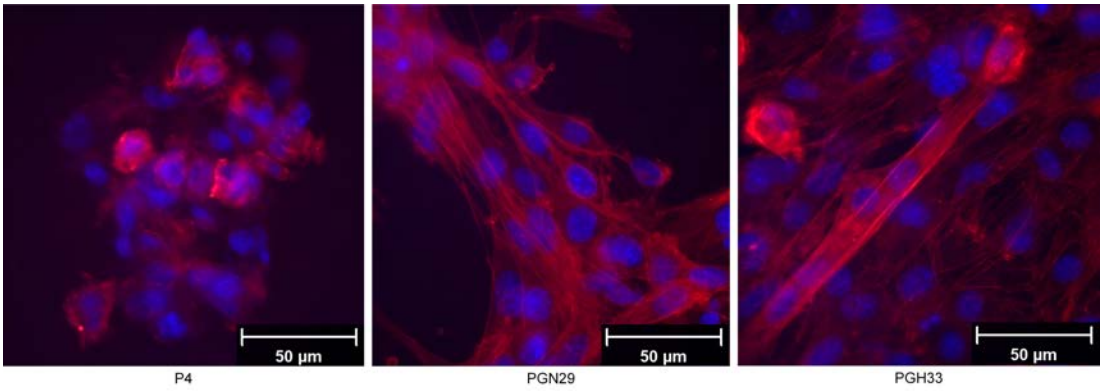

Figure 3.21: Beginning stages of C2C12 cell differentiation on hydrogels 2. The C2C12 cells were cultured in proliferation medium and fixed on day 6 with 4% paraformaldehyde and stained with rhodamine phalloidin (red) and DAPI (blue), scale bars show 50 µm.

3.3.5 Enzyme Linked ImmunoSorbant Assay

The ELISA results showed that more of the basic fibroblast growth factor was absorbed and eluted from the HS modified scaffold than PHEMA or the other

hydrogels. The hydrogels with immobilised HS bound 1.7-100 times more growth factor compared to PHEMA, P(HEMA:GMA) and P(HEMA:GMA)-NH_2. These results were demonstrated in 3 separate assays as seen in Figure 3.22. These results showed a consistently lower signal from PHEMA, P(HEMA:GMA) and P(HEMA:GMA)-NH_2, which were not markedly different to one another. The low values were likely due to physically entrapped growth factor in the 3D hydrogels. The signals from P(HEMA:GMA)-HS were consistently and notably higher, this confirmed the bioactivity of the immobilised HS. The 2 hydrogels used, PGH8 and PGH10, had 3.09 ± 0.05 μmol HS/g hydrogel and 0.6 ± 0.2 μmol HS/g hydrogel respectively. The ELISA results were 417 and 497 ng bFGF for PGH8 and 83 ng bFGF for PGH10, these results had a fold difference of 5 - 6 times which correlated with the approximate 5 fold difference in immobilised HS. Therefore the assay was sufficiently sensitive to measure the fold differences in HS immobilisation which translated to equivalent fold differences in bFGF binding.

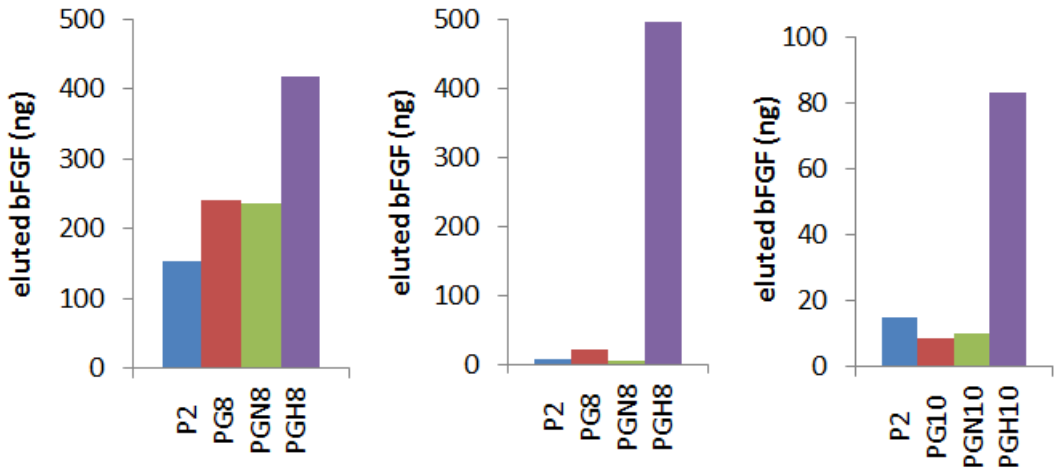

Figure 3.22: Bioactivity of immobilised HS on hydrogels, the amount of bFGF bound to the hydrogels by immobilised HS as determined by ELISA, n = 1.

Assays with duplicate discs (Figure 3.23) confirmed the trend despite the high standard deviation observed. A higher signal was obtained from P(HEMA:GMA)-HS compared to the other hydrogels, but the measured amount of growth factor

varied substantially. The results were 3.8 times greater for PGH10 than in the previous assay. Therefore the assay was repeated with more replicate hydrogel discs to reduce the experimental variability.

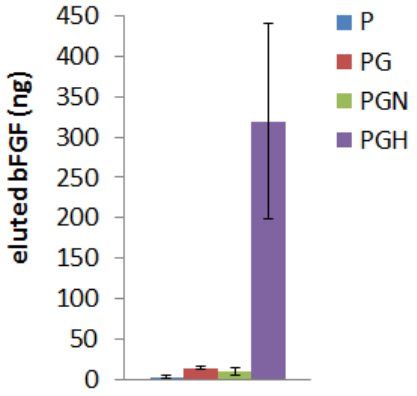

Figure 3.23: Bioactivity of immobilised HS on the hydrogels 2. The amount of bFGF bound to the immobilised HS on the hydrogels as determined by ELISA. The assays had duplicate discs and duplicate technical replicates, n = 4, error bars show the standard deviation.

ELISAs with 4 replicate hydrogel discs attempted to further reduce the experimental variability. As there were no large differences between the other hydrogels, only P(HEMA:GMA)-NH_2 was used as the control. The HS modified discs were shown to elute 100 ng bFGF/disc compared to 30 ng bFGF/disc from P(HEMA:GMA)-NH_2(Figure 3.24). The assay showed a 3 fold increase in signal from P(HEMA:GMA)-HS compared to P(HEMA:GMA)-NH_2. The trend was consistent with the previous assays and the increase in replicate discs resulted in a decrease in the standard deviation. The overall results demonstrated that the immobilised HS retained its bioactivity as P(HEMA:GMA)-HS was able to specifically bind bFGF. These results provided evidence for the enhanced bioactivity of P(HEMA:GMA)-HS over PHEMA which was shown to improve cell adhesion and proliferation of both cell types on P(HEMA:GMA)-HS. These improvements were likely due to the ability of the immobilised HS to bind and interact with proteins to provide signals that enhanced cell behaviour on the hydrogels.

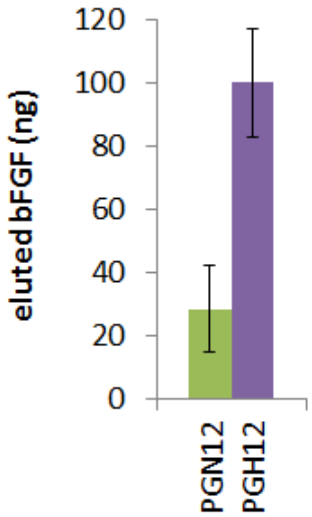

Figure 3.24: Bioactivity of immobilised HS on the hydrogels 3. The amount of bFGF bound to immobilised HS on the hydrogels as determined by ELISA. The assays had 4 discs of each hydrogel and duplicate technical replicates, n = 8, error bars show the standard deviation.

3.3.6 Immunofluorescence of Cell Expressed Fibronectin

Matrix protein expression, specifically the expression of fibronectin is beneficial for cell adhesion as fibronectin acts as an adhesive protein in binding cells to a surface[158]. Additionally the complete adhesion of fibroblasts requires the binding of extracellular fibronectin to cell surface receptors and HS proteoglycans[207]. The expression of fibronectin was examined to explain any observed differences in cell adhesion to the hydrogels, as fibronectin expression is one of the prominent cell responses for successful cell adhesion and cell spreading[208]. Therefore differences in the amount of fibronectin visualised on the hydrogels should match the trends observed with cell adhesion and cell proliferation.

The cells were cultured on the hydrogels, fixed and stained to visualise the fibronectin produced by the cells. As a control the hydrogels were also stained for fibronectin without any cells present. This was to observe whether the protein was specifically absorbed by the hydrogels after incubation in serum. No specific staining was observed and no staining was seen when the hydrogels were incubated in a concentrated solution of fibronectin (data not shown). Controls were also performed by growing the cells on the hydrogels and replacing

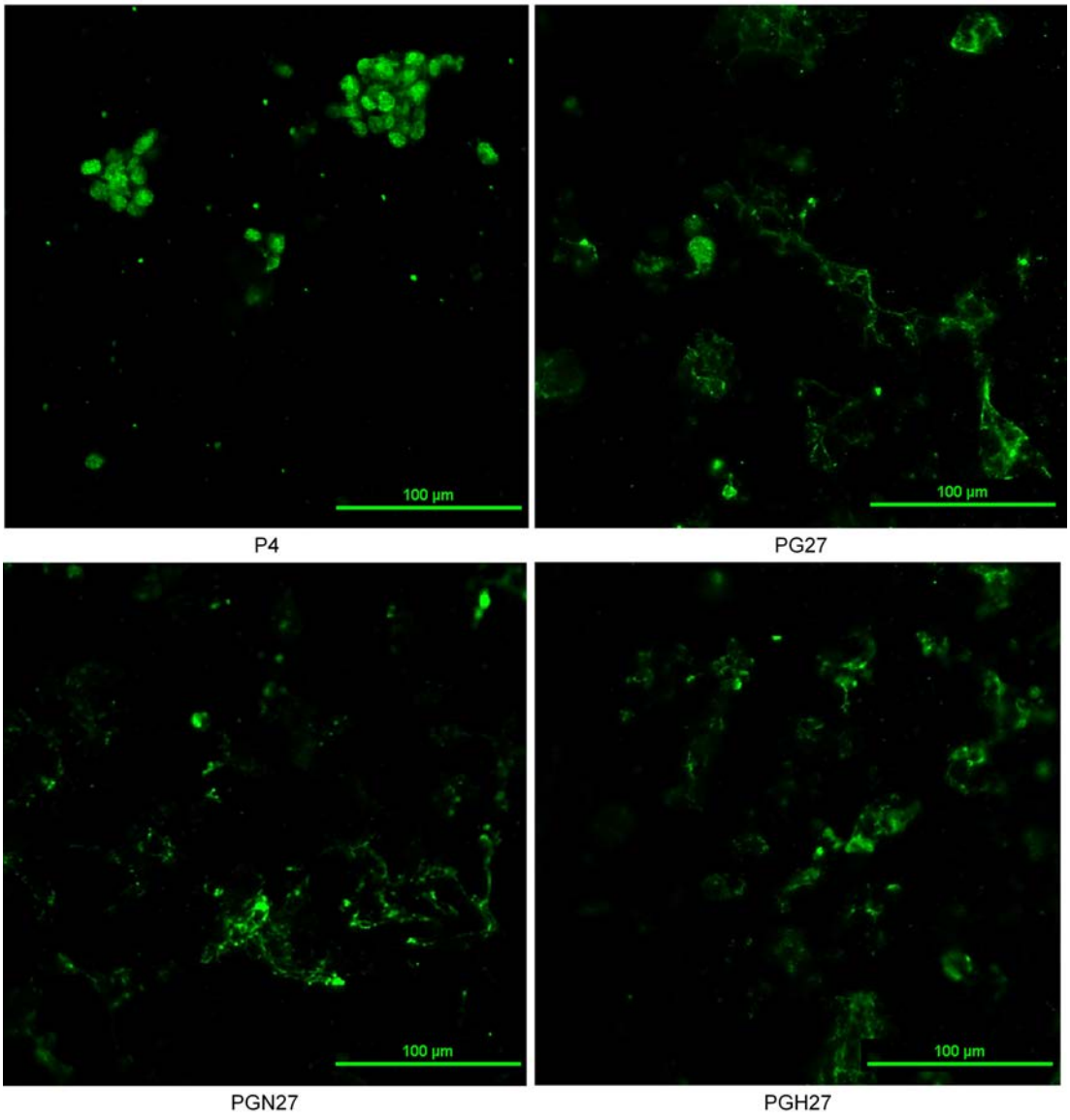

Figure 3.25: Examination of fibronectin expression of 3T3 cells grown on the hydrogels. The cells were grown for 3 days, fixed with 4% paraformaldehyde and stained with fibronectin antibody (ab2413) followed by secondary antibody (Alexa Fluor® 488 F(ab')2 goat anti-rabbit IgG, green), scale bars are 100 µm.

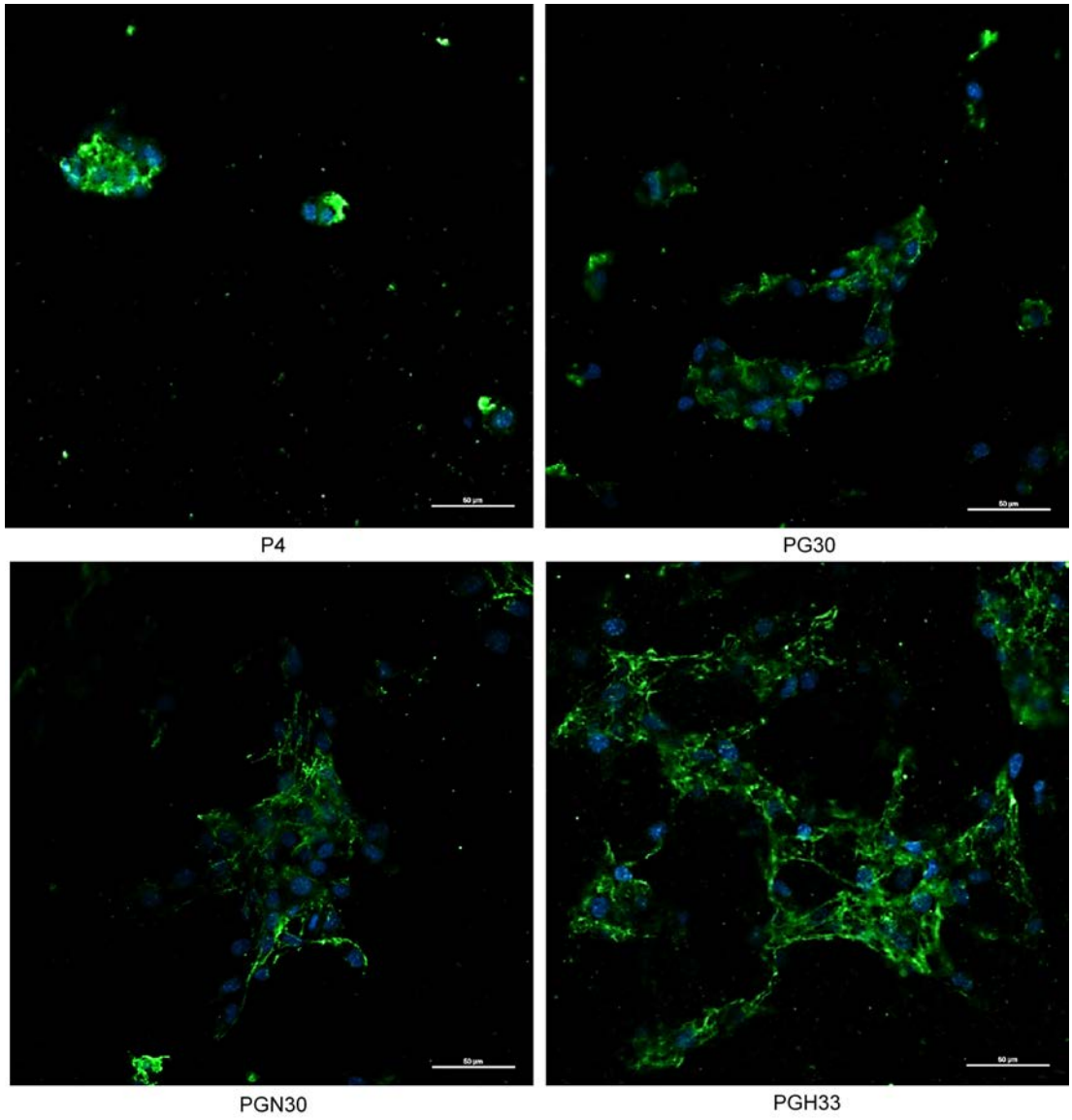

Figure 3.26: Examination of Fibronectin expressed by C2C12 cells grown on the hydrogels**.** The cells were grown for 2 days, fixed with 4% paraformaldehyde, stained with fibronectin antibody (ab2413) followed by secondary antibody (Alexa Fluor® 488 F(ab')2 goat anti-rabbit IgG, green) and DAPI for the nucleus (blue), scale bars are 50 μm.

the incubation of the primary antibody to fibronectin with a buffer incubation. This tested for any unspecific absorption of the secondary fluorescent antibody by the cells or the hydrogels and was negligible (Figure A.3).

The fibronectin staining for the 3T3 and C2C12 cells grown on the hydrogels is shown in Figure 3.25 and Figure 3.26 respectively. The lowest fibronectin expression was seen for both of the cell types grown on PHEMA. The fibronectin was only observed close to the centre of the cells, which correlated with the cell morphology, small and spherical. The size of a fibronectin coated area has been shown to influence cell behaviour such as morphology and cell spreading[209]. Therefore as the cells on PHEMA were not expressing large amounts of fibronectin, they were unable to create a large enough fibronectin coated area to spread onto. This in turn affected their adhesion, the poor cell adhesion then further inhibited cell proliferation.

Similar fibronectin expression was observed by the 3T3 cells grown on the other hydrogels (Figure 3.25). The expressed fibronectin was seen to be fibrillar and occasionally spanned between cells. This indicated that the fibronectin had been organised by the cells, this happened during cell spreading as the secretion of their own fibronectin assisted in their adhesion[210]. It has been demonstrated that cells have the ability to sense the macromolecular composition of the surface and adjust their biosynthetic activity[211]. Therefore as the 3T3 cells produced similar amounts of fibronectin with similar organisation, it could be said that the different hydrogels were equally suitable for fibroblast adhesion and all hydrogels were more suitable than PHEMA.

The fibronectin staining of the hydrogels after C2C12 culture showed extensive fibronectin production by the cells (Figure 3.26). As with the 3T3 cells, the C2C12 cells had the lowest fibronectin expression when grown on PHEMA. The other hydrogels showed similar fibronectin expression to each other and all were markedly greater than that seen on PHEMA. The fibronectin staining was observed as long fibres stretched between the C2C12 cells. This fibrillar structure of fibronectin indicated that the cells had organised the protein to optimise cell processes such as adhesion and spreading.

HS has a known affinity for fibronectin, the HS-fibronectin binding is impor-

tant for integrin associated cell adhesion which has a role in focal adhesion formation[212]. Therefore HS was expected to assist in greater fibronectin deposition by both cell types, there was no observable increase for the 3T3 cells and the C2C12 cells had a moderate increase. There were a few possibilities to explain why an increase was not observed for the 3T3 cells and why the increase was only moderate for the C2C12 cells. Firstly HS-fibronectin binding is relatively weak (100-1000 fold weaker than HS-bFGF binding) and therefore consists of multiple reversible interactions[212]. Secondly the synthesis of fibronectin is known to change during myogenesis[211] therefore if the myoblasts were approaching confluency and preparing to differentiate they would rely less on having a fibronectin matrix around themselves[34]. Despite this, there was a clear improvement in fibronectin organisation by the C2C12 cells on P(HEMA:GMA)-HS. Many fibronectin fibres were stretched between the cells to form a substantial protein network. In conclusion all of the modified hydrogels showed enhanced cell expression and organisation of fibronectin in comparison to PHEMA, therefore all of the modifications were successful in improving cell behaviour.

3.4 Conclusions

Cell adhesion of 3T3 and C2C12 cells was observed to be better on the modified PHEMA hydrogels. This was seen visually with the fluorescent staining of the cells and was also confirmed by assay. The imaged cells were observed to be more spread and show protrusions coming from the cells when cultured on P(HEMA:GMA)-NH_2 and P(HEMA:GMA)-HS. The increased cell attachment on P(HEMA:GMA)-HS was shown with ImageJ analysis of cell images and confirmed with the assay results.

The proliferation of 3T3 and C2C12 cells was observed to be faster and superior on the modified PHEMA hydrogels. This was observed visually with the fluorescent staining of the cells and was quantified by assay. The AQueous

One system proved that there were no adverse effects on either cell type after their culture on all of the hydrogels. Both cell lines proliferated similarly to control cells grown on tissue culture plastic. Direct quantification of cell number on the hydrogel scaffolds was successful with the CellTiter-Glo assay.

The proliferation of both cell lines on PHEMA was observed to be very variable, but with a general increasing trend. The cell proliferation on P(HEMA:GMA)-NH_2 and P(HEMA:GMA)-HS was better with the best cell proliferation observed on P(HEMA:GMA)-HS. These results indicated that the presence of the HS had a significant effect on cell behaviour. The differentiation of C2C12 cells was only observed on P(HEMA:GMA)-HS. This result indicated that the presence of HS was required for the initiation of differentiation and the successful formation of myotubes.

The ELISA results confirmed the bioactivity of the HS after immobilisation on the hydrogels. The signal from P(HEMA:GMA)-HS was significantly above the other hydrogels indicating that the growth factor was specifically bound to the HS. The ELISA results correlated well with the improvement in cell behaviour that was seen on P(HEMA:GMA)-HS compared to the other hydrogels. Cell expression of fibronectin was greater and more organised on the modified hydrogels in comparison to PHEMA. These results indicated that all of the modifications of PHEMA improved the bioactivity of the hydrogel. The improvement in bioactivity resulted in the enhancement of cell behaviour including; cell adhesion, proliferation and differentiation. The best cell behaviour was observed on P(HEMA:GMA)-HS indicating that this was the most successfully modified PHEMA hydrogel.

Chapter 4

Biological Characterisation of P(HEMA:GMA)-RGD, P(HEMA:GMA)-HS and RGD and Intermediates

4.1 Introduction

This chapter focuses on the characterisation of the bioactivity of P(HEMA:GMA)-RGD and P(HEMA:GMA)-HS&RGD. While the peptide from fibronectin and other extracellular matrix proteins that facilitate cell adhesion, have been immobilised on a variety of materials, to my knowledge there is only one previous report of RGD immobilisation on sponge PHEMA[144]. These researchers found immobilised RGD improved cell invasion of the hydrogel. In contrast, the incorporation of RGD with other forms of PHEMA have been investigated by a number of groups. For example, GRGD immobilised on a PHEMA film was found to increase 3T3 fibroblast spreading when the cells were grown in serum-free medium[72]. A PHEMA brush has similarly been functionalised with an RGD containing peptide and this improved the adhesion and spreading of human umbilical vascular endothelial cells[204]. Another PHEMA brush was modified with RGD and PHSRN (which is a synergistic site from fibronectin), the co-

presentation of the peptides resulted in synergistic effects that enhanced cell adhesion[130].

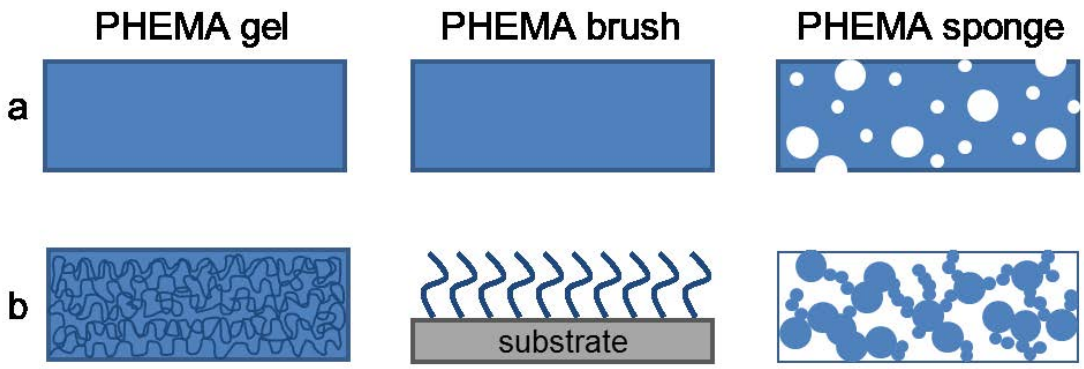

Figure 4.1: The different forms that PHEMA has been synthesised as. a) macroscale schematic of the different forms of PHEMA, gel and brush surfaces are smooth and continuous, sponge PHEMA has large pores, b) microscale schematic showing the difference in the arrangement of the polymer.

The immobilisation of both HS and RGD on the same scaffold has not been reported for PHEMA scaffolds or scaffolds of any other material. The immobilisation or incorporation of multiple biomolecules in scaffolds has generally been confined to a protein or GAG with a growth factor, multiple growth factors or multiple peptides. For example, a peptide that binds heparin has been covalently attached to a fibrin scaffold, and the heparin in turn bound and presented bFGF[176]. The incorporation of all 3 components (peptide, heparin and bFGF) was shown to be required for enhanced neurite extension, with an 100% increase compared to the fibrin scaffold alone[176]. Heparin has been attached to a number of different scaffolds to improve their bioactivity; such as a collagen scaffold, which improved fibroblast adhesion and proliferation[177]. The possibility that heparin may act synergistically with lactose to promote chondrocyte adhesion, proliferation and viability has been explored using a chitosan scaffold[213]. Additionally heparin was crosslinked within a hyaluronan scaffold in the hope of sequestering vascular endothelial growth factor and angiopoietin-1. The scaffold with heparin produced intact microvessel beds with mature vessels walls *in vivo*[24].

Co-presentation of various peptides known to be involved in cell adhesion have been found to improve cell adhesion and cell proliferation when immobilised on scaffolds. For example CDRGDS and CWQPPRARI enhanced the endothelial cell proliferation on a polytetrafluoroethylene surface[214] A mixture of GRGDSS with KKKTTK was used to create a self-assembled monolayer which demonstrated increased cell adhesion and spreading of 3T3 cells[215]. The immobilisation of PDSGR and YIGSR on a PEG scaffold promoted greater cell survival of pancreatic β-cells and glucose stimulated greater insulin release compared to that seen when the β-cells were cultured on the scaffolds with each peptide individually[216]. Importantly RGD has been co-immobilised on alginate with a heparin binding peptide, GGGGSPPRRARVTY, allowing RGD and heparin to be present on the same scaffold. These scaffolds provided the best support for cardiac tissue development in comparison to the scaffolds functionalised with only one of the molecules[217]. These results suggest there is great potential for co-immobilised biomolecules to act synergistically to improve cell functions and hence improve their application as tissue engineering scaffolds.

This current work investigated the effect of the co-immobilisation of HS and RGD on sponge PHEMA, and provided comparison of each end modification, that is: P(HEMA:GMA)-HS, P(HEMA:GMA)-RGD and P(HEMA:GMA)-HS&RGD (from here referred to collectively as end modification hydrogels). The end modification hydrogels were additionally compared with the intermediate hydrogels (P(HEMA:GMA) and P(HEMA:GMA)-NH_2) to demonstrate any improvement in cell behaviour that was attributed to the immobilisation of RGD or HS and RGD. The comparisons allowed for the investigation of any synergistic effects of having both HS and RGD immobilised on the same hydrogel. The bioactivity of the hydrogels was assessed with the culture of 2 cell types on the hydrogels, immunofluorescent staining of cell expressed fibronectin and ELISA.

4.2 Experimental Procedure

Kwikdiff was purchased from Thermo electron corporation. Other reagents, the cell culture procedure and the immunofluorescent staining of fibronectin were the same as those used in Chapter 3.

Cell Staining For Kwikdiff staining the cells were first fixed by incubating them in 0.5 mL of warm 4% formaldehyde at room temperature for 30 min in the dark. The discs were rinsed twice with 1 mL PBS and the cells were then permeabilised with 0.5 mL cold 0.1% (v/v) TX-100 and incubated at 4°C for 4 min. The discs were rinsed twice with 1 mL PBS and then 50 μL of Kwikdiff solution 3 was added. The discs were rinsed 4 times in 1 mL ultra-pure water and then incubated in ultra-pure water for 16 h at room temperature.

Cell Proliferation with CellTiter-Glo Assay The same procedure outlined in chapter 3 was used except for the introduction of rinses for the hydrogel discs immediately before the addition of the CellTiter-Glo reagent.

Enzyme Linked ImmunoSorbant Assay The ELISA protocol was identical to that described in chapter 3 except for the increase in elution time, from 10 to 30 min, and the dilution factors used for the samples was 20 times.

4.3 Results and Discussion

4.3.1 Cell Adhesion

The cell adhesion was investigated 2 hours after cell seeding on the hydrogels. Both cell types had poor adhesion on PHEMA as discussed in chapter 3. The 3T3 cell adhesion on P(HEMA:GMA)-RGD was observed to be similar to that on P(HEMA:GMA)-NH_2 and P(HEMA:GMA) (Figure 4.2). There

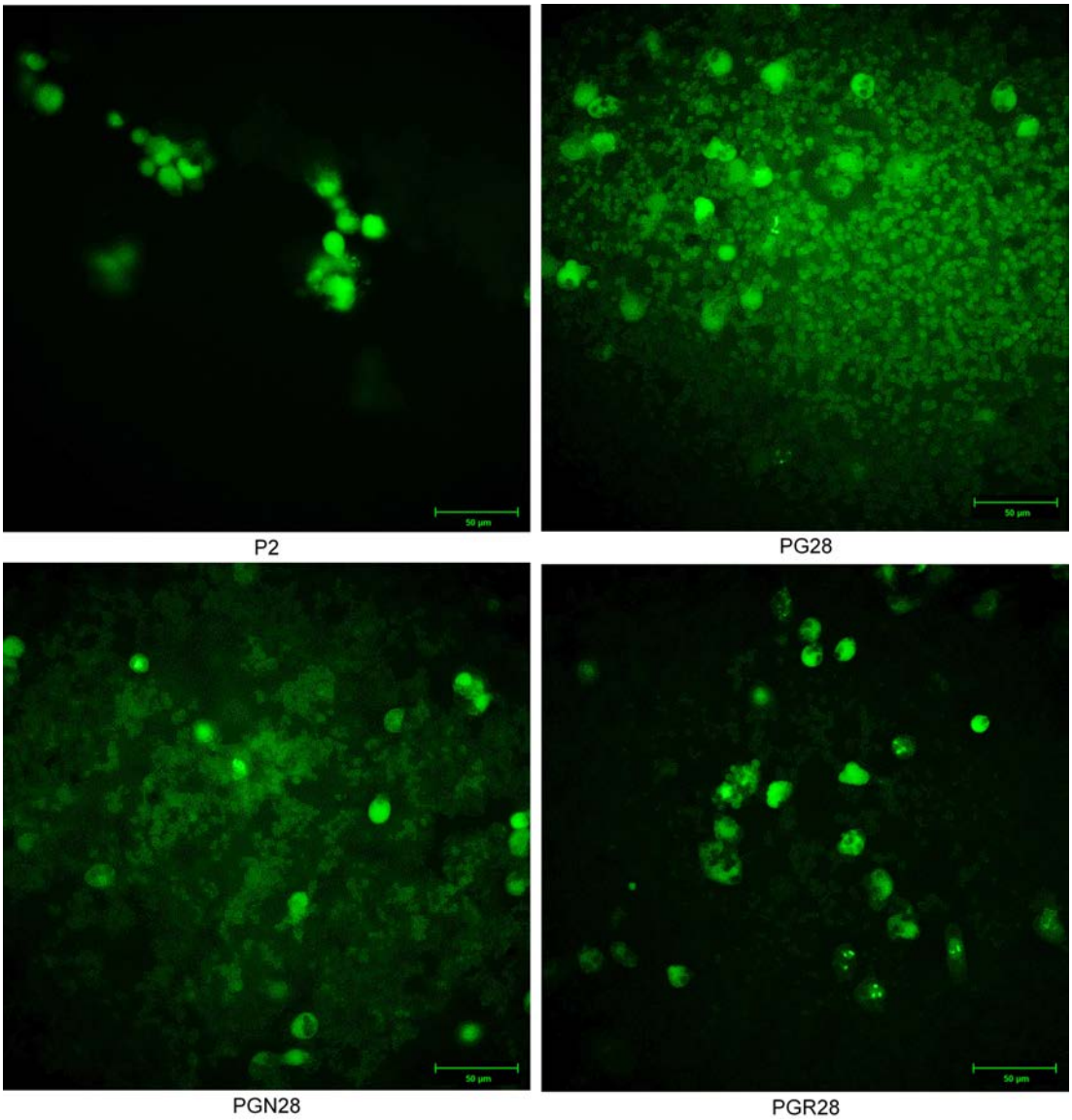

Figure 4.2: Adhesion of 3T3 cells on the hydrogels. The cells were stained with CFSE 2 h after cell seeding and the experiment was performed in duplicate, scale bars show 50 μm.

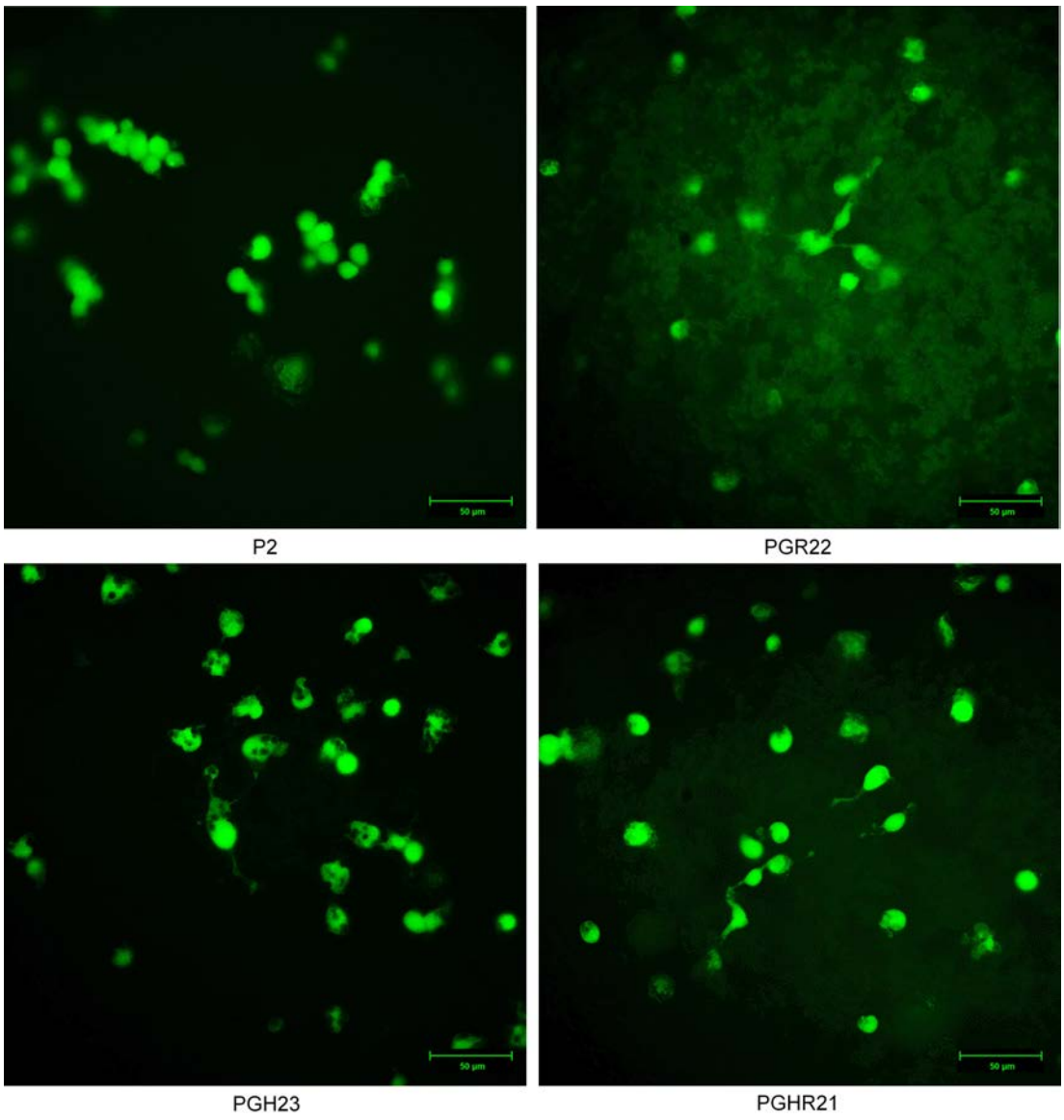

Figure 4.3: Adhesion of 3T3 cells on the end modification hydrogels. The cells were stained with CFSE 2 h after cell seeding, the scale bars show 50 μm.

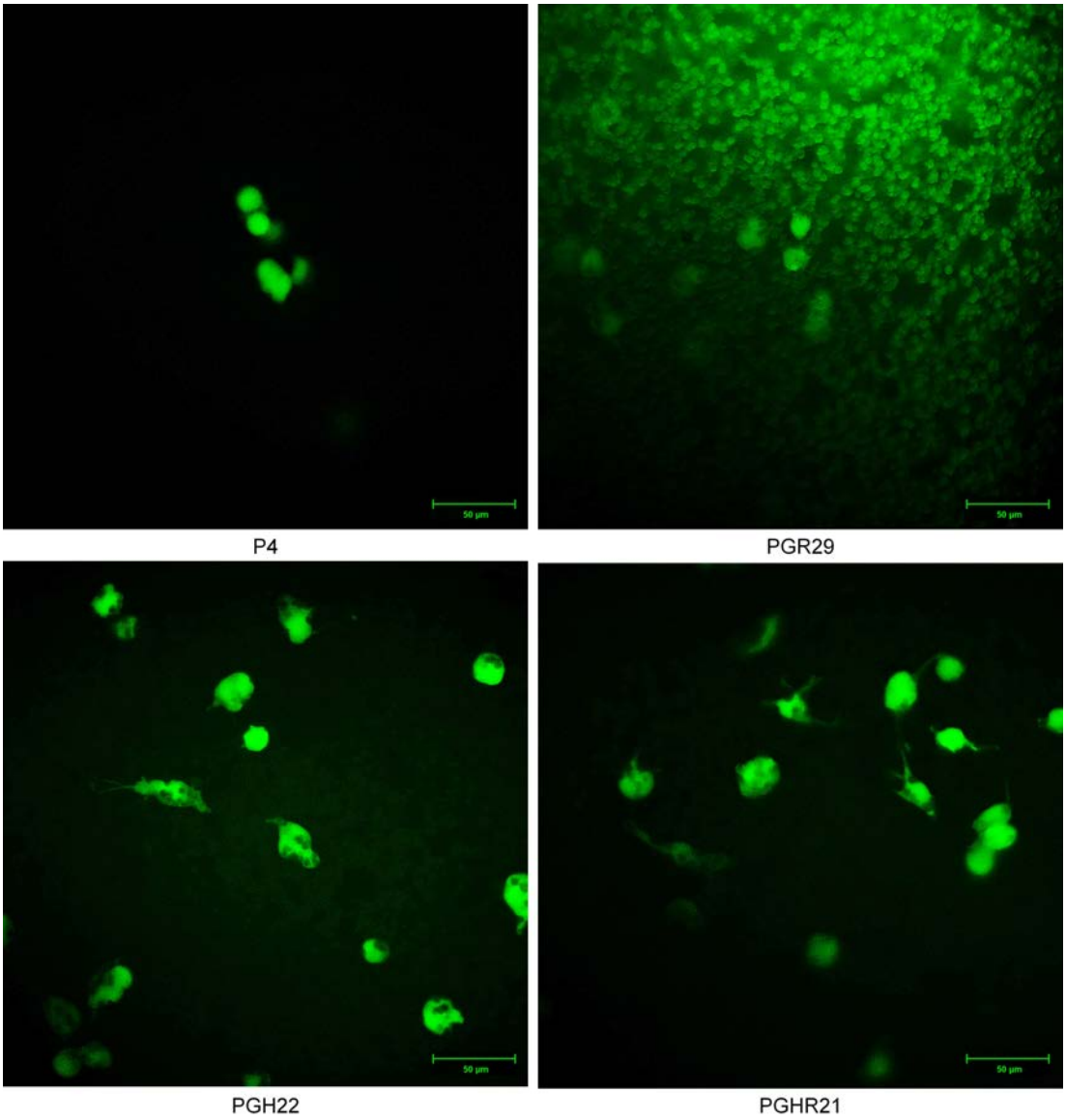

Figure 4.4: Adhesion of C2C12 cells on the end modification hydrogels. Cells were stained with CFSE 2 h after cell seeding, the experiment was performed in duplicate, scale bars show 50 μm.

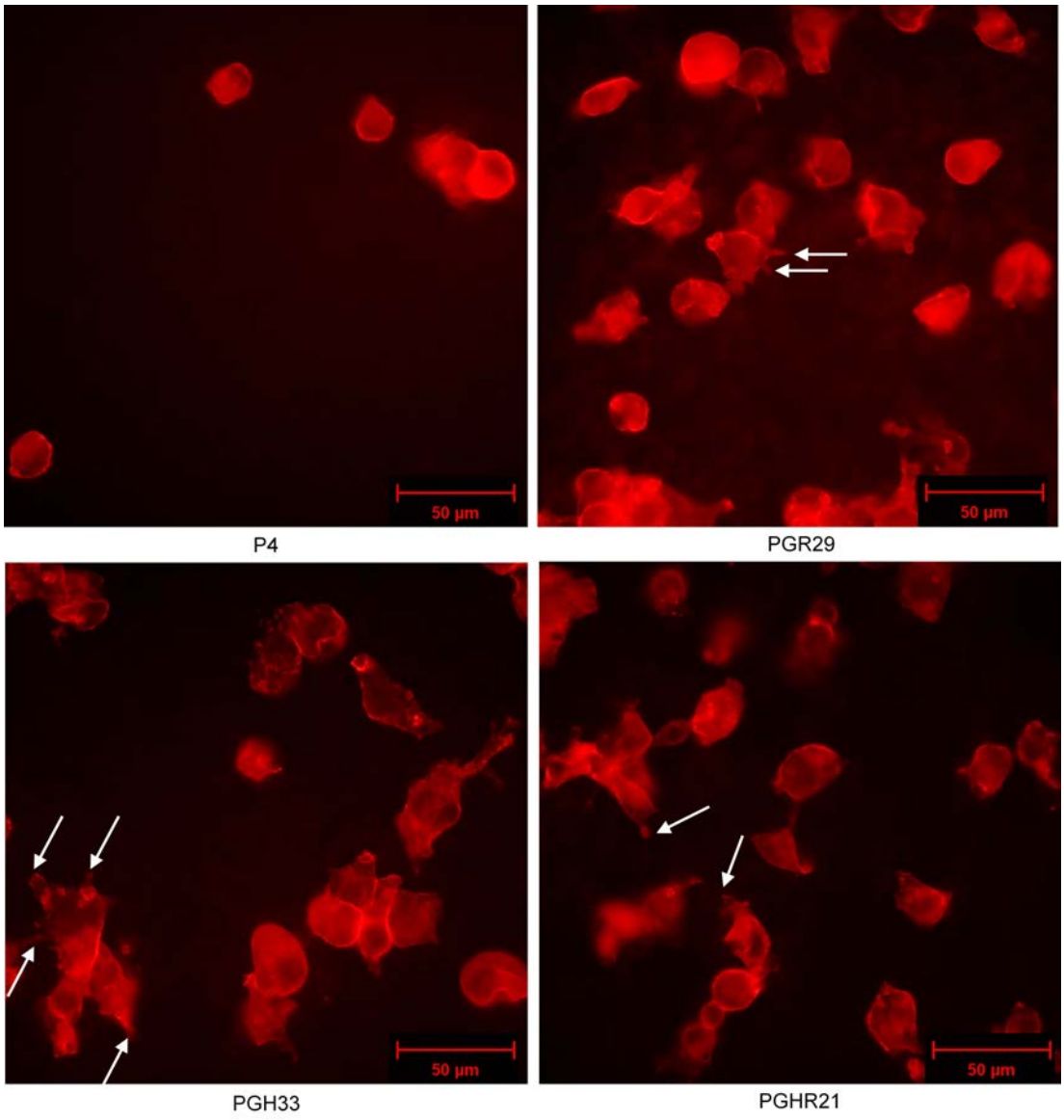

Figure 4.5: Adhesion of C2C12 cells on the end modification hydrogels 2. The cells were fixed with 4% paraformaldehyde and stained with rhodamine phalloidin 2 h after cell seeding. White arrows indicate cell protrusions, scale bars show 50 µm.

were some spread cells on P(HEMA:GMA)-RGD which were larger than those on the other hydrogels and some cells had protrusions extending from them which indicated better cell adhesion (Figure 4.3). Overall the 3T3 cells on P(HEMA:GMA)-RGD varied their morphology, it appeared that the RGD did not consistently improve the adhesiveness of the hydrogel towards fibroblasts. PGR28 had 1.7 times the amount of RGD as that on PGR22, the cells had protrusions on PGR22 but more cell adhesion occurred on PGR28. The best 3T3 cell adhesion was observed on P(HEMA:GMA)-HS&RGD. More cells had protrusions extending from them which showed stronger cell adhesion than on the other hydrogels. The improved cell adhesion could have been due to the synergistic effect of having HS and RGD present on the same hydrogel.

Similar to the 3T3 cells, the C2C12s were more spread on P(HEMA:GMA)-RGD than on PHEMA, as seen in Figure 4.4 and Figure 4.5. Cell protrusions extended from the cells grown on P(HEMA:GMA)-RGD, indicating better adhesion. However the best cell adhesion was seen on P(HEMA:GMA)-HS&RGD, where the C2C12 cells were consistently spread and visibly larger with multiple protrusions. The improvement could have been due to synergistic effects as the presence of both biomolecules could have enabled the cells to form more focal adhesions to the hydrogel which would explain the presence of multiple cell protrusions. Such enhanced cell adhesion and spreading has been demonstrated with the co-immobilisation of different peptides[130,215].

The lack of an increase in cell adhesion after RGD immobilisation was observed. The critical RGD surface concentration is considered to be between 1-10 pmol/cm^2 [167,218]**?** . By making the assumption that most of the immobilised RGD was on the surface of the hydrogels their concentrations were estimated to be between 0.3-0.5 μmol/cm^2, this was significantly higher than the critical concentration. The difference is likely due to the different forms of the materials, brush and gel polymers are markedly more dense than sponge PHEMA creating the large difference in RGD concentration, such as the estimated 23 pmol/cm^2 on a PHEMA brush surface[130]. Therefore it was unlikely that the concentration of the immobilised RGD on the hydrogels, created in this work, was too low to support and enhance cell adhesion.

The lack of consistent cell adhesion was observed with lower cell adhesion in Figure 4.4 compared to Figure 4.5. Both experiments used the same hydrogel therefore the variability could have been due to the method of RGD immobilisation or the spacing of the immobilised RGD. A copolymer of PHEMA and GMA has been used to immobilise various densities of a peptide to the scaffold[167]. The lowest peptide density tested was 22 pmol peptide/mg polymer, alternatively represented as 0.14 peptide chains/nm^3. The RGD density on the hydrogels synthesised in this project was 33 and 52 nmol RGD/mg hydrogel (PGR29 and PGR28 respectively) which equated to approximately 0.004 and 0.006 peptide chains/nm^3. Therefore while the RGD concentration was sufficient, the RGD density may have been too small. This may have been the reason for the lack of a significant increase in cell adhesion as the immobilised RGD sites were spread too far apart to optimise cell adhesion. It has been demonstrated that additional to the positive relationship between RGD concentration and cell adhesion, the distance between adjacent RGD molecules is also important. Clusters of immobilised RGD, where the molecules were on average closer together, are better at enhancing cell proliferation than the same concentration of RGD with the molecules more spread apart[73]. This is due to the link between integrin clustering during focal adhesion maturation and myosin-actin interactions[73].

RGD might not have improved cell adhesion as much as anticipated due to its presentation, this may have been due to the method of immobilisation. While may other researchers use NHS to form a peptide bond between RGD and the scaffold, most utilise one of the amine groups on the RGD for the immobilisation[219]. In this work the amine was present on the scaffold and the carboxylic acid group on the RGD was used. The difference in the site through which the RGD was attached may have affected the ability of the RGD to interact with cells. For example, it has been shown that cyclic RGD has a 10-fold greater ability than the linear version to bind $\alpha V\beta 3$, $\alpha V\beta 5$ and $\alpha 5\beta 1$ integrins. It has also been shown that a kinked conformation of RGD enhances binding to $\alpha 5\beta 3$ while the linear conformation prefers $\alpha IIb\beta 3$. One of the prodominant integrins used in C2C12 adhesion are the $\alpha V\beta 3$, therefore the immobilisation of the RGD

in this work may have presented the RGD in a more linear conformation than that used by others. In addition, the activity of RGD is lower than fibronectin and recombinant fragments (that mimic the monomer of the dimer structure of fibronectin), which mediate stronger cell adhesion[220]. These results suggest that RGD alone may not be sufficient, and longer peptides are necessary for superior cell adherence[221].

4.3.2 Cell Proliferation

The proliferation of 3T3 cells was low on PHEMA and P(HEMA:GMA). Visually the cell number was not seen to increase greatly, however there was a small increase on PHEMA from day 1 to 2 and a small increase on P(HEMA:GMA) from day 3 to 4. These observations indicated little to no cell proliferation on PHEMA and P(HEMA:GMA) (Figure 4.6). Some cell proliferation was seen on P(HEMA:GMA)-NH_2, as an increase in cell number was observed from day 2 to 4. These results were consistent with those observed in chapter 3. Better cell proliferation was seen on P(HEMA:GMA)-RGD, the cell number increased daily up to day 4. These results demonstrated that the immobilisation of RGD introduced bioactivity to the hydrogel which improved and increased 3T3 cell proliferation. The proliferation of 3T3 cells was greatest on P(HEMA:GMA)-HS&RGD and similar to the proliferation observed on P(HEMA:GMA)-HS (Figure 4.7).

The proliferation of C2C12 cells was similar on PHEMA and P(HEMA:GMA). Little to no cell proliferation was observed on either hydrogel (Figure 4.8). More cell proliferation was seen on P(HEMA:GMA)-NH_2. The C2C12 cells were spread on P(HEMA:GMA)-NH_2 on day 1, protrusions from the cells indicated better cell adhesion which lead to increased cell proliferation. The same occurred on P(HEMA:GMA)-RGD, the spread morphology of the cells on day 1 resulted in higher cell proliferation by day 6. The cell proliferation was greater on P(HEMA:GMA)-RGD than P(HEMA:GMA)-NH_2. Additionally the orientation of the cells was different on the hydrogels on day 6. The C2C12 cells were sparsely populated on PHEMA and P(HEMA:GMA) with no partic-

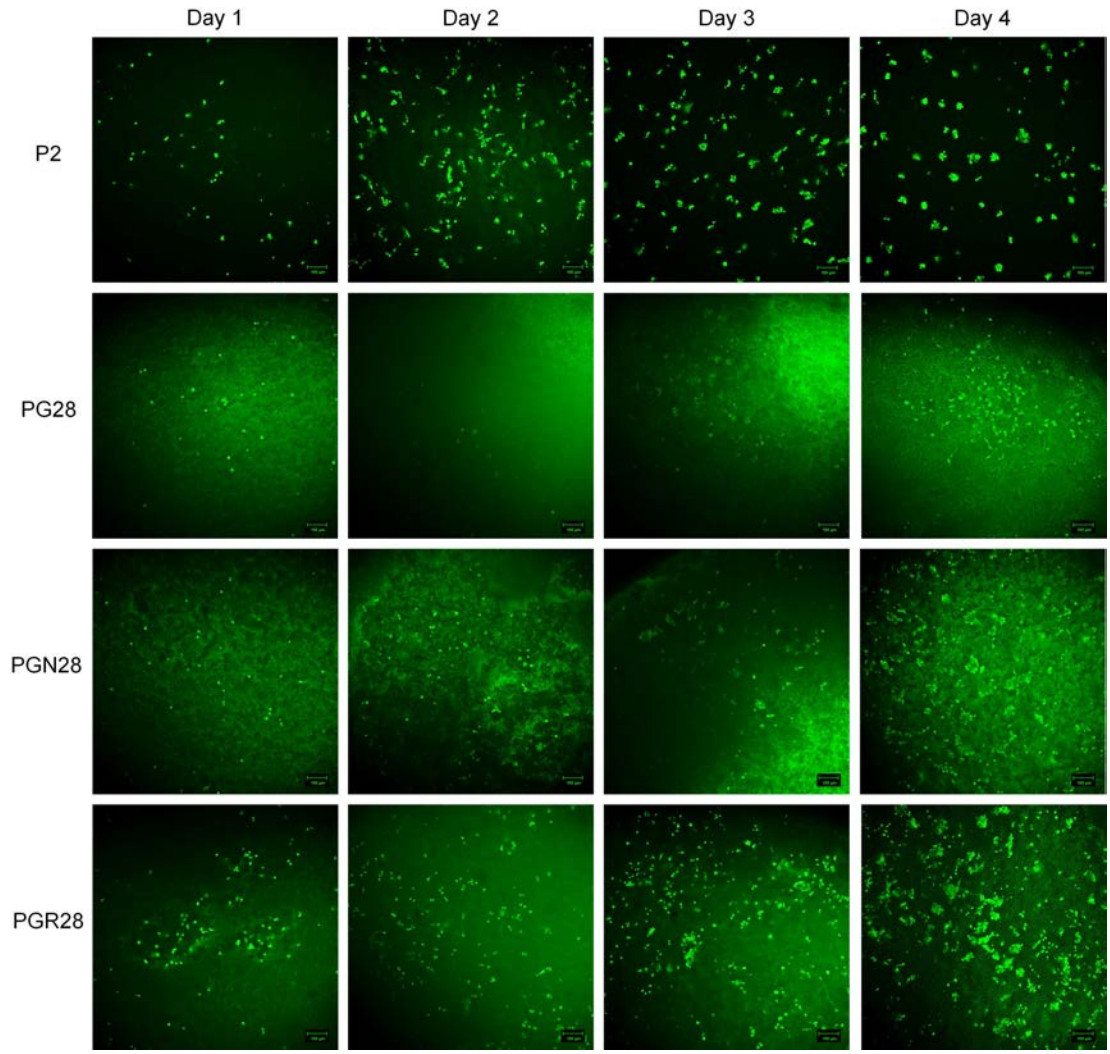

Figure 4.6: 3T3 cell proliferation on the hydrogels. The cells were stained with CFSE and the experiment was performed in duplicate, the scale bars show 100 μm.

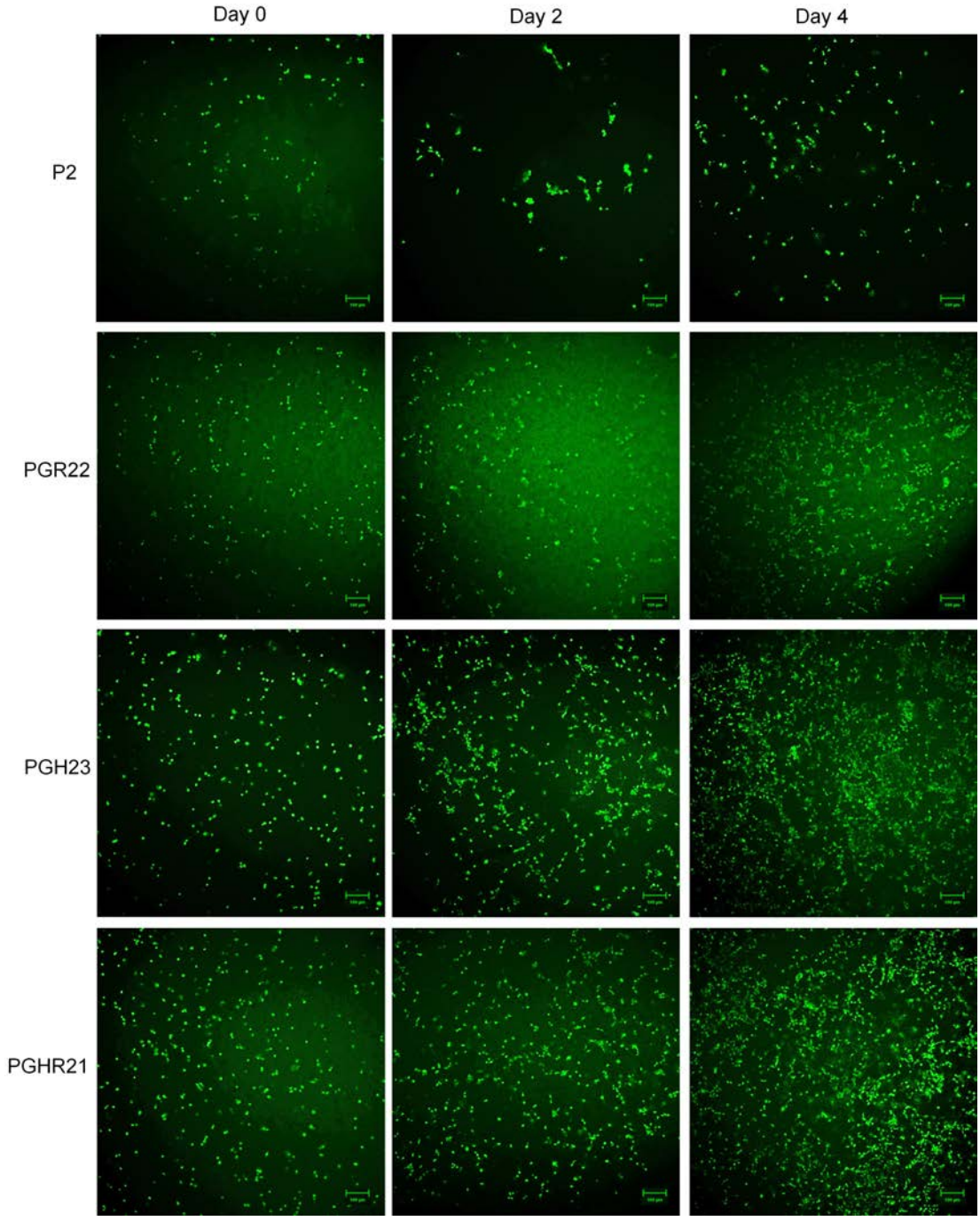

Figure 4.7: Proliferation of 3T3 cells on the end modification hydrogels. The cells were stained with CFSE and the experiment was performed in duplicate, scale bars show 100 μm.

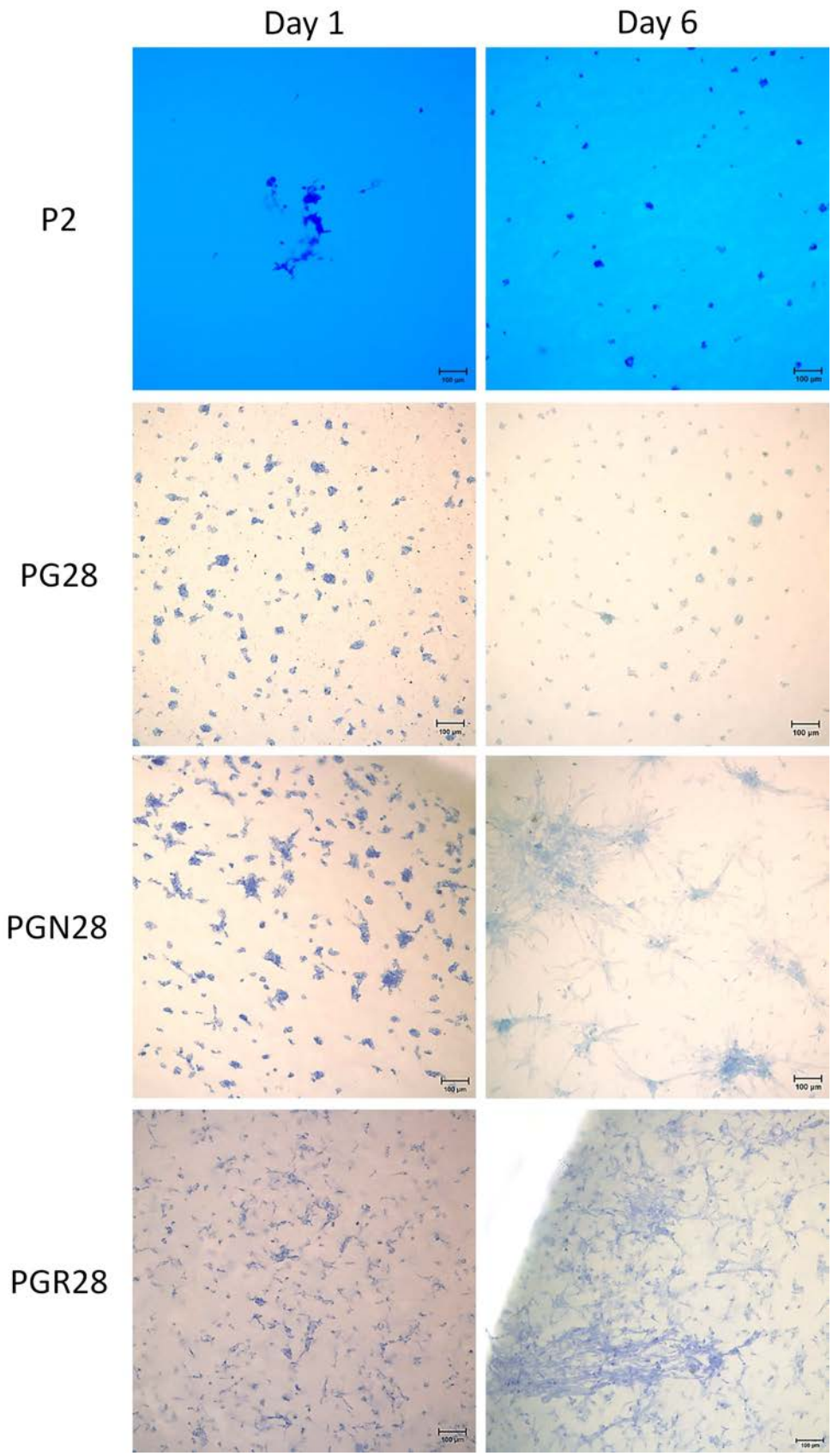

Figure 4.8: Proliferation of C2C12 cells on the hydrogels. Cells were fixed with 4% paraformaldehyde before Kwikdiff staining. PHEMA irreversibly absorbed Kwikdiff resulting in the blue background, experiment was performed in triplicate, scale bars show 100 μm.

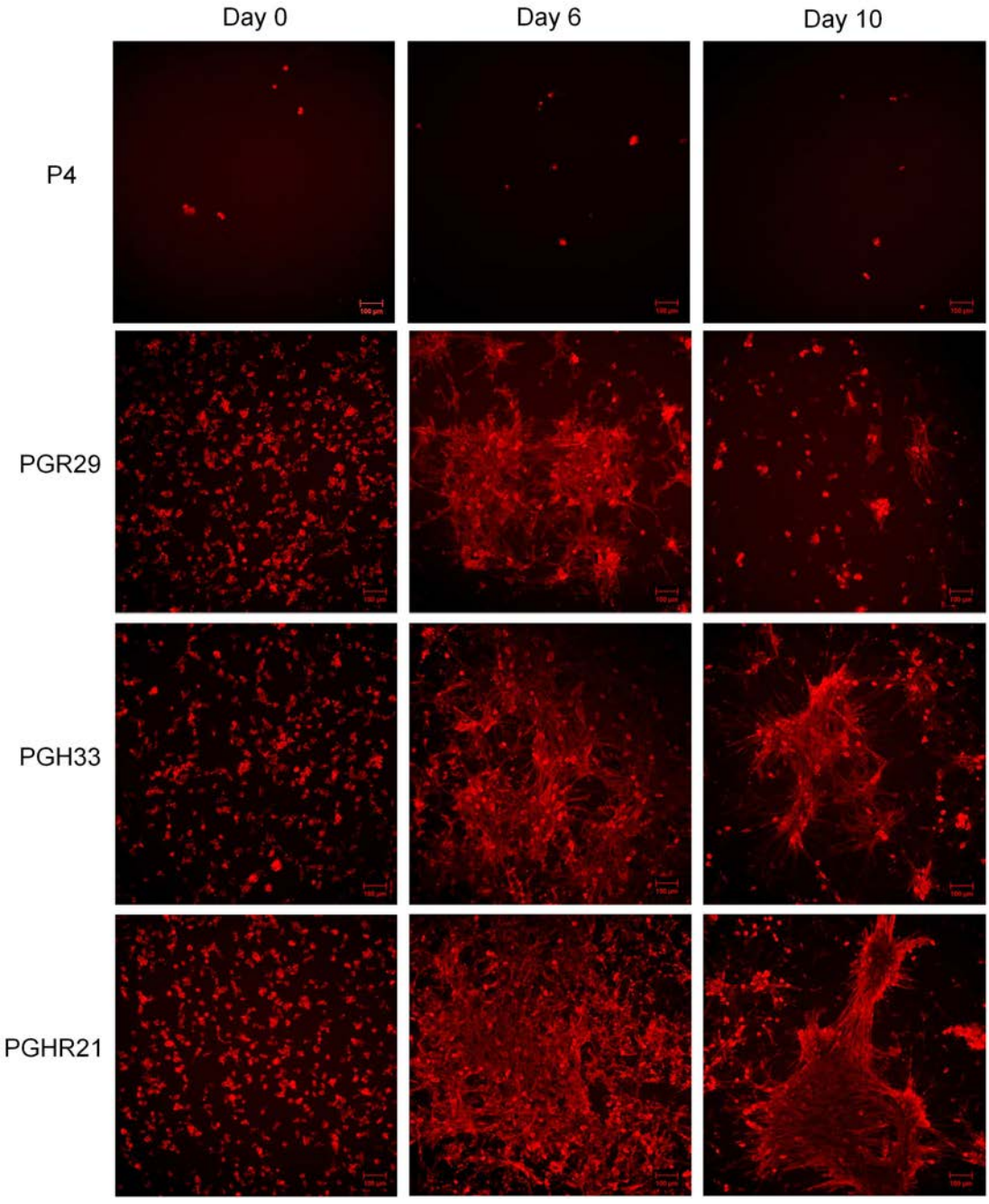

Figure 4.9: Proliferation of C2C12 cells on the end modification hydrogels. The cells were fixed with 4% paraformaldhyde and stained with rhodamine phalloidin. The experiment was performed in duplicate, scale bars show 100 μm.

ular orientation. In contrast the cells on P(HEMA:GMA)-NH_2 had aggregated into large cell colonies creating a sunburst shape. The cells in these aggregates still maintained a spread morphology that was significantly different to the round cell clusters on PHEMA and P(HEMA:GMA). The aggregated cells on P(HEMA:GMA)-RGD were aligned along one another. The alignment of C2C12 cells is one of the first steps towards cell differentiation. Therefore the RGD on the hydrogel had assisted the C2C12 cells in their organisation and they had begun cell differentiation. These results indicated that the RGD immobilised on the hydrogel had improved the bioactivity of the hydrogel resulting in enhanced cell behaviour with respect to cell proliferation and organisation.

The proliferation of 3T3 and C2C12 cells was compared on all end modification hydrogels (Figure 4.7 and Figure 4.9). On P(HEMA:GMA)-HS and P(HEMA:GMA)-HS&RGD the cell number increase from day 0 to 2 was more obvious and was followed by a larger increase from day 2 to 4. The highest 3T3 cell proliferation was observed on the hydrogels with HS immobilised, followed by P(HEMA:GMA)-RGD. The C2C12 cells proliferated on all end modification hydrogels from day 0 to day 6 (Figure 4.9), and the highest cell number was on P(HEMA:GMA)-HS&RGD on day 6. From day 6 to 10 the cells organised and aligned on the hydrogels with immobilised HS, but on P(HEMA:GMA)-RGD the cell number decreased. These results showed that C2C12 cell proliferation was enhanced on all end modification hydrogels up to day 6 but HS was required on the hydrogel to support the cells past this timepoint. All end modification hydrogels had higher cell proliferation than PHEMA, therefore all modifications were successful in improving cell proliferation of both cell types.

4.3.3 Cell Quantification with CellTiter-Glo

The number of 3T3 cells on the hydrogels was quantified with the CellTiter-Glo assay on day 0 and 2 of culture. P(HEMA:GMA)-NH_2 was included in the assays as a control to determine whether any improvement in cell behaviour was due to the immobilisation of RGD or due to the preceding modification steps. The lowest luminescent signal and therefore lowest cell number was

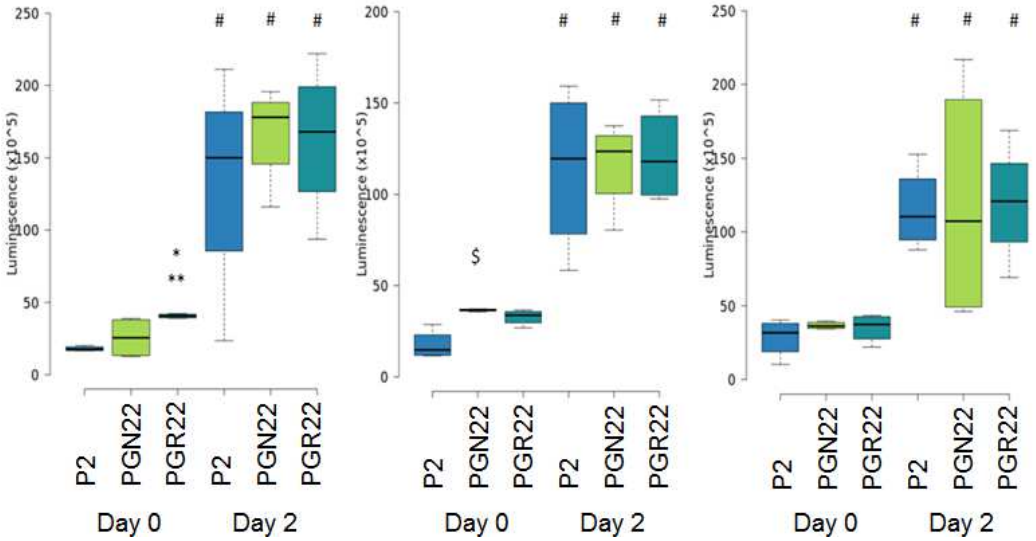

Figure 4.10: Proliferation of 3T3 cells on RGD hydrogels. Figures left to right show 3 independent experiments, n = 4. Statistics were analysed using a non parametric model to compare the median values ($p<0.05$), * PGR22 > P2, ** PGR22 > PGN22, $ PGN22 > P2, # all day 2 results > day 0.

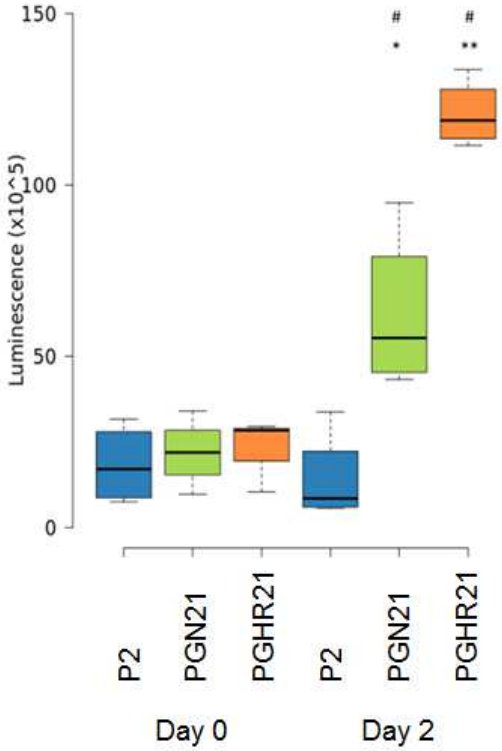

Figure 4.11: Proliferation of 3T3 cells on HS&RGD hydrogels, n = 4. Statistics were analysed using a non parametric model to compare the median values ($p<0.05$), * PGN21 > P2, ** PGHR21 > PGN21 & P2, # day 2 results > day 0.

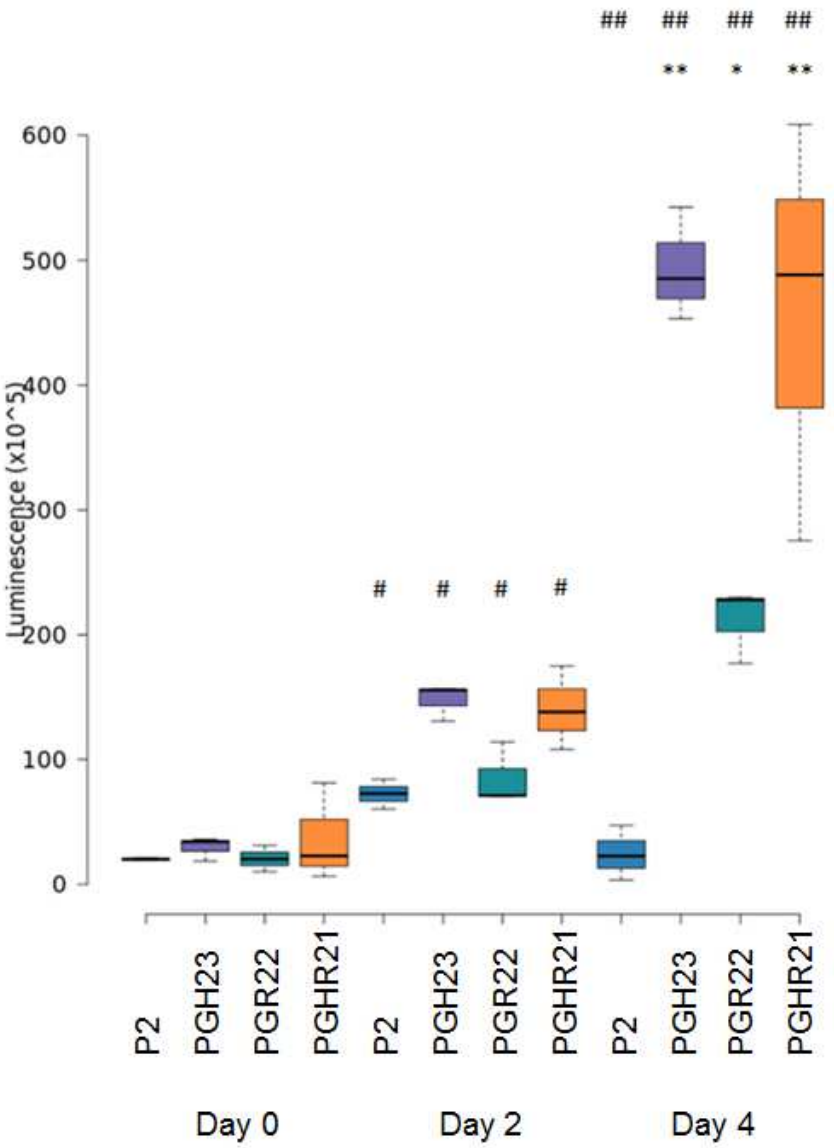

Figure 4.12: Proliferation of 3T3 cells on end modification hydrogels, n = 3. Statistics were analysed using a non parametric model to compare the median values (* and #, p<0.05), on day 6, * PGR22 > P2, ** PGH23 and PGHR21 > P2 & PGR22, # all day 2 results > day 0, ## all day 4 results > day 2 except PHEMA which was < day 2 results.

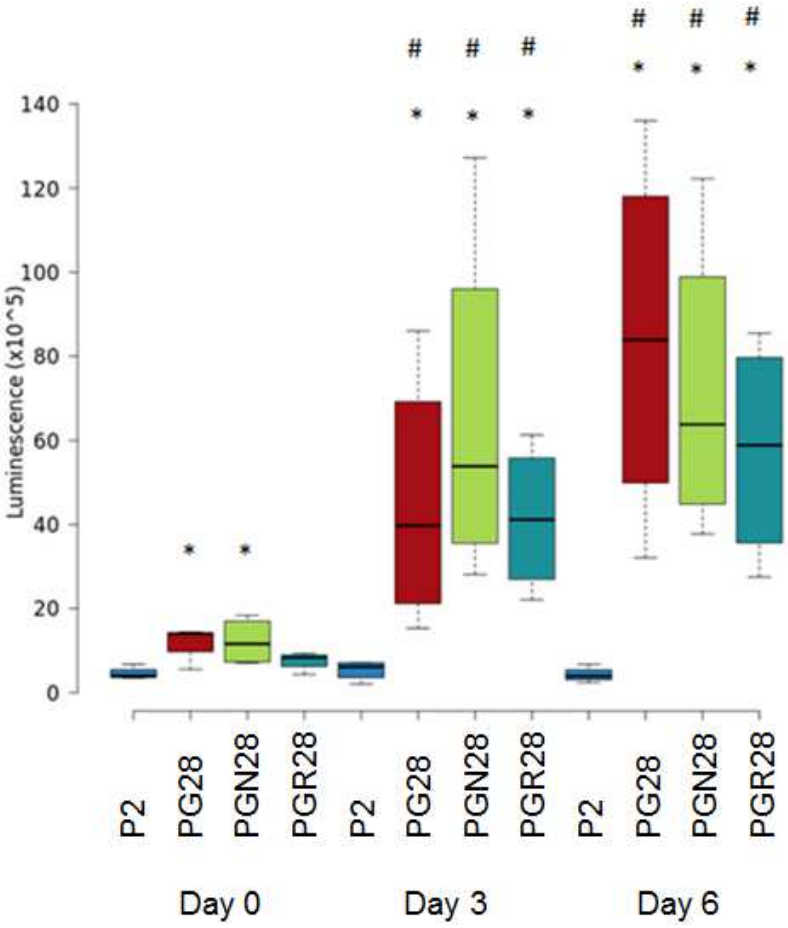

Figure 4.13: Proliferation of C2C12 cells on RGD hydrogels, n = 3. Statistics were analysed using a non parametric model to compare the median values ($p<0.05$), *day 0: PG28 & PGN28 > P2, *days 3 & 6: PG28, PGN28 & PGR28 > P2, # day 3 & 6 results > day 0.

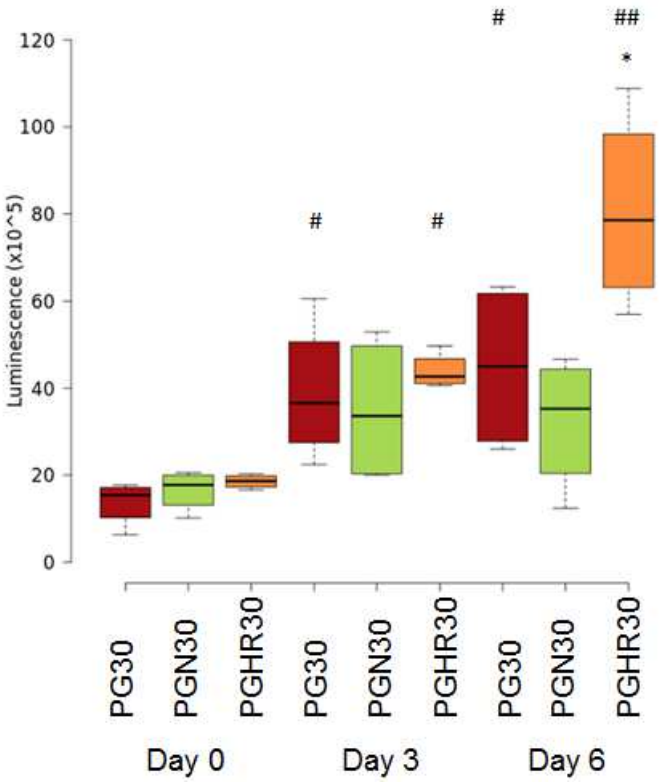

Figure 4.14: Proliferation of C2C12 cells on HS&RGD hydrogels, n = 3. Statistics were analysed using a non parametric model to compare the median values ($p<0.05$), *PGHR30 > PGN30, # day 3 & 6: PG30 & PGHR30 > day 0, ## day 6: PGHR30 > day 3.

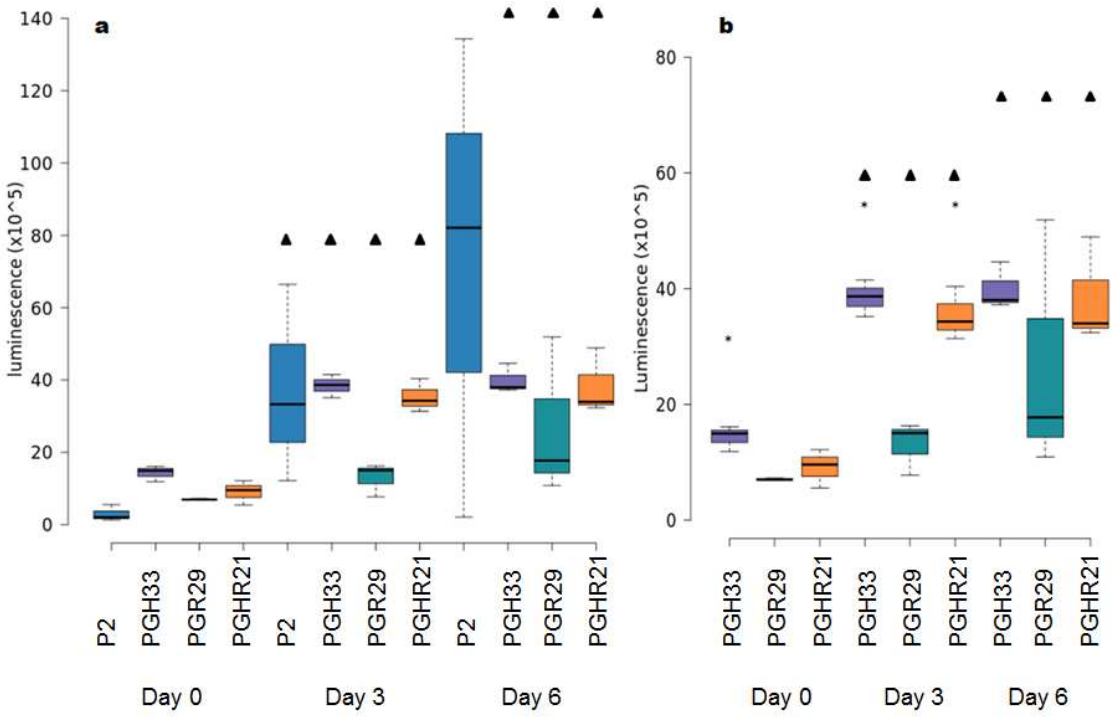

Figure 4.15: Proliferation of C2C12 cells on end modification hydrogels, n = 3. Statistics were analysed using a non parametric model to test for an increasing trend with the Jonckheere-Terpstra test (▲, $p<0.05$), ▲all day 3 results > day 0, ▲day 6: PGH33, PGR29 & PGHR21 > day 0. b) same data as a) presented without PHEMA results, *day 0 PGH33 > PGR29, *day 3 PGH33 & PGHR21 > PGR29, ▲all day 3 results > day 0, ▲all day 6 results > day 0.

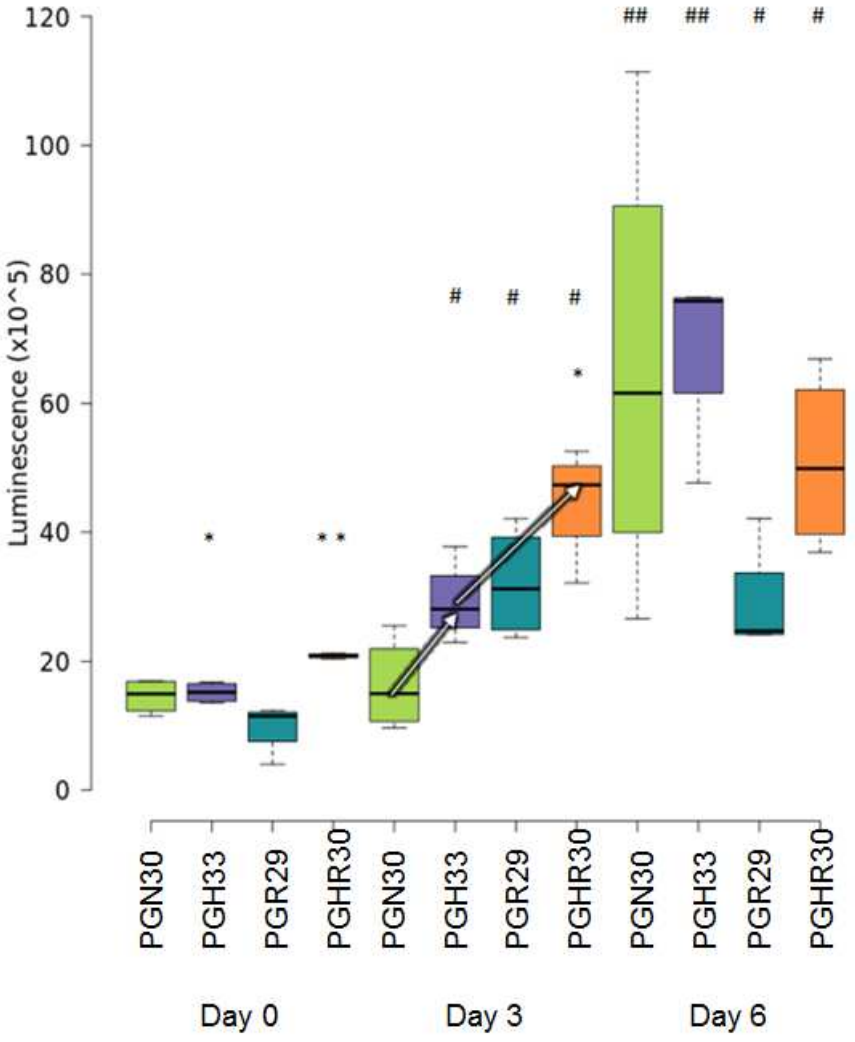

Figure 4.16: Proliferation of C2C12 cells on end modification hydrogels 2, n = 3. Statistics were analysed using a non parametric model to test to compare the median values (* and #) and for an increasing trend with the Jonckheere-Terpstra test (white arrows, $p<0.05$), * day 0 PGH33 > PGR29, ** day 0 PGHR30 > all other hydrogels, * day 3: PGHR30 > PGN30, ** PGHR30 > all other hydrogels, # day 3 & 6 > day 0, ## day 6 > days 0 & 3.

on PHEMA on day 0 (Figure 4.10). This indicated that the cell adhesion on PHEMA was lower than the other hydrogels. There was an increase in cell number on all hydrogels on day 2, compared to day 0, demonstrating proliferation on all hydrogels. There were no statistical differences between the cell number on the different hydrogels on day 2. These results were consistent with the observations of the fluorescently stained cells on the hydrogels, which showed an increase in cell number from day 0 to day 2 but no significant difference in cell number between the hydrogels (Figure 4.2).

To observe the 3T3 cell proliferation due to the immobilisation of both HS and RGD the hydrogel was first compared with the controls, PHEMA and P(HEMA:GMA)-NH_2. There was no difference in the cell number between the hydrogels on day 0, however there were differences between all hydrogels on day 2 (Figure 4.11). The cell number on PHEMA was the lowest and the cell number had not increased from day 0, the cells had not proliferated on PHEMA. The cell number on P(HEMA:GMA)-NH_2 had increased from day 0 and was significantly higher than PHEMA. The highest increase in cell number was seen on P(HEMA:GMA)-HS&RGD. These results were similar to those obtained for the P(HEMA:GMA)-HS hydrogels (Figure 3.16). Similar amounts of HS was immobilised, 0.6 and 1.8 μmol/g for the P(HEMA:GMA)-HS hydrogels and 1.4 μmol/g for P(HEMA:GMA)-HS&RGD, therefore the improvement in cell proliferation may have been due to the higher concentration of HS.

The 3T3 cell proliferation on the end modification hydrogels was directly compared. The cell number increased on PHEMA from day 0 to day 2 but then decreased to day 4 (Figure 4.12). As the lowest cell number was seen on PHEMA on day 4, PHEMA demonstrated the worst cell proliferation. The cell number on P(HEMA:GMA)-RGD increased from day 0 to 2 and again to day 4, therefore the day 4 timepoint was able to differentiate the cell proliferation and show that it was significantly better than on PHEMA. The highest increase in cell number was on P(HEMA:GMA)-HS and P(HEMA:GMA)-HS&RGD, the cell number increased continually from day 0 to 4. The highest cell proliferation occurred on these hydrogels and these results correlated well with the observations by fluorescent staining (Figure 4.6). The immobilisation of RGD was

seen to improve 3T3 cell proliferation, the immobilisation of both biomolecules resulted in similar proliferation to that observed on P(HEMA:GMA)-HS.

The C2C12 cell number on day 0 on P(HEMA:GMA) and P(HEMA:GMA)-NH_2 was greater than that on PHEMA (Figure 4.13). On days 3 and 6 the cell number on P(HEMA:GMA), P(HEMA:GMA)-NH_2 and P(HEMA:GMA)-RGD were higher than that on PHEMA. These results indicated that the copolymer provided a better substrate for C2C12 cell proliferation than PHEMA. The cell number on these hydrogels was also significantly above the number on day 0, this showed that the cells had proliferated over 6 days. However there were no significant differences in cell number between these hydrogels, indicating that the immobilised RGD had limited impact on cell proliferation. This was interesting since the images of the cells (Figure 4.8) showed less cell coverage on P(HEMA:GMA) on day 6 compared to the other hydrogels. These results highlight the limitations of visual inspection and the importance of reliable quantitative cell assays.

The cells proliferated on all of the hydrogels with the highest cell proliferation on P(HEMA:GMA)-HS&RGD (Figure 4.14). As with the previous results,Figure 4.13, no significant difference was seen in cell number between P(HEMA:GMA) and P(HEMA:GMA)-NH_2. These results indicated that the improvement in cell proliferation was likely due to the copolymerisation of HEMA with GMA with no further improvement after the addition of a free amine. Co-immobilisation of HS and RGD significantly increased cell proliferation, with the highest cell number observed on P(HEMA:GMA)-HS&RGD on day 6. These results were similar to the results obtained for P(HEMA:GMA)-HS, which also showed a continuous increase in cell number from day 0 to 6 (Figure 3.18).

The C2C12 cell number was directly compared on each end modification hydrogel and to PHEMA. There were no statistical differences between the median values on the different hydrogels or across the time points (Figure 4.15). These results implied that the variability seen in the cell number on PHEMA could have obscured any significant difference between the other hydrogels. Indeed when the statistics were applied without the PHEMA data, the cell numbers on P(HEMA:GMA)-HS and P(HEMA:GMA)-HS&RGD were significantly

higher than on P(HEMA:GMA)-RGD on day 3. There was an increasing trend in the median values of all hydrogels from day 0 to day 3 and an increasing trend for all end modifications from day 0 to day 6. These results contrasted with the cell proliferation seen in previous assays (Figure 3.18 and Figure 4.14) which showed statistically significant increases in C2C12 cell number on P(HEMA:GMA)-HS and P(HEMA:GMA)-HS&RGD at all time points.

The C2C12 cell number was then directly compared between P(HEMA:GMA)-NH_2 and the end modification hydrogels. On day 0 the cell number was higher on P(HEMA:GMA)-HS&RGD than the other hydrogels (Figure 4.16). This indicated better cell adhesion on P(HEMA:GMA)-HS&RGD than the other hydrogels which confirmed the results from the fluorescent staining of the cells on the hydrogels (Figure 4.5). On day 3 the cell number was significantly higher on P(HEMA:GMA)-HS&RGD than P(HEMA:GMA)-NH_2 and there was an increasing trend in cell number from P(HEMA:GMA)-NH_2 to P(HEMA:GMA)-HS and to P(HEMA:GMA)-HS&RGD. All end modification hydrogels had higher cell numbers on days 3 and 6 compared to day 0 but only on P(HEMA:GMA)-HS did the cell number increase sequentially from day 0 to 6. These results suggested that the variability on PHEMA did obscure some of the differences in cell number across the hydrogels and timepoints. Nonetheless cell proliferation was observed on all end modification hydrogels from day 0 to 3 with further proliferation to day 6 on P(HEMA:GMA)-HS. There were no significant differences in C2C12 cell proliferation on day 6 which was likely due to the cells decreasing their proliferation rate as they initiated differentiation.

While the overall C2C12 cell number may have been similar on the hydrogels, the cell morphology was clearly different. The cells on P(HEMA:GMA)-NH_2 and P(HEMA:GMA)-RGD had the typical fusiform morphology and were well spread, in stark contrast to the cells on P(HEMA:GMA) which were spherical and not spread (Figure A.5). These results highlight the importance of multiple observations of the cell proliferation as the cell assays alone would indicate similar applicability of the hydrogels, while the cell images show differences in cell morphology which affect cell behaviour.

In conclusion the results from the CellTiter-Glo assays showed that both cell

types proliferated on all of the hydrogels. Cell proliferation on PHEMA was very variable, some assays showed an increase in cell number where others showed no change or even a decrease. No significant difference was observed between cell proliferation on P(HEMA:GMA) and P(HEMA:GMA)-NH_2 hydrogels, however some assays indicated that the cell proliferation was improved in comparison to PHEMA. Most assays showed no significant increase in cell proliferation after the addition of RGD when compared to P(HEMA:GMA) and P(HEMA:GMA)-NH_2. Most assays showed the highest cell proliferation on P(HEMA:GMA)-HS&RGD which was sometimes greater than the proliferation on P(HEMA:GMA)-NH_2. Importantly the improvement in cell proliferation of both cell types on P(HEMA:GMA)-HS&RGD was seen to follow the cell proliferation observed on P(HEMA:GMA)-HS. Therefore these results indicated a more significant effect on cell proliferation by HS than RGD immobilisation. Work by others has also observed no significant increase in 3T3 cell proliferation after the incorporation of RGD into the scaffold, in fact a decrease in cell proliferation was found[222].

4.3.4 Cell Differentiation

The C2C12 cells were observed to orientate themselves along one another and approach confluency on the hydrogels. This cell behaviour was seen from day 6 of culture on all of the end modification hydrogels (Figure 4.17). The C2C12 cells were cultured for 10 days to investigate whether they would differentiate on the hydrogels, the differentiation was assisted by changing the media from proliferation to differentiation media on day 6. The C2C12 cells were struggling to survive on PHEMA, most likely due to their poor adhesion and proliferation on PHEMA. The cells on P(HEMA:GMA)-NH_2 and P(HEMA:GMA)-RGD were networked, some cells were aligned on P(HEMA:GMA)-RGD but no myotubes were formed. The lack of cell differentiation on P(HEMA:GMA)-RGD could have been due to a couple of reasons. Firstly there was a difference in the organisation of the cells on day 6, the cells were arranged in a sunburst shape (Figure 4.17). This was in contrast with the cells on the HS immobilised

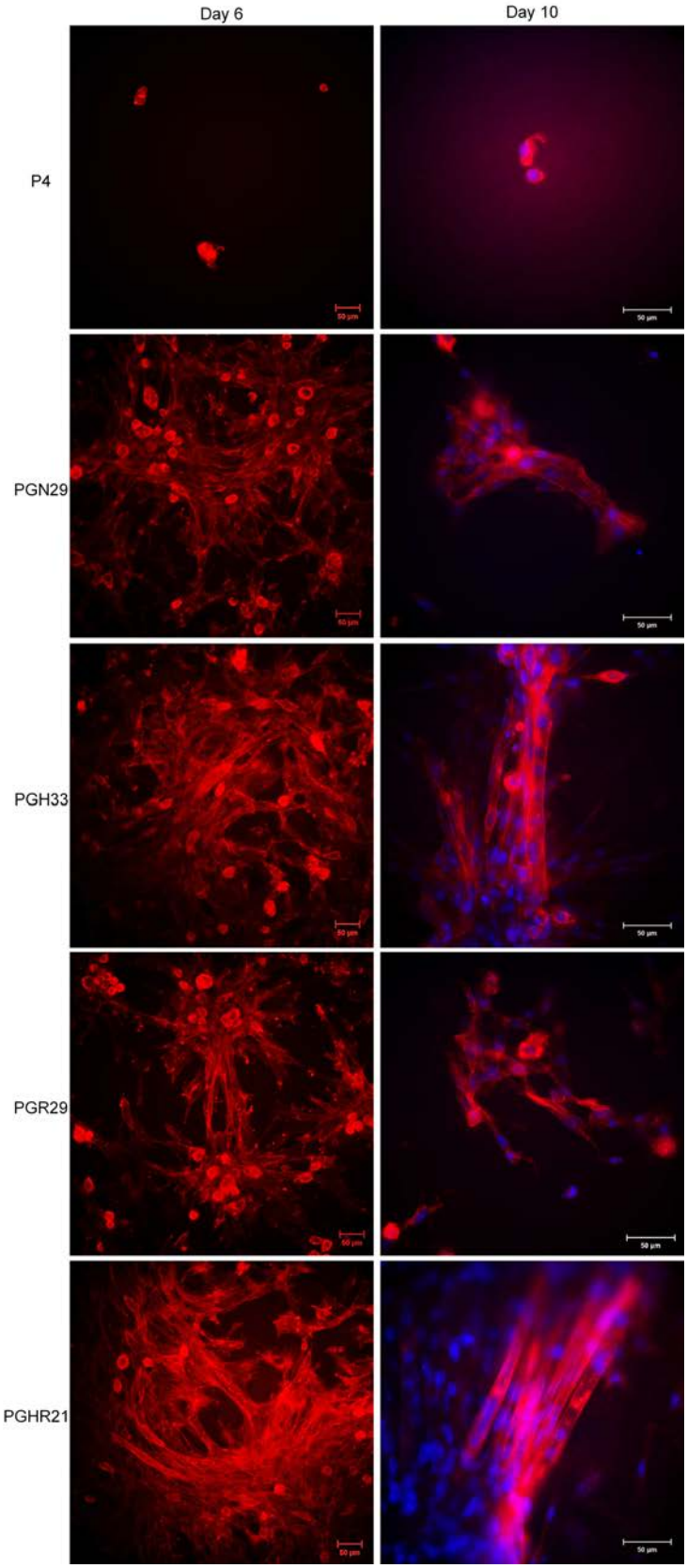

Figure 4.17: Stages of C2C12 cell differentiation on the hydrogels. The cells were fixed with 4% paraformaldhyde and stained with rhodamine phalloidin on day 6, day 10 the cells were additionally counter-stained with DAPI (blue). The experiment was performed in duplicate, scale bars show 50 μm**.**

hydrogels which were aligned along one another. The re-orientation of the cells is important for cell fusion which leads to myotube formation. The other potential reason is that the cells reached their peak on day 6 (or earlier) and were declining so that by day 10 there were insufficient cells present for successful differentiation.

As the distance between the immobilised RGD molecules was likely unoptimised for cell adhesion it was also likely to have affected the development of actin fibres. This is turn could have affected the ability of the C2C12 cells towards differentiation. Optimisation of the distance between immobilised RGD molecules has been demonstrated to enhance actin fibre and focal adhesion formation and maturation[73]. These events are vital to initiate cell signals which control other cell behaviours such as proliferation and differentiation.

The cells on P(HEMA:GMA)-HS&RGD were confluent, had aligned themselves and the cells were fused together forming myotubes. Differentiation of the C2C12s was abundant on P(HEMA:GMA)-HS&RGD but absent on all other hydrogels except P(HEMA:GMA)-HS. Single mytubes were formed on P(HEMA:GMA)-HS while bundles of aligned myotubes were seen on P(HEMA:GMA)-HS&RGD. The differentiation of the C2C12 cells was compared on all of the end modification hydrogels. The C2C12 cells only formed multinucleated myotubes on hydrogels with immobilised HS. Myotubes formed on P(HEMA:GMA)-HS were surrounded by cells in varying states of alignment and fusion, whereas areas of multiple myotubes were seen on P(HEMA:GMA)-HS&RGD. These bundles of aligned myotubes mimicked the myofibril structure of myofibres. These results showed that the presence of HS was required by the cells for successful differentiation. Additionally the presence of both HS and RGD resulted in multiple myotube formation which created areas of aligned myotubes that mimicked muscle fibre structure. Therefore the presence of both HS and RGD were required to enhance cell adhesion and cell proliferation so that the cells could approach confluency and successfully differentiate.

4.3.5 Enzyme Linked ImmunoSorbant Assay

The activity of HS immobilised on P(HEMA:GMA)-HS&RGD was confirmed with the bFGF ELISA. The calculated amount of bFGF eluted from P(HEMA:GMA)-HS&RGD was 9 fold larger than the amount from P(HEMA:GMA)-NH_2, which was used as the control (Figure 4.18). The results showed that the HS immobilised on P(HEMA:GMA)-HS&RGD bound bFGF while the signal from P(HEMA:GMA)-NH_2 was due to physical entrapment of the growth factor in the hydrogel. This trend was consistent with the values obtained when the hydrogels with only HS immobilised were assayed (discussed in chapter 3). There was a small difference in the amount of HS immobilised when it was immobilised alone and when together with RGD, PGH12 and PGHR21 had 1.0 ± 0.4 and 1.4 ± 0.3 μmol HS/g hydrogel respectively. The 2 hydrogels were compared and the results showed that PGH12 and PGHR21 bound and eluted 337 ± 119 and 378 ± 138 ng bFGF. The hydrogels bound a similar amount of bFGF, therefore the HS bioactivity was maintained on P(HEMA:GMA)-HS&RGD with similar bioactivity to P(HEMA:GMA)-HS.

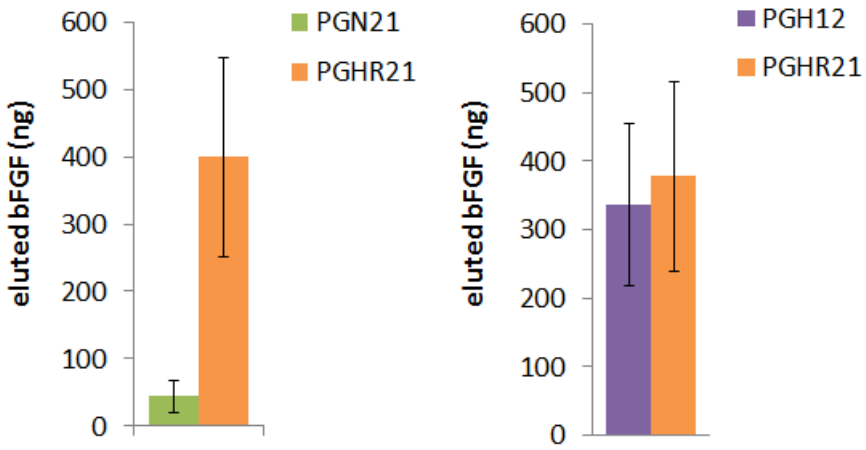

Figure 4.18: Bioactivity of immobilised HS on P(HEMA:GMA)-HS&RGD. Calculated bFGF bound to hydrogels as determined by ELISA, the assays had 3 discs of each hydrogel and duplicate technical replicates, n = 6, error bars show the standard deviation.

4.3.6 Immunofluorescence of Cell Expressed Fibronectin

The expression of fibronectin by 3T3 and C2C12 cells on the end modification hydrogels was visualised with immunofluorescence. The lowest fibronectin production was by the 3T3 cells that were cultured on PHEMA, as discussed in Chapter 3. Fibronectin expressed by the 3T3 cells on P(HEMA:GMA)-HS was more abundant and observed to stretch between cells with the highest fibronectin production on P(HEMA:GMA)-HS&RGD (Figure 4.19). Organisation of cell expressed fibronectin occurred on both HS immobilised hydrogels, however the maturation of the fibronectin network was markedly better on P(HEMA:GMA)-HS&RGD. As the amount of HS immobilised on P(HEMA:GMA)-HS was 2.4 ± 0.2 μmol/g hydrogel and 1.4 ± 0.3 μmol/g hydrogel on P(HEMA:GMA)-HS&RGD, these differences in fibronectin expression were likely due to a synergistic effect. Therefore the immobilisation of both HS and RGD enhanced cell expression of fibronectin and enabled better maturation of cell expressed ECM proteins. These results demonstrated that the co-immobilisation of HS and RGD provided a surface that was able to interact with the 3T3 cells to provide signals which enhanced cell behaviour.

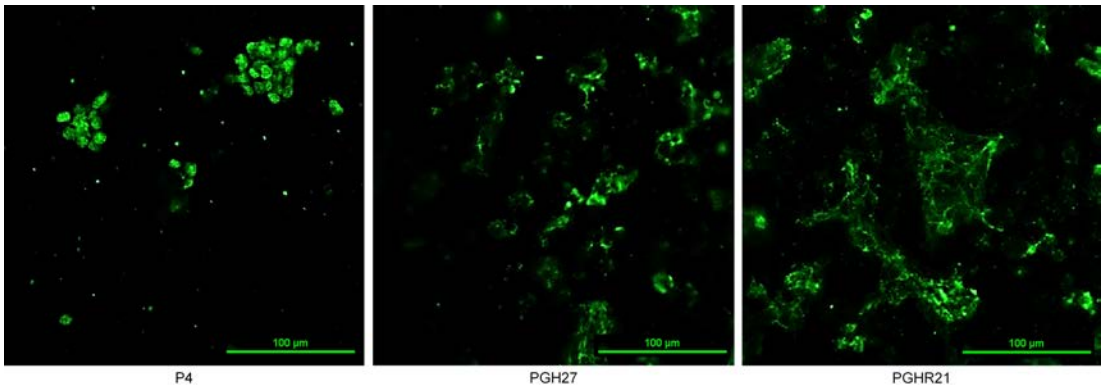

Figure 4.19: Immunofluorescence of fibronectin produced by 3T3 cells on the hydrogels. The cells were stained for fibronectin after 3 days of culture on the hydrogels, fibronectin antibody (ab2413) followed by secondary antibody (Alexa Fluor® 488 F(ab')2 goat anti-rabbit IgG, green). Images taken with a Nikon confocal microscope, scale bars are 100 μm.

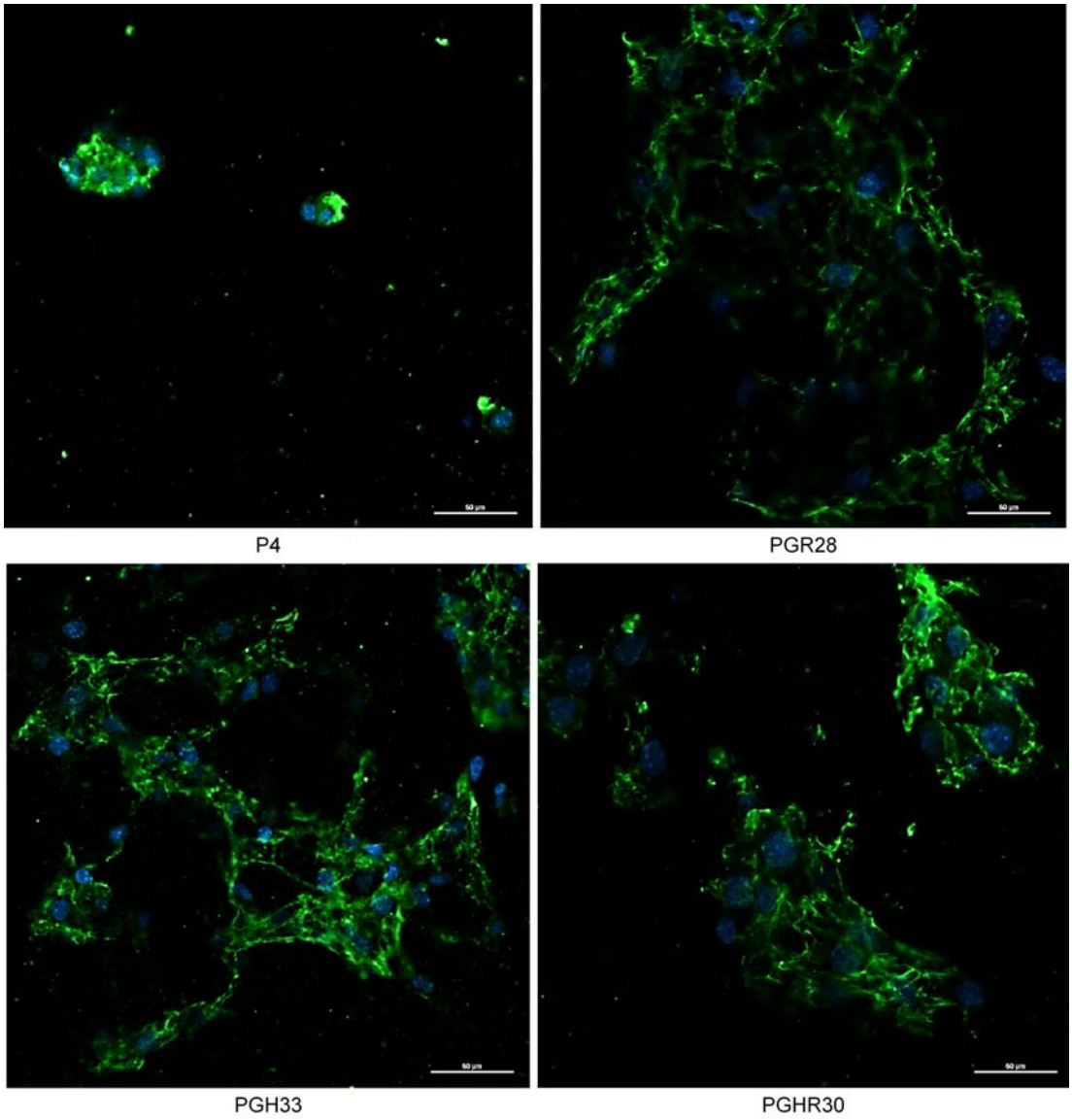

Figure 4.20: Immunofluorescence of fibronectin produced by C2C12 cells on the end modification hydrogels. The cells were stained for fibronectin after 3 days of culture on the hydrogels, fibronectin antibody (ab2413) followed by secondary antibody (Alexa Fluor® 488 F(ab')2 goat anti-rabbit IgG, green) and the nuclei were stained blue (DAPI). Images taken with a Nikon confocal microscope, scale bars show 50 μm.

The C2C12 cells expressed fibronectin on all hydrogels, with the lowest expression on PHEMA as shown in Chapter 3. In contrast the fibronectin expressed by the C2C12 cells on the other hydrogels was more abundant and stretched between cells (Figure 4.20). The organisation of the fibronectin created a fibrillar network between the cells, this resulted in better cell adhesion and spreading as was demonstrated by the fluorescent staining of the cells on the hydrogels. The amount and structure of the fibronectin was very similar on P(HEMA:GMA)-HS and P(HEMA:GMA)-RGD but there was less fibronectin on P(HEMA:GMA)-HS&RGD. The reduction in fibronectin could have been due to the beginning stages of cell differentiation, as the synthesis of fibronectin is known to change during myogenesis[211]. Therefore if the myoblasts were approaching confluency and preparing to differentiate they would rely less on having a fibronectin matrix around themselves[34]. These results have shown that all of the end modifications on PHEMA created hydrogels that enhanced the matrix protein expression of both cell types.

In summary the combination of techniques used have shown that all modifications on PHEMA have improved the bioactivity of the hydrogel. The best cell results were on the end modification hydrogels, especially those with immobilised HS. All end modification hydrogels showed enhanced cell adhesion, proliferation and differentiation. The presence of both HS and RGD have shown some synergistic effect with respect to the differentiation of the C2C12 cells. It is likely that the combination of the two biomolecules provided an environment for the cells that enhanced cell adhesion which in turn increased cell proliferation and differentiation. The ELISA and immunofluorescence results demonstrated the bioactivity of the immobilised HS, this proved that the HS was able to bind proteins similar to *in vivo* processes. A potential mechanism for the synergistic effect of HS and RGD is presented. It has been shown that α5 expression increases during the myogenesis of C2C12 cells, which can link actin to form actin-membrane interactions which reinforce cell-cell interactions[223]. The binding of α5 to nescharin begins the pathway to cell migration and the upregulation of heparanase leads to cell fusion[223]. Therefore the presence of HS and RGD on the hydrogels increased the integrin binding and presented bioactive HS

which in combination enhanced cell migration and cell fusion resulting in the promotion of cell differentiation.

To further examine the how the immobilised HS and RGD improved the cell behaviour, a few additional experiments could be performed. These would include serum free conditions to observe whether the cells maintain their cell behaviour. This would indicate whether the bioactivity of the hydrogels is sufficient to promote the cell behaviour observed in this work or whether additional factors from the serum were involved (i.e. to test whether the improvements with HS were partially due to the binding of bFGF to the hydrogel). Specifically serum free conditions for the cell deposition of fibronectin would be useful to observe and correlate with any changes in cell behaviour. With serum free conditions it would also be interesting to test for any changes in cell adhesion when soluble HS or RGD are present in the medium. Decreased cell adhesion would indicate that the HS and RGD were being directly used to assist with the adhesion of the cells to the hydrogels.

4.4 Conclusions

The modification of PHEMA with RGD resulted in a small improvement in cell adhesion of both 3T3 and C2C12 cells. The cells had a more spread morphology than the controls, PHEMA, P(HEMA:GMA) and P(HEMA:GMA)-NH_2. The cells were observed to form small protrusions which were the beginning stages of better cell adhesion and potential focal adhesion maturation. The improvement in cell adhesion on P(HEMA:GMA)-RGD also improved cell proliferation of both cell types. Significantly more cells were seen on P(HEMA:GMA)-RGD at later time points than the controls. These visual observations were confirmed with the assay results. The modification of PHEMA with both HS and RGD resulted in the most drastic improvements in cell behaviour. P(HEMA:GMA)-HS&RGD demonstrated the best cell adhesion, proliferation and also assisted in the best C2C12 differentiation.

The activity of immobilised HS on P(HEMA:GMA)-HS&RGD was tested and compared to P(HEMA:GMA)-HS. The results showed that both hydrogels, that contained similar amounts of HS, were able to bind a similar amount of bFGF. This indicated that the co-immobilisation of HS and RGD on the same hydrogel did not adversely affect the activity of the HS. The expression of fibronectin by the 3T3 cells was higher on the end modification hydrogels than PHEMA. This indicated that the cells were better adhered and spread on the modified hydrogels which lead to better cell proliferation.

Myotube formation only occurred on P(HEMA:GMA)-HS and P(HEMA:GMA)-HS&RGD. The ELISA results indicated that both of the hydrogels with HS bound similar amounts of bFGF therefore the HS bioactivity was similar. The myotube formation on P(HEMA:GMA)-HS&RGD was more abundant and the formed myotubes were aligned, characteristic of muscle fibre alignment *in vivo.* These results suggested that there was a synergistic effect from the co-immobilisation of HS and RGD on the same hydrogel. This synergistic effect was observed to have minimal effects on the adhesion and proliferation of the cells, however they resulted in the best C2C12 differentiation creating aligned bundles of myotubes that mimicked muscle fibre formation.

In conclusion each end modification hydrogel demonstrated improved cell adhesion and proliferation of fibroblasts and myoblasts over PHEMA. The cell adhesion and proliferation of both cell types was similar on each end modification hydrogel. The important difference between the hydrogels was that the presence of HS was required by the myoblasts for successful cell differentiation. Additionally the myotube formation was best on P(HEMA:GMA)-HS&RGD suggesting a synergistic effect of the co-immobilisation on the cells. These results show 3 successful modifications on PHEMA that improved the bioactivity of the hydrogel and created materials that have potential for tissue engineering applications.

Chapter 5

Conclusions

This project focused on the modification of PHEMA, a widely used and FDA approved bio-inert hydrogel, with HS and RGD to improve its bioactivity for possible uses as a tissue engineering scaffold. This included the design, synthesis, physical and chemical characterisation, and cellular evaluation of six different hydrogels; PHEMA, P(HEMA:GMA), P(HEMA:GMA)-NH2 , P(HEMA:GMA)-HS, P(HEMA:GMA)-RGD and P(HEMA:GMA)-HS&RGD, where P(HEMA:GMA) and P(HEMA:GMA)-NH2 acted as intermediates for the immobilisation of HS and RGD. The work firstly revealed , that the covalent immobilisation of HS or RGD to the hydrogel did not markedly alter the physical properties of the hydrogel, and secondly, that the biological activities of the immobilised entities were conserved. The overall outcomes were hydrogels with enhanced cell attachment properties and, in the case of hydrogels containing the HS structures, support for cell differentiation. Collectively the modified hydrogels demonstrated superior functionality compared to that of the unmodified PHEMA, with functions that are appropriate for a tissue engineering scaffold.

In summary, the hydrogel maintained high water content, high surface area, interconnected pore structure and elastic properties, which are important for a tissue scaffold. Increased thermal stability of the modified PHEMA hydrogels was observed and likely due to the increased crosslinking with the comonomer. The viscoelastic properties of all of the hydrogels were within the ranges for soft to intermediate tissues. The elastic recovery of the hydrogels

was high and their performance under repeated stress demonstrated their potential for long term implant applications.

Clear improvements in cell adhesion, proliferation and differentiation were shown on the modified hydrogels. Copolymerisation increased cell adhesion of fibroblasts and myoblasts and the immobilisation of the biomolecules increased cell proliferation and differentiation. Specifically, the behaviour of 3T3 and C2C12 cells was indicative of healthier cells on all the modified hydrogels compared to those on PHEMA. The cells were observed to attach, proliferate and differentiate best on the end modification hydrogels. The best cell results occurred on P(HEMA:GMA)-HS and P(HEMA:GMA)-HS&RGD. C2C12 cell differentiation was only observed on the hydrogels modified with HS. This indicated that the HS hydrogels were able to promote cell organisation and orientation which led to successful cell differentiation. The most interesting finding was the formation of aligned myotubes on P(HEMA:GMA)-HS&RGD. Their orientation in bundles mimicked the in vivo structure of muscle fibres. The results from immunofluorescent staining showed that the cells expressed more fibronectin on the end modification hydrogels which correlated to the improved cell behaviour observed on those hydrogels. Image analysis showed that the fibronectin was better organised on the HS immobilised hydrogels which indicated the first stages of a mature ECM microenvironment around the cells.

Results showed that HS can be easily attached in a bioactive form, with evidence showing that the immobilised HS bound and sequestered bFGF in the same way as is observed in vivo. Thus, the created scaffold provided a method to mimic ECM signalling that promoted fibroblast proliferation and myoblast differentiation. Application of this hydrogel in vivo may support wound healing by enhancing the fibroblast population to create ECM while simultaneously supporting the differentiation of myoblasts to create muscle tissue. The exact structure and biological interactions of muscle ECM and muscle cells has not been determined[224]. The hydrogels created here could be used as a model to gain insights into how cell-ECM interactions change during muscle injury and repair. The methodology developed can be applied to immobilise other GAGs enabling the investigation of each GAG type individually or in various combina-

tions. In this way the complex roles of the GAG component of the ECM would be better revealed than has been previously possible. A better understanding of these interactions will assist in designing scaffolds to facilitate muscle regeneration.

Technically the quantification of cells on the porous, opaque, 3D hydrogels was a major challenge. Several methods were trialled, but the CellTitre-Glo assay was proven the most effective and reproducible. The luminescent signal, produced as a result of cell metabolism and monitored in the assay, is advantageous for scaffolds where absorbance or fluorescent techniques create significant background. Success with this assay allowed a rigorous, unbiased assessment of the effects of the immobilised entities on cell behaviour. In contrast to the visual assessments commonly used in this field which are subject to bias, as cells rarely attach evenly across the scaffolds.

The elasticity of the hydrogel was between the range that has been measured for whole skin, 0.36-0.45 kPa[172], and individual fibroblasts, 3-12 kPa[169], hence, it was expected to provide a suitable mechanical environment for fibroblasts. Interestingly the same hydrogel was also able to support and enhance the differentiation of myoblasts despite having lower elasticity than muscle tissue, 31-450 kPa[225]. This work has shown that a single hydrogel can support and enhance the cell behaviours of different cell types. This would be useful for the regeneration of deep wounds as the hydrogel would be able to integrate with both muscle and skin tissue. As all current commercial products for wound healing are only applicable to skin depth wounds, this hydrogel has the potential to fill this deficiency.

Overall, this project provided a facile method for the functionalisation and the chemical immobilisation of the well-known and relatively inert PHEMA hydrogels with biomolecules to create a scaffold more appropriate for tissue engineering applications. The project also developed a reliable method to quantify cells on the porous and opaque 3D hydrogels. The produced 3D bioactive hydrogel scaffolds demonstrated promise for deep tissue wound healing and muscle regeneration treatments. The work has shown that using the synthetic pathway designed, it is possible to immobilise HS and maintain its bioactivity.

This bioactivity was proven to mirror the effect of soluble HS on cell behaviour, mimicking in vivo signalling. The results from this work will enhance the current knowledge on cell-scaffold interactions enabling better scaffold design in the future.

Future Directions

While further investigations are required to understand how the immobilised biomolecules have interacted with the investigated cell lines, and to prove the concept in vivo, the developed scaffold could also be used as a model for the investigation and advanced understanding of the cell interaction with the biomolecules immobilised on the surface of the hydrogels. One particular interest in this direction is to use the scaffold, which has demonstrated high elastic recovery under repeated stress, to investigate the responses of different cells to the tension and stress in the biological environment to evaluate the potential of scaffolds as long-term implants.

References

[1] Williams, D. F. *Biomaterials* **2009**, *30*, 5897–909.

[2] Freed, L. E.; Guilak, F.; Guo, X. E.; Gray, M. L.; Tranquillo, R.; Holmes, J. W.; Radisic, M.; Sefton, M. V.; Kaplan, D.; Vunjak-novakovic, G. *Tissue Engineering* **2006**, *12*, 3285–3305.

[3] Hunziker, E.; Spector, M.; Libera, J.; Gertzman, A.; Woo, S. L.-Y.; Ratcliffe, A.; Lysaght, M.; Coury, A.; Kaplan, D.; Vunjak-Novakovic, G. *Tissue engineering* **2006**, *12*, 3341–64.

[4] Ingber, D. E. *Annals of biomedical engineering* **2010**, *38*, 1148–61.

[5] Mikos, A. G.; Atala, A.; Kasper, F. K. *Tissue Engineering* **2006**, *12*, 3307–3339.

[6] Cook, a. D.; Hrkach, J. S.; Gao, N. N.; Johnson, I. M.; Pajvani, U. B.; Cannizzaro, S. M.; Langer, R. *Journal of biomedical materials research* **1997**, *35*, 513–23.

[7] Albert, B.; Johnson, A.; Lewis, J. *Shock*, 4th ed.; Garland Science: New York, 2002; Vol. 18.

[8] Raeber, G. P.; Lutolf, M. P.; Hubbell, J. a. *Acta biomaterialia* **2007**, *3*, 615–29.

[9] Daley, W. P.; Peters, S. B.; Larsen, M. *Journal of cell science* **2008**, *121*, 255–64.

[10] Behonick, D. J.; Werb, Z. *Mechanisms of Development* **2003**, *120*, 1327–1336.

[11] Roskelley, C. D.; Srebrow, a.; Bissell, M. J. *Current opinion in cell biology* **1995**, *7*, 736–47.

[12] Pérez, R. a.; Won, J.-E.; Knowles, J. C.; Kim, H.-W. *Advanced drug delivery reviews* **2013**, *65*, 471–96.

[13] Beck, K.; Hunter, I.; Engel, J. *FASEB Journal* **1990**, *4*, 148–160.

[14] Kirker, K. R.; Luo, Y.; Nielson, J. H.; Shelby, J.; Prestwich, G. D. *Biomaterials* **2002**, *23*, 3661–71.

[15] Veiseh, M.; Turley, E. A.; Bissell, M. J. *Structure*; 2008; pp 33–51.

[16] Jha, A. K.; Yang, W.; Kirn-Safran, C. B.; Farach-Carson, M. C.; Jia, X. *Biomaterials* **2009**, *30*, 6964–75.

[17] Tibbitt, M. W.; Anseth, K. S. *Biotechnology and bioengineering* **2009**, *103*, 655–63.

[18] Patterson, J.; Martino, M. M.; Hubbell, J. a. *Materials Today* **2010**, *13*, 14–22.

[19] Mouw, J. K.; Case, N. D.; Guldberg, R. E.; Plaas, a. H. K.; Levenston, M. E. *Osteoarthritis and cartilage / OARS, Osteoarthritis Research Society* **2005**, *13*, 828–36.

[20] Vinatier, C.; Magne, D.; Weiss, P.; Trojani, C.; Rochet, N.; Carle, G. F.; Vignes-Colombeix, C.; Chadjichristos, C.; Galera, P.; Daculsi, G.; Guicheux, J. *Biomaterials* **2005**, *26*, 6643–51.

[21] Rodgers, K. D.; San Antonio, J. D.; Jacenko, O. *Developmental dynamics : an official publication of the American Association of Anatomists* **2008**, *237*, 2622–42.

[22] A, V.; RD, C.; JD, E. In *Trends in Cell Biology*, 2nd ed.; A, V., RD, C., JD, E., Eds.; Cold Spring Harbour Laboratory Press: New York, 2009; Vol. 10.

[23] Pieper, J. S.; Hafmans, T.; Veerkamp, J. H.; Kuppevelt, T. H. V. *Biomaterials* **2000**, *21*, 581–593.

[24] Riley, C. M.; Fuegy, P. W.; Firpo, M. a.; Shu, X. Z.; Prestwich, G. D.; Peattie, R. a. *Biomaterials* **2006**, *27*, 5935–43.

[25] Pierce, G. F.; Mustoe, T. A. *Annual Review of Medicine* **1995**, *46*, 467–481.

[26] Deuel, T.; Kawahara, R.; Mustoe, T.; Pierce, G. *Annual Review of Medicine* **1991**, *42*, 567–584.

[27] Mustoe, T. a.; Pierce, G. F.; Morishima, C.; Deuel, T. F. *The Journal of clinical investigation* **1991**, *87*, 694–703.

[28] Jackson, R. a.; Nurcombe, V.; Cool, S. M. *Gene* **2006**, *379*, 79–91.

[29] Luong-Van, E.; Grøndahl, L.; Song, S.; Nurcombe, V.; Cool, S. *Journal of molecular histology* **2007**, *38*, 459–68.

[30] Schwarz, U. S.; Gardel, M. L. *Journal of cell science* **2012**, *125*, 3051–60.

[31] Mattila, P. K.; Lappalainen, P. *Nature reviews. Molecular cell biology* **2008**, *9*, 446–54.

[32] Freudenberg, U.; Hermann, A.; Welzel, P. B.; Stirl, K.; Schwarz, S. C.; Grimmer, M.; Zieris, A.; Panyanuwat, W.; Zschoche, S.; Meinhold, D.; Storch, A.; Werner, C. *Biomaterials* **2009**, *30*, 5049–60.

[33] Stevens, M. M.; George, J. H. *Science* **2005**, *310*, 1135–8.

[34] Gullberg, D.; Ekblom, P. *International Journal of Developmental Biology* **1995**, *39*, 845–854.

[35] Langer, R.; Vacanti, J. P. *Science* **1993**, *260*, 920–926.

[36] Yeung, T.; Georges, P. C.; Flanagan, L. a.; Marg, B.; Ortiz, M.; Funaki, M.; Zahir, N.; Ming, W.; Weaver, V.; Janmey, P. a. *Cell motility and the cytoskeleton* **2005**, *60*, 24–34.

[37] Seo, J.-H.; Kakinoki, S.; Inoue, Y.; Nam, K.; Yamaoka, T.; Ishihara, K.; Kishida, A.; Yui, N. *Biomaterials* **2013**, *34*, 3206–14.

[38] Kong, H. J.; Polte, T. R.; Alsberg, E.; Mooney, D. J. *Proceedings of the National Academy of Sciences of the United States of America* **2005**, *102*, 4300–5.

[39] Zhang, Y.-H.; Zhao, C.-Q.; Jiang, L.-S.; Dai, L.-Y. *Matrix biology* **2011**, *30*, 135–44.

[40] Mager, M. D.; LaPointe, V.; Stevens, M. M. *Nature chemistry* **2011**, *3*, 582–9.

[41] a.F. Von Recum,; Van Kooten, T. *Journal of Biomaterials Science, Polymer Edition* **1996**, *7*, 181–198.

[42] Thapa, A.; Webster, T. J.; Haberstroh, K. M. *Journal of biomedical materials research. Part A* **2003**, *67*, 1374–83.

[43] Thasneem, Y. M.; Sharma, C. P. *Characterization of Biomaterials*; Elsevier, 2013; pp 175–205.

[44] Holzapfel, B. M.; Reichert, J. C.; Schantz, J.-T.; Gbureck, U.; Rackwitz, L.; Nöth, U.; Jakob, F.; Rudert, M.; Groll, J.; Hutmacher, D. W. *Advanced drug delivery reviews* **2013**, *65*, 581–603.

[45] Lackie, J. *Chambers Dictionary of Science and Technology*; 2007.

[46] Curtis, A.; Wilkinson, C. *Biochemical Society Symposium* **1999**, *65*.

[47] Ma, Z.; Mao, Z.; Gao, C. *Colloids and surfaces. B, Biointerfaces* **2007**, *60*, 137–57.

[48] Teixeira, A. I.; Nealey, P. F.; Murphy, C. J. *Journal of biomedical materials research. Part A* **2004**, *71*, 369–76.

[49] Yim, E. K. F.; Reano, R. M.; Pang, S. W.; Yee, A. F.; Chen, C. S.; Leong, K. W. *Biomaterials* **2005**, *26*, 5405–13.

[50] Andersson, A.-S.; Bäckhed, F.; von Euler, A.; Richter-Dahlfors, A.; Sutherland, D.; Kasemo, B. *Biomaterials* **2003**, *24*, 3427–3436.

[51] Zinger, O.; Zhao, G.; Schwartz, Z.; Simpson, J.; Wieland, M.; Landolt, D.; Boyan, B. *Biomaterials* **2005**, *26*, 1837–47.

[52] Teixeira, A. I.; Abrams, G. a.; Bertics, P. J.; Murphy, C. J.; Nealey, P. F. *Journal of cell science* **2003**, *116*, 1881–92.

[53] Pattison, M. a.; Wurster, S.; Webster, T. J.; Haberstroh, K. M. *Biomaterials* **2005**, *26*, 2491–500.

[54] Thapa, A.; Miller, D. C.; Webster, T. J.; Haberstroh, K. M. *Biomaterials* **2003**, *24*, 2915–2926.

[55] Kubinová, S.; Horák, D.; Kozubenko, N.; Vanecek, V.; Proks, V.; Price, J.; Cocks, G.; Syková, E. *Biomaterials* **2010**, *31*, 5966–75.

[56] Petersen, O. W.; Rønnov-Jessen, L.; Howlett, a. R.; Bissell, M. J. *Proceedings of the National Academy of Sciences of the United States of America* **1992**, *89*, 9064–8.

[57] Cukierman, E.; Pankov, R.; Stevens, D. R.; Yamada, K. M. *Science* **2001**, *294*, 1708–12.

[58] Roskelley, C. D.; Bissell, M. J. *Biochemistry and Cell Biology* **1995**, *73*, 391–7.

[59] Friedl, P.; Bröcker, E. B. *Cellular and Molecular Life Sciences* **2000**, *57*, 41–64.

[60] Raeber, G. P.; Lutolf, M. P.; Hubbell, J. a. *Biophysical journal* **2005**, *89*, 1374–88.

[61] Schmeichel, K. L.; Bissell, M. J. *Journal of cell science* **2003**, *116*, 2377–88.

[62] Cukierman, E.; Pankov, R.; Yamada, K. M. *Current opinion in cell biology* **2002**, *14*, 633–9.

[63] Barralet, J. E.; Wang, L.; Lawson, M.; Triffitt, J. T.; Cooper, P. R.; Shelton, R. M. *Journal of materials science: Materials in medicine* **2005**, *16*, 515–9.

[64] Mahoney, M. J.; Anseth, K. S. *Biomaterials* **2006**, *27*, 2265–74.

[65] Elsdale, T.; Bard, J. *The Journal of Cell Biology* **1972**, *54*, 626–637.

[66] Lewandowska, K.; Pergament, E.; Sukenik, C. N.; Culp, L. A. *Journal of Biomedical Materials Research* **1992**, *26*, 1343–1363.

[67] Hern, D. L.; Hubbell, J. a. *Journal of biomedical materials research* **1998**, *39*, 266–76.

[68] Hersel, U.; Dahmen, C.; Kessler, H. *Biomaterials* **2003**, *24*, 4385–4415.

[69] Rahmany, M. B.; Van Dyke, M. *Acta biomaterialia* **2013**, *9*, 5431–7.

[70] Yang, C.; Cheng, K.; Weng, W.; Yang, C. *Journal of materials science. Materials in medicine* **2009**, *20*, 2349–52.

[71] Benoit, D. S. W.; Anseth, K. S. *Biomaterials* **2005**, *26*, 5209–20.

[72] Massia, S. P.; Hubbell, J. a. *Annals of the New York Academy of Sciences* **1990**, *589*, 261–70.

[73] Maheshwari, G.; Brown, G.; Lauffenburger, D. a.; Wells, a.; Griffith, L. G. *Journal of cell science* **2000**, *113 (Pt 1*, 1677–86.

[74] Hojo, K.; Susuki, Y.; Maeda, M.; Okazaki, I.; Nomizu, M.; Kamada, H.; Yamamoto, Y.; Nakagawa, S.; Mayumi, T.; Kawasaki, K. *Bioorganic & medicinal chemistry letters* **2001**, *11*, 1429–32.

[75] Kao, W. J.; Lee, D.; Schense, J. C.; Hubbell, J. a. *Journal of biomedical materials research* **2001**, *55*, 79–88.

[76] Rees, M. D.; McNiven, T. N.; Davies, M. J. *The Biochemical journal* **2007**, *401*, 587–96.

[77] Ingavle, G. C.; Gehrke, S. H.; Detamore, M. S. *Biomaterials* **2014**, *35*, 3558–70.

[78] Peattie, R. a.; Rieke, E. R.; Hewett, E. M.; Fisher, R. J.; Shu, X. Z.; Prestwich, G. D. *Biomaterials* **2006**, *27*, 1868–75.

[79] Jackson, R. A.; Mcdonald, M. M.; Nurcombe, V.; Little, D. G.; Cool, S. M. *Journal of Orthopaedic Research* **2006**, 636–644.

[80] Cool, S. M.; Nurcombe, V. *Journal of cellular biochemistry* **2006**, *99*, 1040–51.

[81] Chipperfield, H.; Bedi, K. S.; Cool, S. M.; Nurcombe, V. *The International journal of developmental biology* **2002**, *46*, 661–70.

[82] Desgranges, P.; Barbaud, C.; Caruelle, J. P.; Barritault, D.; Gautron, J. *FASEB journal : official publication of the Federation of American Societies for Experimental Biology* **1999**, *13*, 761–6.

[83] Vowden, P.; Romanelli, M.; Price, P. *Journal of Wound Care* **2007**, *16*, 189–195.

[84] Marston, W.; Hanft, J.; Norwood, P.; Pollak, R. *Diabetes Care* **2003**, *26*, 1701–1705.

[85] Grefte, S.; Vullinghs, S.; Kuijpers-Jagtman, A. M.; Torensma, R.; Von den Hoff, J. W. *Biomed Mater* **2012**, *7*, 55004.

[86] Spinazzi, R.; Petrelli, L.; Guidolin, D.; Carraro, G.; Casale, V.; Tortorella, C.; Neri, G.; Albertin, G.; Andreis, P. G.; Nussdorfer, G. G. *International Journal of Molecular Medicine* **2006**, *17*, 1101–1110.

[87] Moradi, F.; Bahktiari, M.; Joghataei, M. T.; Nobakht, M.; Soleimani, M.; Hasanzadeh, G.; Fallah, A.; Zarbakhsh, S.; Hejazian, L. B.; Shirmohammadi, M.; Maleki, F. *Journal of Neuroscience Research* **2012**, *90*, 2335–2348.

[88] Bichsel, C. A.; Gobaa, S.; Kobel, S.; Secondini, C.; Thalmann, G. N.; Cecchini, M. G.; Lutolf, M. P. *Lab Chip* **2012**, *12*, 2313–2316.

[89] Peppas, N. a.; Moynihan, H. J.; Lucht, L. M. *Journal of biomedical materials research* **1985**, *19*, 397–411.

[90] DeForest, C. a.; Anseth, K. S. *Annual review of chemical and biomolecular engineering* **2012**, *3*, 421–44.

[91] Jeyanthi, R.; Panduranga, K. *Biomaterials* **1990**, *11*, 238–243.

[92] Bach, L. G.; Islam, M. R.; Jeong, Y. T.; Gal, Y. S.; Lim, K. T. *Applied Surface Science* **2012**, *258*, 2816–2822.

[93] Carbonetto, S.; Gruver, M.; Turner, D. *Science* **1982**, *216*, 897–899.

[94] Carbonetto, S.; Gruver, M.; Turner, D. *The Journal of Neuroscience* **1983**, *3*, 2324–2335.

[95] Skotadis, E.; Tanner, J.; Stathopoulos, S.; Tsouti, V.; Tsoukalas, D. *Sensors and Actuators B: Chemical* **2012**, *175*, 85–91.

[96] Lydon, M. J.; Minett, T. W.; Tighe, B. J. *Biomaterials* **1985**, *6*, 396 – 402.

[97] Özgür, E.; Bereli, N.; Türkmen, D.; Ünal, S.; Denizli, A. *Materials Science and Engineering: C* **2011**, *31*, 915–920.

[98] Denizli, F.; Arica, Y.; Denizli, A. *Reactive and Functional Polymers* **2000**, *44*, 207–217.

[99] Ishihara, K.; Kim, M.; Shinohara, I.; Okano, T.; Kataoka, K.; Sakurai, Y. *Journal of Applied Polymer Science* **1983**, *28*, 1321–1329.

[100] Li, C.; Zheng, Y.-F.; Lou, X. *Journal of materials science. Materials in medicine* **2009**, 2215–2222.

[101] Trigo, R. M.; Blanco, M. D.; Teijón, J. M.; Sastre, R. *Biomaterials* **1994**, *15*, 1181–6.

[102] Dziubla, T. D.; Torjman, M. C.; Joseph, J. I.; Murphy-Tatum, M.; Lowman, a. M. *Biomaterials* **2001**, *22*, 2893–9.

[103] Hsiue, G. H.; Guu, J. a.; Cheng, C. C. *Biomaterials* **2001**, *22*, 1763–9.

[104] Efthimiadou, E. K.; Tziveleka, L.-a.; Bilalis, P.; Kordas, G. *International journal of pharmaceutics* **2012**, *428*, 134–42.

[105] Kumar, S. S. D.; Surianarayanan, M.; Vijayaraghavan, R.; Mandal, A. B.; MacFarlane, D. R. *European journal of pharmaceutical sciences : official journal of the European Federation for Pharmaceutical Sciences* **2014**, *51*, 34–44.

[106] Murugesan, S.; Xie, J.; Linhardt, R. J. *Current topics in medicinal chemistry* **2008**, *8*, 80–100.

[107] Denizli, A. *Journal of Applied Polymer Science* **1999**, *74*, 655–662.

[108] Akgöl, S.; Kaçar, Y.; Özkara, S.; Yavuz, H.; Denizli, A.; Arica, M. *Journal of Molecular Catalysis B: Enzymatic* **2001**, *15*, 197–206.

[109] Arica, M. Y.; Alaeddinoglu, N. G.; Hasirci, V. *Enzyme and Microbial Technology* **1998**, *22*, 152–157.

[110] Danisman, T.; Tan, S.; Kacar, Y.; Ergene, A. *Food Chemistry* **2004**, *85*, 461–466.

[111] Chirila, T. V. *Biomaterials* **2001**, *22*, 3311–7.

[112] Lloyd, a. W.; Faragher, R. G.; Denyer, S. P. *Biomaterials* **2001**, *22*, 769–85.

[113] Hicks, C. R.; Morris, I. T.; Vijayasekaran, S.; Fallon, M. J.; McAllister, J.; Clayton, a. B.; Chirila, T. V.; Crawford, G. J.; Constable, I. J. *British Journal of Ophthalmology* **1999**, *83*, 616–621.

[114] Kliment, K.; Stol, M.; Fahoun, K.; Stockar, B. *Journal of biomedical materials research* **1968**, *2*, 237–43.

[115] Wichterle, O.; Lim, D. *Nature* **1960**, *185*, 117–118.

[116] Fox, C. L.; Modak, S.; Stanford, J. W.; Bradshaw, W. *Burns* **1981**, *7*, 295–297.

[117] Young, C. D.; Wu, J. R.; Tsou, T. L. *Biomaterials* **1998**, *19*, 1745–52.

[118] Corkhill, P. H.; Hamilton, C. J.; Tighe, B. J. *Biomaterials* **1989**, *10*, 3–10.

[119] Tomić, S. L.; Mićić, M. M.; Dobić, S. N.; Filipović, J. M.; Suljovrujić, E. H. *Radiation Physics and Chemistry* **2010**, *79*, 643–649.

[120] Belkas, J. S.; Munro, C. a.; Shoichet, M. S.; Johnston, M.; Midha, R. *Biomaterials* **2005**, *26*, 1741–9.

[121] Katayama, Y.; Montenegro, R.; Freier, T.; Midha, R.; Belkas, J. S.; Shoichet, M. S. *Biomaterials* **2006**, *27*, 505–518.

[122] Reynolds, L. F.; Bren, M. C.; Wilson, B. C.; Gibson, G. D.; Shoichet, M. S.; Murphy, R. J. L. *Spinal cord : the official journal of the International Medical Society of Paraplegia* **2008**, *46*, 58–64.

[123] Plant, G. W.; Woerly, S.; Harvey, a. R. *Experimental neurology* **1997**, *143*, 287–99.

[124] Woerly, S.; Laroche, G.; Marchand, R.; Pato, J.; Subr, V.; Ulbrich, K. *Journal of neural transplantation & plasticity* **1995**, *5*, 245–55.

[125] Woerly, S.; Pinet, E.; de Robertis, L.; Van Diep, D.; Bousmina, M. *Biomaterials* **2001**, *22*, 1095–111.

[126] Long, T. J.; Sprenger, C. C.; Plymate, S. R.; Ratner, B. D. *Biomaterials* **2014**, *35*, 8164–8174.

[127] Hradil, J.; Horák, D. *Reactive and Functional Polymers* **2005**, *62*, 1–9.

[128] Xu, F.; Neoh, K.; Kang, E. *Progress in Polymer Science* **2009**, *34*, 719–761.

[129] Rezaei, S. M.; Mohd Ishak, Z. a. *Express Polymer Letters* **2014**, *8*, 39–49.

[130] Desseaux, S.; Klok, H.-A. *Biomaterials* **2015**, *44*, 24–35.

[131] Sun, L.; Li, D.; Hemraz, U. D.; Fenniri, H.; Webster, T. J. *Journal of Biomedical Materials Research - Part A* **2013**, 3446–3451.

[132] Ren, T.; Yu, S.; Mao, Z.; Moya, S. E.; Han, L.; Gao, C. *Biomacromolecules* **2014**, *15*, 2256–2264.

[133] Wu, J.; Mao, Z.; Han, L.; Xi, J.; Zhao, Y.; Gao, C. *Journal of Bioactive and Compatible Polymers* **2013**, *28*, 605–620.

[134] Horak, D, Dvorak, P, Hampl, A & Slouf, M. *Journal of Applied Polymer Science* **2003**, *87*, 425–432.

[135] Horák, D.; Kroupová, J.; Slouf, M.; Dvorák, P. *Biomaterials* **2004**, *25*, 5249–60.

[136] Kroupova, J.; Horak, D.; Pachernik, J.; Dvorak, P.; Slouf, M. *Journal of Biomedical Materials Research - Part B Applied Biomaterials* **2006**, *76*, 315–325.

[137] Kubinova, S.; Horak, D.; Sykova, E. *Biomaterials* **2009**, *30*, 4601–9.

[138] Bayramoglu, G.; Bitirim, V.; Tunali, Y.; Arica, M. Y.; Akcali, K. C. *Materials Science and Engineering C* **2013**, *33*, 801–810.

[139] Brynda, E.; Houska, M.; Kysilka, J.; Pradny, M.; Lesny, P.; Jendelova, P.; Michalek, J.; Sykova, E. *Journal of Materials Science: Materials in Medicine* **2009**, *20*, 909–915.

[140] Arslantunali, D.; Budak, G.; Hasirci, V. *Journal of Biomedical Materials Research - Part A* **2014**, *102*, 828–841.

[141] Plant, G. W.; Harvey, a. R.; Chirila, T. V. *Brain Research* **1995**, *671*, 119–130.

[142] Pertici, V.; Trimaille, T.; Laurin, J.; Felix, M. S.; Marqueste, T.; Pettmann, B.; Chauvin, J. P.; Gigmes, D.; Decherchi, P. *Biomaterials* **2014**, *35*, 6248–6258.

[143] Dalton, P. D.; Shoichet, M. S. *Biomaterials* **2001**, *22*, 2661–9.

[144] Paterson, S. M.; Shadforth, A. M. a.; Shaw, J. a.; Brown, D. H.; Chirila, T. V.; Baker, M. V. *Materials science & engineering. C, Materials for biological applications* **2013**, *33*, 4917–22.

[145] Kumar, D.; Gerges, I.; Tamplenizza, M.; Lenardi, C.; Forsyth, N. R.; Liu, Y. *Acta Biomaterialia* **2014**, *10*, 3463–3474.

[146] Higa, O. Z.; Faria, H. A. M.; a.a. de Queiroz, A. *Radiation Physics and Chemistry* **2014**, *98*, 118–123.

[147] Volkmer, T.; Magalhães, J.; Sousa, V.; Santos, L.; Burguera, E.; Blanco, F.; Román, J.; Rodríguez-Lorenzo, L. *Polymers* **2014**, *6*, 2510–2525.

[148] Cetin, D.; Kahraman, a. S.; Gumusderelioglu, M. *Journal of biomaterials science Polymer edition* **2011**, *22*, 1157–1178.

[149] Huang, J.; Ten, E.; Liu, G.; Finzen, M.; Yu, W.; Lee, J. S.; Saiz, E.; Tomsia, A. P. *Polymer* **2013**, *54*, 1197–1207.

[150] Zainuddin,; Chirila, T. V.; Brnard, Z.; Watson, G. S.; Toh, C.; Blakey, I.; Whittaker, A. K.; Hill, D. J. T. *Radiation Physics and Chemistry* **2011**, *80*, 219–229.

[151] Lou, X.; Munro, S.; Wang, S. *Biomaterials* **2004**, *25*, 5071–80.

[152] Lou, X.; Vijayasekaran, S.; Chirila, T. V.; Maley, M. a.; Hicks, C. R.; Constable, I. J. *Journal of biomedical materials research* **1999**, *47*, 404–11.

[153] Pieper, J. S.; Hafmans, T.; van Wachem, P. B.; van Luyn, M. J. A.; Brouwer, L. A.; Veerkamp, J. H.; van Kuppevelt, T. H. *Journal of Biomedical Materials Research* **2002**, *62*, 185 – 194.

[154] Meade, K. a.; White, K. J.; Pickford, C. E.; Holley, R. J.; Marson, A.; Tillotson, D.; van Kuppevelt, T. H.; Whittle, J. D.; Day, A. J.; Merry, C. L. R. *The Journal of biological chemistry* **2013**, *288*, 5530–8.

[155] Cushing, M. C.; Liao, J.-T.; Jaeggli, M. P.; Anseth, K. S. *Biomaterials* **2007**, *28*, 3378–87.

[156] Farndale, R. W.; Buttle, D. J.; Barrett, a. J. *Biochimica et biophysica acta* **1986**, *883*, 173–7.

[157] Farndale, R. W.; Sayers, C. a.; Barrett, a. J. *Connective tissue research* **1982**, *9*, 247–8.

[158] Rimmer, S.; Johnson, C.; Zhao, B.; Collier, J.; Gilmore, L.; Sabnis, S.; Wyman, P.; Sammon, C.; Fullwood, N. J.; MacNeil, S. *Biomaterials* **2007**, *28*, 5319–31.

[159] Teixeira, S.; Yang, L.; Dijkstra, P. J.; Ferraz, M. P.; Monteiro, F. J. *Journal of materials science. Materials in medicine* **2010**, *21*, 2385–92.

[160] Arica, M. Y.; Bayramoglu, G. *Journal of Molecular Catalysis B: Enzymatic* **2004**, *27*, 255–265.

[161] Geurts, J. M.; Jacobs, P. E.; Muijs, J. G.; Steven Van Es, J. J. G.; German, A. L. *Journal of Applied Polymer Science* **1996**, *61*, 9–19.

[162] Morita, S. *Frontiers in chemistry* **2014**, *2*, 10.

[163] Zhang, L.; Zheng, G.-J.; Guo, Y.-T.; Zhou, L.; Du, J.; He, H. *Asian Pacific journal of tropical medicine* **2014**, *7*, 136–40.

[164] Tomić, S. L. J.; Mićić, M. M.; Filipović, J. M.; Suljovrujić, E. H. *Radiation Physics and Chemistry* **2007**, *76*, 1390–1394.

[165] Islam, M. R.; Bach, L. G.; Park, J. M.; Hong, S. S.; Lim, K. T. *Journal of Applied Polymer Science* **2013**, *127*, 1569–1577.

[166] Baker, M. V.; Brown, D. H.; Casadio, Y. S.; Chirila, T. V. *Polymer* **2009**, *50*, 5918–5927.

[167] Santander-Borrego, M.; Green, D. W.; Chirila, T. V.; Whittaker, A. K.; Blakey, I. *Journal of Polymer Science, Part A: Polymer Chemistry* **2014**, *52*, 1781–1789.

[168] Meakin, J. R.; Hukins, D. W. L.; Aspden, R. M.; Imrie, C. T. *Journal of Materials Science: Materials in Medicine* **2003**, *4*, 783–787.

[169] Rotsch, C.; Jacobson, K.; Radmacher, M. *Proceedings of the National Academy of Sciences of the United States of America* **1999**, *96*, 921–6.

[170] Wakatsuki, T.; Kolodney, M. S.; Zahalak, G. I.; Elson, E. L. *Biophysical journal* **2000**, *79*, 2353–68.

[171] Thoumine, O.; Ott, A. *Journal of Cell Science* **1997**, *110*, 2109–2116.

[172] Holt, B.; Tripathi, A.; Morgan, J. *Journal of Biomechanics* **2008**, *41*, 2689–2695.

[173] Berfield, M.; Gotte, M.; Park, P. W.; Reizes, O.; Fitzgerald, M. L.; Linceecum, J.; Zako, M. *Annual Review of Biochemistry* **1999**, *68*, 729–777.

[174] Garcia, A. J.; Vega, M. D.; Boettiger, D. *Molecular Biology of the Cell* **1999**, *10*, 785–798.

[175] Duncan, a. *European Polymer Journal* **2001**, *37*, 1821–1826.

[176] Sakiyama-Elbert, S. E.; Hubbell, J. a. *Journal of controlled release : official journal of the Controlled Release Society* **2000**, *65*, 389–402.

[177] Ruozi, B.; Parma, B.; Croce, M. A.; Tosi, G.; Bondioli, L.; Vismara, S.; Forni, F.; Vandelli, M. A. *International journal of pharmaceutics* **2009**, *378*, 108–15.

[178] Casar, J. C.; Cabello-Verrugio, C.; Olguin, H.; Aldunate, R.; Inestrosa, N. C.; Brandan, E. *Journal of cell science* **2004**, *117*, 73–84.

[179] Huang, C.; Cheng, C.; Su, H.; Lin, Y. *Cellular Physiology and Biochemistry* **2015**, *36*, 1291–1304.

[180] Galderisi, U.; Peluso, G.; Bernardo, S.; Calarco, A.; D'Apolito, M.; Petillo, O.; Cipollaro, M.; Fusco, F. R.; Melone, M. A. B. *Stem Cell Research* **2013**, *10*, 85–94.

[181] Rapraeger, A. C.; Krufka, A.; Olwin, B. B. *Science* **1991**, *252*, 1705–08.

[182] Kleinman, H. K.; Luckenbill-Edds, L.; Cannon, F. W.; Sephel, G. C. *Analytical biochemistry* **1987**, *166*, 1–13.

[183] Chaturvedi, V, Dye, D, Kinnear, B, Kuppevelt, T, Grounds, M, Coombe, D. *PLoS One* **2015**,

[184] Corporation, I. alamarBlue ® Assay. 2007.

[185] Goegan, P.; Johnson, G.; Vincent, R. *Toxicology in Vitro* **1995**, *9*, 257–266.

[186] Quent, V. M. C.; Loessner, D.; Friis, T.; Reichert, J. C.; Hutmacher, D. W. *Journal of Cellular and Molecular Medicine* **2010**, *14*, 1003–1013.

[187] O'Brian, J.; Wilson, I.; Orton, T.; Pognan, F. *European Journal of Biochemistry* **2000**, *267*, 5421–5426.

[188] Riss, T. L.; Moravec, R. A.; Niles, A. L.; Benink, H. A.; Worzella, T. J.; Minor, L. *Assay Guidance Manual*; National Institutes of Health, 2013.

[189] Omidian, H.; Park, K.; Rocca, J. G. *International Journal of Polymeric Materials* **2010**, *59*, 693–709.

[190] Peluso, G.; Petillo, O.; Anderson, J. M.; Ambrosio, L.; Nicolais, L.; Melone, M. A. B.; Eschbach, F. O.; Huang, S. J. *Journal of Biomedical Materials Research* **1997**, *34*, 327–336.

[191] McCracken, J. M.; Badea, A.; Kandel, M. E.; Gladman, A. S.; Wetzel, D. J.; Popescu, G.; Lewis, J. A.; Nuzzo, R, G. *Advanced Healthcare Materials* **2016**,

[192] Truskey, G. A.; Proulx, T. L. *Biomaterials* **1993**, *14*, 243–254.

[193] Tamariz, E.; Grinnell, F. *Molecular Biology of the Cell* **2002**, *13*, 3915–3929.

[194] Parsons, J. T.; Horwitz, A. R.; Schwartz, M. a. *Nature reviews. Molecular cell biology* **2010**, *11*, 633–43.

[195] Pokharna, H. K.; Zhong, Y.; Smith, D. *Journal of Bioactive and Compatible Polymers* **1990**, *5*, 42–52.

[196] Arima, Y.; Iwata, H. *Acta Biomaterialia* **2015**, *26*, 72–81.

[197] Keselowsky, B. G.; Collard, D. M.; Garcia, A. J. *Proceedings of the National Academy of Sciences of the United States of America* **2005**, *102*, 5953–5957.

[198] Hejcl, A.; Lesny, P.; Pradny, M.; Michalek, J.; Jendelova, P.; Stulik, J.; Sykova, E. *Physiology Research* **2008**, *57*, S121–132.

[199] Bruyrre, J.; Roy, E.; Ausseil, J.; Lemonnier, T.; Teyre, G.; Bohl, D.; Etienne-Manneville, S.; Lortat-Jacob, H.; Heard, J. M.; Vitry, S. *Journal of Molecular Biology* **2015**, *427*, 775–791.

[200] Yang, D.; Lü, X.; Hong, Y.; Xi, T.; Zhang, D. *Biomaterials* **2013**, *34*, 5747–58.

[201] Freier, T.; Montenegro, R.; Koh, H. S.; Shoichet, M. S. *Biomaterials* **2005**, *26*, 4624–4632.

[202] Freier, T.; Koh, H. S.; Kazazian, K.; Shoichet, M. S. *Biomaterials* **2005**, *26*, 5872–5878.

[203] Singh, D.; Nayak, V.; Kumar, A. *International Journal of Biological Sciences* **2010**, *6*, 371–381.

[204] Tugulu, S.; Silacci, P.; Stergiopulos, N.; Klok, H.-A. *Biomaterials* **2007**, *28*, 2536–46.

[205] Chirila, T. V.; Constable, I. J.; Crawford, G. J.; Vijayasekaran, S.; Thompson, D. E.; Chen, Y.-c.; Fletcher, W. A.; Griffin, B. J. *Biomaterials* **1993**, *14*, 26–38.

[206] Montesano, A.; Luzi, L.; Senesi, P.; Terruzzi, I. *International Journal of Biological Sciences* **2013**, *9*, 391 – 402.

[207] Laterra, J.; Silbert, J. E.; Culp, L. A. *The Journal of Cell Biology* **1983**, *96*, 112–123.

[208] Couchman, J. R.; Hook, M.; Rees, D. A.; Timpl, R. *The Journal of Cell Biology* **1983**, *96*, 177–183.

[209] Patwari, P.; Lee, R. T. *Circulation Research* **2008**, *103*, 234–43.

[210] Grinnell, F.; Feld, M. *Cell* **1979**, *17*, 117–129.

[211] Thyberg, J.; Hedin, U.; Sjolund, M.; Palmberg, L.; Bottger, B. a. *Arteriosclerosis, Thrombosis, and Vascular Biology* **1990**, *10*, 966–990.

[212] Lyon, M.; Gallagher, J. T. *Matrix Biology* **1998**, *17*, 485–493.

[213] Tan, H.; Lao, L.; Wu, J.; Gong, Y.; Gao, C. *Polymers for Advanced Technologies* **2008**, *19*, 15–23.

[214] Gagne, L.; Rivera, G.; Laroche, G. *Biomaterials* **2006**, *27*, 5430–5439.

[215] Pulsipher, A.; Park, S.; Dutta, D.; Luo, W.; Yousaf, M. N. *Langmuir* **2014**, *30*, 13656–13666.

[216] Weber, L. M.; Hayda, K. N.; Haskins, K.; Anseth, K. S. *Biomaterials* **2007**, *28*, 3004–3011.

[217] Sapir, Y.; Kryukov, O.; Cohen, S. *Biomaterials* **2011**, *32*, 1838–1847.

[218] Elbert, D. L.; Hubbell, J. a. *Biomacromolecules* **2001**, *2*, 430–441.

[219] Irvine, D. J.; Mayes, a. M.; Griffith, L. G. *Biomacromolecules* **2001**, *2*, 85–94.

[220] Petrie, T. A.; Capadona, J. R.; Reyes, C. D.; Garcia, A. J. *Biomaterials* **2006**, *27*, 5459–5470.

[221] Higuchi, A.; Ling, Q.; Kumar, S. S.; Munusamy, M.; Alarfajj, A. A.; Umezawa, A.; Wu, G. *Progress in Polymer Science* **2014**, *39*, 1348–1374.

[222] Bradshaw, M.; Ho, D.; Fear, M. W.; Gelain, F.; Wood, F. M.; Iyer, K. S. *Scientific reports* **2014**, *4*, 6903.

[223] Grassot, V.; Da Silva, A.; Saliba, J.; Maftah, A.; Dupuy, F.; Petit, J. *BMC Genomics* **2014**, *15*, 621.

[224] Gillies, A. R.; Lieber, R. L. *Muscle & nerve* **2011**, *44*, 318–31.

[225] Chino, K.; Takahashi, H. *Clinical Biomechanics* **2015**, *30*, 1230–1235.

Appendix

Table A.1: Equilibrium water content of hydrogels in phosphate buffered saline

Hydrogel	EWC%[1]
PG26	78.1 ± 0.4
PGN26	78.8 ± 0.5
PGR26	79.1 ± 0.7

[1]values were the average of 5 samples ± standard deviation

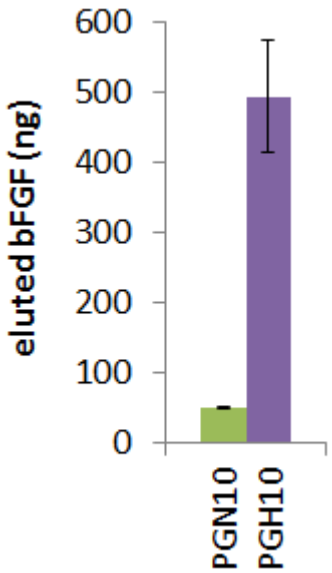

Figure A.1: Bioactivity of immobilised HS on the hydrogels 4. The amount of bFGF bound to immobilised HS on the hydrogels as determined by ELISA, n=8, error bars show standard deviation.

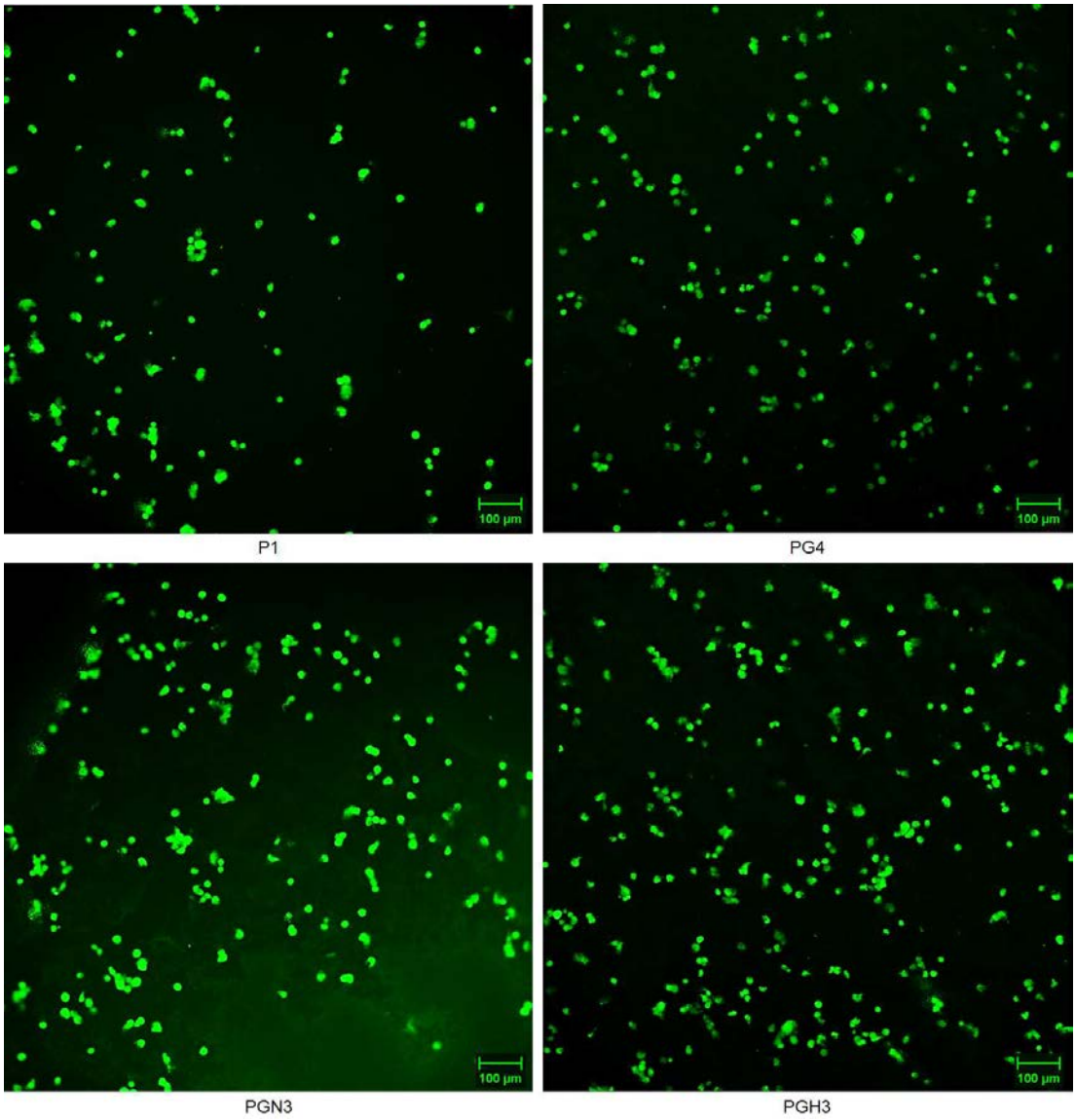

Figure A.2: C2C12 cell adhesion on the hydrogels 2. The cells were stained with CFSE 2 h after seeding on the hydrogels and imaged with fluorescent microscopy, scale bars show 100 µm.

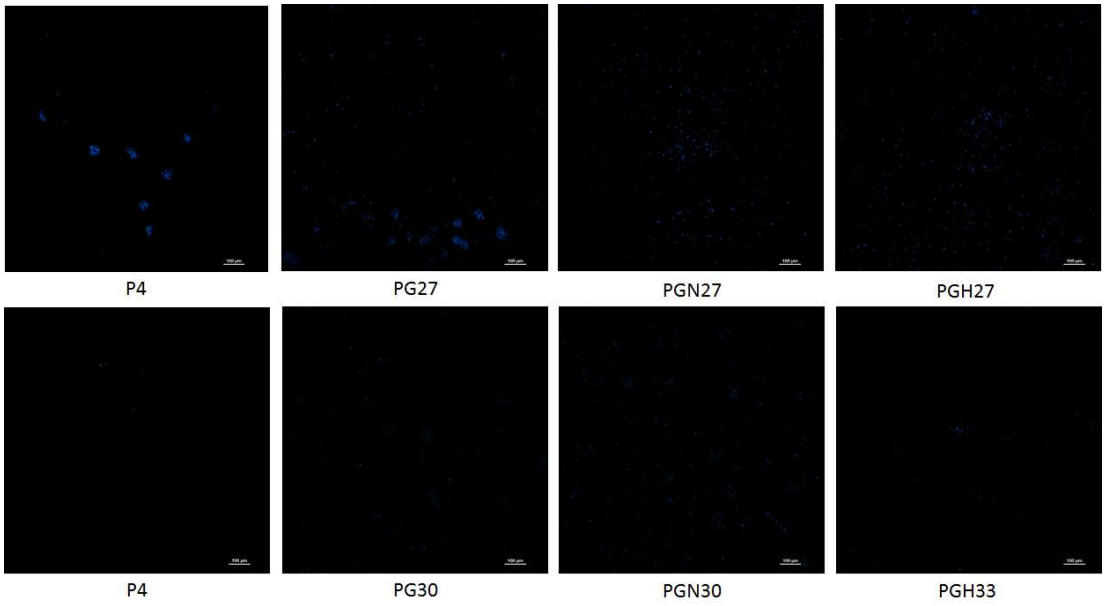

Figure A.3: Control images for Fibronectin staining on hydrogels. The cells were grown on the hydrogels, top row, 3T3 cells, bottom row C2C12 cells. The cells were fixed with 4% paraformaldehyde, incubated in buffer followed by the secondary fluorescent antibody (Alexa Fluor® 488 F(ab')2 goat anti-rabbit IgG, green) and DAPI for the nucleus (blue), the scale bars are 100 μm.

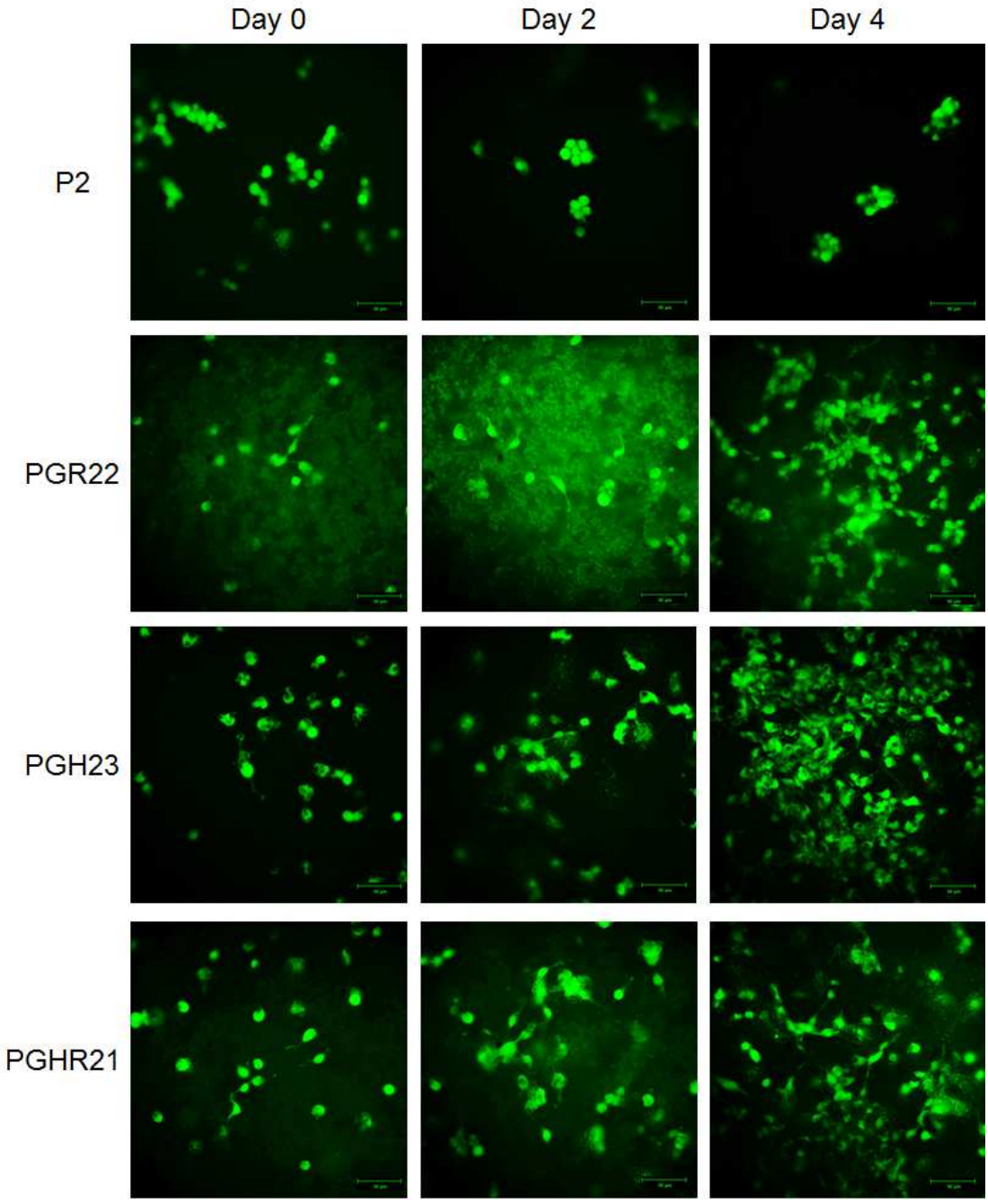

Figure A.4: Morphology of 3T3 cells on end modification hydrogels. The cells were stained with CFSE and imaged with fluorescent microscopy, scale bars show 50 μm.

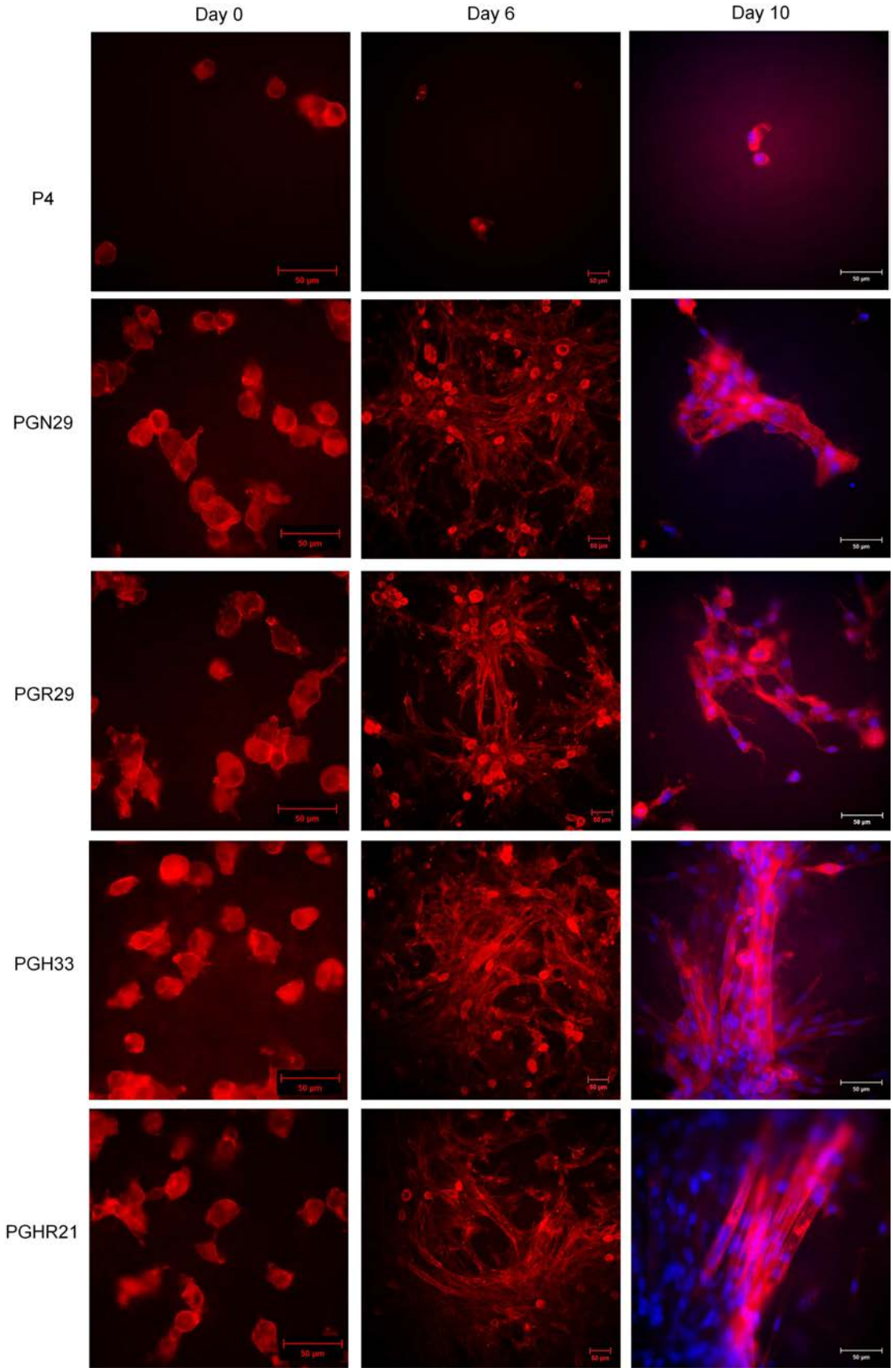

Figure A.5: Morphology of C2C12 cells on end modification hydrogels.

Every reasonable effort has been made to acknowledge the owners of copyright material. I would be pleased to hear from any copyright owner who has been omitted or incorrectly acknowledged.